GRIFFITH UNIVERSITY

Measurement and Analysis of Electron Mobility in GaN Power HEMTs

Author

Aminbeidokhti, Amirhossein

Published

2016

Thesis Type

Thesis (PhD Doctorate)

School

Griffith School of Engineering

DOI

10.25904/1912/2231

Rights statement

The author owns the copyright in this thesis, unless stated otherwise.

Downloaded from

http://hdl.handle.net/10072/368007

Griffith Research Online

https://research-repository.griffith.edu.au

Measurement and Analysis of Electron Mobility in GaN Power HEMTs

A Thesis

Submitted to

The Griffith School of Engineering

Griffith University

Brisbane, Australia

by

Amirhossein Aminbeidokhti

B. Eng, M. Eng

Submitted in fulfilment of the requirements of the degree

of

Doctor of Philosophy

June 2016

ABSTRACT

High-electron-mobility transistor (HEMT) is a promising device for power applications because of their high breakdown voltage, high electron mobility in two-dimensional electron gas (2DEG) area, fast switching capability, high-temperature operating capabilities, compatibility with standard electronic circuits, and low production cost.

In contrast to the gate in metal–oxide–semiconductor field-effect transistor (MOSFET), which extends from source to drain, the gate in HEMT splits the device into two main sections: field-effect (section under the gate) and resistive (section outside the gate). Resistances of the 2DEG outside the gate sections are constant and modelled by fixed resistors. However, the 2DEG resistance under the gate section is dependent to the gate voltage, which can be modelled by channel resistance of a field-effect transistor (FET). Since these resistances depend on the mobility of electrons in the 2DEG, it is important to separate the electron mobility in the resistive and field-effect sections. Therefore, existence of the resistive section in the HEMT structure leads to requiring new methods for the HEMT mobility measurement. Also, since there is no model for the HEMT in SPICE, novel models are required for the SPICE simulation of the HEMT. In order to solve these issues:

- A novel method for measurement of electron mobility in the 2DEG section of the HEMT is introduced, in which the 2DEG between the source and drain is separated to the field-effect and resistive sections. In addition, this method enables the potential impact of the gate voltage on the 2DEG mobility under the gate to be measured without the error of the resistive 2DEG sections. Utilising this method leads to measure the mobility under and outside the gate, separately. Applying this method to fabricated HEMTs, utilising modified field-effect and effective mobility measurement techniques, shows similar results for the 2DEG mobilities under and outside the gate. Although the value of 2DEG mobility under the gate measured by field-effect and effective techniques are close to each other, these measurement techniques show different behaviour with the gate voltage. Effective mobility measurement technique is independent from the gate voltage, however field-effect mobility measurement technique shows dependence to the gate voltage. Also, it should be noted that this method requires utilising an extra sample–Hall sample.

- In order to address issues with the first presented mobility measurement method, a new measurement method for the electron mobility of the 2DEG section just under the gate is introduced, which does not require any extra samples. Utilising this method leads to the electron mobility investigation for a wide range of temperature, from 25°C to 300°C. It is experimentally demonstrated that the electron mobility in the 2DEG under the gate of the HEMT is not dependent on the gate voltage. Furthermore, it is shown that the HEMT mobility decreases with increasing the temperature according to the power-law (T^{-k}) and with a high value of the power-law coefficient ($k = 2.45$).

- Mobility at high temperatures is a function of phonon scattering. Regarding to the HEMT mobility dependence on temperature, the power-law co-efficient, which shows the rate of change for the phonon-limited electron mobility with temperature, for the phonon scattering is 1.5. However, this value is between 2.14 and 3.42 for the GaN-based devices such as AlGaN/GaN HEMT. The increase of the power-law coefficient in the GaN-based devices is explained physically that leads to the better understanding of electron mobility behaviour in GaN structures at high temperature.

- In addition, a method for using standard MOSFET equations and parameters for SPICE simulation of circuits with the HEMT is presented. The proposed method is demonstrated and verified by measured transfer and output characteristics of fabricated HEMTs. In addition, parameter-extraction techniques to determine the values of selected parameters from measured HEMT characteristics are presented.

To my beloved parents, sisters, brother, brother in-law, niece, and grandparents

for their love, endless support

and encouragement.

ACKNOWLEDGEMENT

Working at Queensland Micro- and Nanotechnology Center, Griffith University has been an incredibly rewarding experience. I believe QMNC to be a unique center in the sense that the sharing of ideas and knowledge extends not only beyond individuals but also between different groups of the center with different backgrounds. I had the opportunity to work with and exchange ideas and information with people from the electrical engineering, materials, and physics backgrounds. I can never express my gratitude enough to the people who have helped me and made a significant contribution to making this thesis possible.

First and foremost, I would like to convey my deepest and sincere gratitude to my principal supervisor, Professor Sima Dimitrijev for taking me on as a student and providing continuous supervision, guidance and encouragement throughout my doctoral journey. Without his endless support, guidance, and enlightened contribution to this research there would be no thesis. And even in his own, difficult, times he never waive red in his leadership and wisdom. Everything you have done for me, your support, time and energy, is greatly appreciated. You will be missed.

Dr. Jisheng Han taught me to understand processing issues, trained me how to perform the fabrication process, and work with fabrication equipment in the cleanroom. In my opinion, he is the best resource in the world for any technical issues regarding the fabrication process. Dr Philip Tanner has been a valuable resource in helping me for electrical measurements. Their guidance and opinions towards my complicated queries and questions has served me well and I owe them my heartfelt appreciation.

My sincere gratitude is extended to Alan Iacopi, Anthony Christian and Glenn Walker for their invaluable technical assistance and guidance for operation of the clean room equipment.

I would also like to acknowledge the financial support and scholarships (GUPRS and GUIPRS) provided by the Griffith University. Also I appreciate Professor Xiangang Xu from the State Key Laboratory of Crystal Materials, Shandong University for supplying the GaN wafers which have been used in this research.

Thanks Lacey Shaw and Kerryn Iacopi for all your help, administrative support and assistance during the whole period of my PhD.

Thank you to all my friends and colleagues for their amazing support throughout my education at the post-graduate level. Thank you, Hamid Amini Moghadam, Daniel Erwin Haasmann, and Sina Aminmansour, you have all helped in more ways that you can imagine. And thanks to all the people that I have forgotten to mention that have made a contribution, no matter how small, in supporting me through my life.

Finally, I would like to express my endless gratitude to my wonderful parents, sisters, brother, brother in-law and my niece for their endless care, support and love throughout the years. I will never be able to thank you enough.

Amirhossein Aminbeidokhti

STATEMENT OF ORIGINALITY

This work has not previously been submitted for a degree or diploma in any university. To the best of my knowledge and belief, the thesis contains no material previously published or written by another person except where due reference is made in the thesis itself.

_Amirhossein Aminbeidokhti__

Author’s Signature

_22/06/2016____

Date

TABLE OF CONTENTS

Abstract I

Acknowledgement V

Statement of originality VII

Table of contents IX

Selected List of Symbols XI

Selected List of Abbreviations XIV

Chapter 1: Introduction 1

1.1. Significance of the research 2

1.2. Material advantages of GaN for power electronic devices 4

1.3. HEMT structure 5

1.4. Current status and practical challenges 6

1.5. Original research contributions 9

1.6. Thesis outline 10

1.7. Related publications 12

1.8. References 14

Chapter 2: Literature review- Electron mobility of GaN power HEMTs 19

2.1. Introduction 21

2.2. Electron mobility measurement methods for HEMT 22

2.2.1. Hall mobility 23

2.2.1.1. Definition 23

2.2.1.2. Measurement method 24

2.2.1.2.1. Sample configuration 24

2.2.1.2.1. Measurement set-up 25

2.2.1.2.2. Two-dimensional electron gas carrier density measurement 26

2.2.1.2.3. Sheet resistance measurement 27

2.2.2. Effective mobility 28

2.2.3. Field-effect mobility 32

2.3. Works performed on electron mobility measurements of the HEMT 35

2.4. Possible sources of error of electron mobility measurements 43

2.5. Temperature dependence of electron mobility of the HEMT.......................................43

2.6. Scattering mechanisms effects on mobility of the HEMT 50

2.7. Application of the measured electron mobility of the HEMT.......................................54

2.7.1. SPICE Simulation of circuits with HEMT...54

2.7.1.1. Importance of SPICE modelling of the HEMT 54

2.7.1.2. Models presented for SPICE simulation of the HEMT 55

2.8. References 62

Chapter 3: A Method for Extraction of Electron Mobility in Power HEMTs[1] 73

Chapter 4: Gate Voltage Independence of Electron Mobility in Power AlGaN/GaN HEMTs[2] 95

Chapter 5: The Power Law of Phonon-Limited Electron Mobility in the Two-Dimensional Electron Gas of AlGaN/GaN Heterostructure[3] 103

Chapter 6: SPICE MOSFET Equations and Parameters as Power HEMT Model[4] 109

Chapter 7: Conclusions and Recommendations 125

7.1. Conclusions 126

7.2. Suggestions for future research 127

[1] Published in *Superlattices and Microstructures*, vol. 85, pp. 543–550, September 2015.
[2] Published in *IEEE Transactions on Electron Devices*, vol. 63, no. 3, pp. 1013-1019, March 2016.
[3] Published in *IEEE Transactions on Electron Devices*, vol. 63, no. 5, pp. 2214-2218, May 2016.
[4] To be submitted to *Microelectronics Reliability* journal.

Selected List of Symbols

B .... Magnetic field
C .... Capacitance per unit area
C_{GC} .... Gate-to-channel capacitance
C_{GD} .... Gate-to-drain capacitance
C_{GS} .... Gate-to-channel capacitance
C_{ox} .... Gate oxide capacitance
cgdo .... Gate-to-drain overlap capacitance per unit width
cgso .... Gate-to-source overlap capacitance per unit width
f .... Frequency
f_T .... Cut-off frequency
g_m .... Transconductance
g_O .... Output conductance
I_H .... Hall current
I_D .... Drain current
KP .... Transconductance parameter
L .... Length
L_{eff} .... Channel effective length
L_T .... Transfer length
L_G .... Gate length
m^* .... Effective mass
n .... Effective number of squares
n_C .... Effective number of squares for source and drain Ohmic contacts
n_D .... Effective number of squares between the drain and source
n_G .... Effective number of squares for the gate
n_S .... Effective number of squares between the gate and source
N_{2DEG} .... Two-dimensional electron gas charge density
N_{SC} .... Concentration of phonons as scattering centers
Q_n .... Mobile channel charge density
Phi .... Surface potential I strong inversion
q .... Electron charge

$R_{Average}$ ....Average resistance

R_{CH} ....Channel resistance

R_{CS}......................Source contact resistance

R_{CD} ....Drain contact resistance

R_{DS}......................Drain-to-source resistance

R_{GD} ....Gate-to-drain resistance

R_{GS}......................Gate-to-source resistance

r_G........................Variable resistance of two-dimensional electron gas under the gate

R_S........................Sheet resistance

$R_{S\text{-}C}$ ....Sheet resistance of source/drain contacts

$R_{S\text{-}O}$ ....Sheet resistance of two-dimensional electron gas outside the gate

$r_{S\text{-}U}$......................Sheet resistance of two-dimensional electron gas under the gate

t_{AlGaN}..................Thickness of aluminium gallium nitride layer

T ....Temperature

V ....Voltage

$V_{2DEG\text{-}U}$ ....Voltage across the two-dimensional electron gas under the gate

V_{DS}......................Drain-to-source voltage

V_{eff} ....Effective electron velocity

V_G ....Applied gate voltage

V_{GS}......................Gate-to-source voltage

V_H ....Hall voltage

$V_{R\text{-}C}$.....................Voltage across the contact resistances of the source and drain

$V_{R\text{-}GD}$..................Voltage across the resistive gate-to-drain section of the 2DEG

$V_{R\text{-}GS}$ ....Voltage across the resistive gate-to-source section of the 2DEG

V_T........................Threshold voltage

V_{th} ....Thermal velocity of electrons

W ....Width

W_G ....Gate width

ε_{AlGaN}..................Permittivity of aluminium gallium nitride

μ_0........................Low-field electron mobility

μ_{eff}.......................Effective mobility

μ_{FE} ....Field-effect mobility

μ_H ....Hall mobility

μ_n........................Electron mobility

γ..........................Power coefficient

θ..........................Mobility degradation factor

τ_{ph} ....Average time between two phonon-scattering events

σ_{SC} ....Phonon-scattering cross-section

SELECTED LIST OF ABBREVIATIONS

2DEG .... Two-dimensional electron gas
AC .... Alternating current
Al_2O_3 .... Aluminium oxide
ALD .... Atomic layer deposition
AlN..................... Aluminium nitride
AlGaN .... Aluminium gallium nitride
CTL .... Circular-transmission-line
DC .... Direct current
DIBL .... Drain-induced barrier lowering
GaAs .... Gallium arsenide
GaN .... Gallium nitride
GCA .... Gradual channel approximation
Ge .... Germanium
HEMT .... High electron mobility transistor
InAlN .... Indium aluminium nitride
MESFET .... Metal-semiconductor field-effect transistor
MOS-HEMT ...... Metal–oxide–semiconductor high electron mobility transistor
MOSFET .... Metal–oxide–semiconductor field-effect transistor
QMSA .... Quantitative mobility spectrum analysis
RF....................... Radio frequency
Si .... Silicon
SiC...................... Silicon carbide
Si_3N_4 .... Silicon nitride
SiO_2 .... Silicon dioxide
SPICE................ Simulation program with integrated circuit emphasis

CHAPTER 1: INTRODUCTION

1.1 Significance of the research 2

1.2 Material advantages of GaN for power electronic devices 4

1.3 HEMT structure 5

1.4 Current status and practical challenges 6

1.5 Original research contributions 9

1.6 Thesis outline 10

1.7 List of publications 13

1.8 References 15

1.1. Significance of the research

In recent years, demand for the high electron mobility transistor (HEMT) for high-power applications has increased significantly [1]. This device was invented by Mimura et al. [2-4], and was fabricated based on gallium arsenide (GaAs). The initial HEMT had several drawbacks, especially in regard to the cost [4] . Therefore, it was necessary to modify the HEMT structure and develop its performance.

It was found that wide bandgap materials with high thermal conductivity, electric field, and high electron saturation velocity, such as gallium nitride (GaN) and silicon carbide (SiC), offer reliable technologies for high-power and high-temperature applications [1]. Comparing the most common wide bandgap semiconductors (GaN and SiC) reveals that GaN is more cost-effective than SiC. Also, it is possible to grow GaN on various substrates (sapphire, Si, and SiC) with large dimensions. Therefore, it is feasible to have larger wafers and larger GaN devices for the same processing cost, which results in achieving cheaper products.

Khan et al. introduced the first AlGaN/GaN HEMT [5, 6]. This device has the advantages of heterojunction, which is formed at the interface of AlGaN and GaN. GaN-based HEMT is considered as the next-generation device technology for high-power and high-speed applications [7], whose wide range of applications for power management and power switching are shown in Figure 1. This device neither needs doped AlGaN and GaN layers nor requires any gate oxides. It has a simple fabrication process, which requires few photolithography steps, and it is cheaper than other common power semiconductor devices based on SiC, such as Schottky and the metal-oxide-semiconductor field-effect transistor (MOSFET). Also, it offers superior performance (higher mobility, higher breakdown voltage, larger drain current, and higher power density) in comparison to Si and SiC-based devices [8], and is more environmentally friendly than GaAs devices. Figure 2 represents a comparison between the power devices fabricated by the most common semiconductor devices.

As the name HEMT indicates, the most significant parameter of this device is its high value of electron mobility. Therefore, understanding the concept of the electron mobility in AlGaN/GaN HEMT, and investigating methods to measure this parameter, are crucial for the performance enhancement of the HEMT. Since the HEMT is capable of operating at high temperatures, it needs mobility measurement methods for measurements above the room temperature. It is also needed

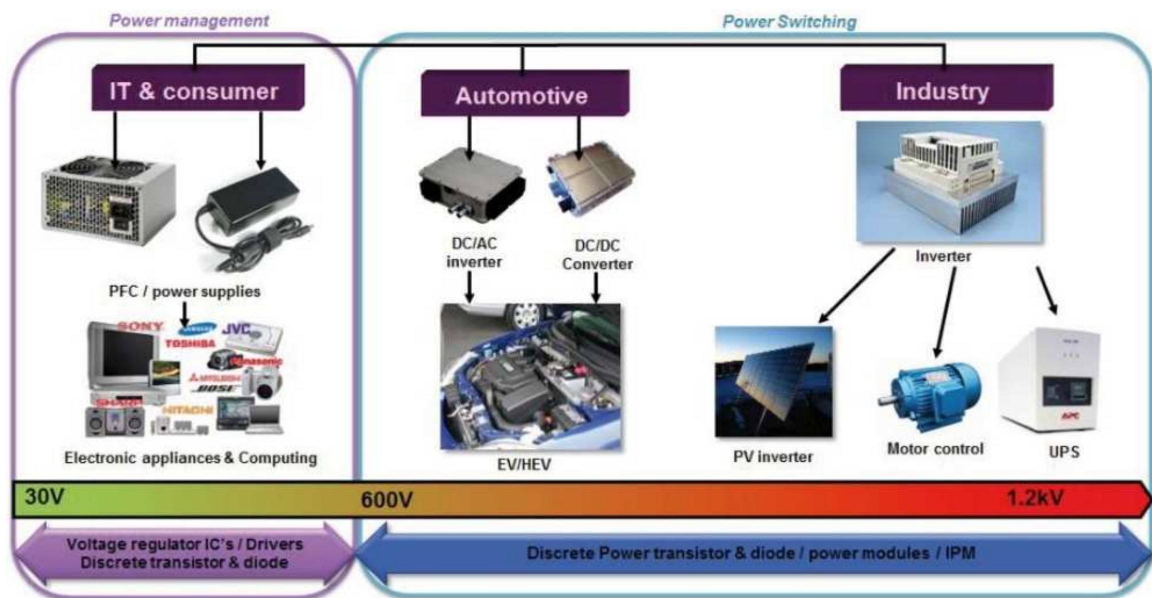

Figure 1. Possible applications for GaN HEMTs in power electronics [9]

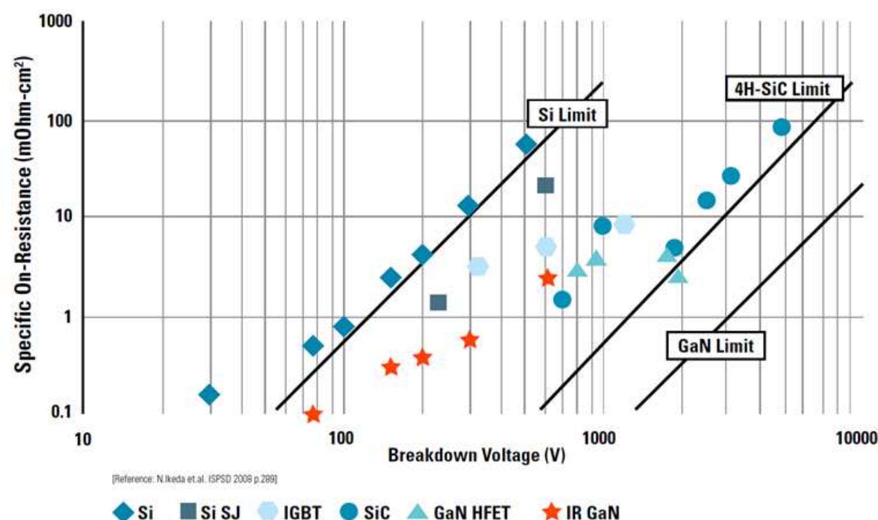

Figure 2. Comparison of the ON-resistance versus the breakdown voltage of GaN HEMT with Si and SiC-based devices [10]

to analyse the effects of temperature on the mobility. In addition, effects of other parameters, such as the gate voltage and various scattering mechanisms, and the physics behind these effects, need to be taken into consideration and analysed. In addition, the application of this measured mobility in developing the HEMT needs to be investigated. One of the main applications of this measured mobility is in the HEMT modelling for circuit designs, analysis,

and simulation purposes. Straightforward models of this device can produce extensive industrial applications for the HEMT.

1.2. Material advantages of GaN for power electronic devices

Power semiconductor devices require wide bandgap materials with high breakdown-field, high saturated electron velocity, high thermal conductivity, and high carrier mobility. In addition, the substrate should have high thermal conductivity. The relation between the material characteristics and the device performance is explained in Table 1.

Table 1. Relation between material characteristics and the device performance [8],[11],[12]

Material property	Device operation	Advantage
High breakdown field	High voltage	High power device
High thermal conductivity	High temperature	Smaller die size, smaller package, cheaper package
Wide bandgap	High breakdown voltage, power density, and high temperature	Compact device, ease of matching, reduced cooling
High electron velocity	High power and frequency	High frequency systems

As can be seen in Table 2, which compares the characteristics of materials competing in the area of power semiconductor devices, GaN has a wide bandgap with the capability of operating at high temperatures. Its wide bandgap combined with its high electron velocity means that GaN-based devices can achieve high breakdown voltage and high currents and, therefore, high power density. In addition, its high thermal conductivity makes GaN-based devices very promising for high-power applications [8]. Although thermal conductivity of GaN is smaller than SiC, excellent properties of GaN at high temperatures make these devices a feasible alternative for high-temperature and high-power applications. An improvement in high-temperature applications of GaN-based power devices can be achieved if self-heating effects are decreased [8].

Table 2. Comparison of competing materials in the area of power semiconductor devices [1]

Material	Mobility (cm^2/V.s)	Relative permittivity	Bandgap (eV)	Maximum operating temperature (°C)
Si	1300	11.4	1.1	300
GaAs	5000	13.1	1.4	300
SiC	260	9.7	2.9	600
GaN	1500	9.5	3.4	700

1.3. HEMT structure

HEMT incorporates a heterojunction between two materials with different bandgaps. The current passes through the channel formed by a sheet of charges at this heterojunction, which is known as two-dimensional electron gas (2DEG). To understand how the 2DEG forms, it is important to know the polarisation charges between materials with different bandgaps, such as AlGaN and GaN. There are two kinds of polarisation charges, including the spontaneous and piezoelectric polarisations. Spontaneous polarisation is the inherent polarisation and it exists because of the characteristic of the material [13]. Also, piezoelectric polarisation occurs when the crystal lattice is changed through applying the strain [14]. In the HEMT structure, both of these polarisations exist and the total polarisation is the sum of these two polarisation charges.

When the polarisation of induced sheet charge density is positive, free electrons tend to compensate the positive polarisation induced charge at the interface of AlGaN/GaN. If the energy level in the quantum well at the AlGaN/GaN interface drops below the Fermi level, these electrons accumulate at the interface of AlGaN and GaN. This is because of the high band offset at the AlGaN/GaN interface and the low interface roughness. These electrons originate from the doping of AlGaN, or they can be induced by the piezoelectric field of strained GaN-based materials. This quantum well is called the two-dimensional electron gas (2DEG) [14].

The 2DEG region has very high electron mobility because of its low ionised impurities scattering. The typical charge density of the 2DEG region is around 1.5×10^{13} cm^{-2} with a mobility of approximately 2000 cm^2/V.s. The high value of the charge density causes low ON-resistance and high current density [11, 15]. In the HEMT structure, which is shown in Figure

3, 2DEG flows from the source to the drain and the gate controls the charges in the channel through the DC voltage and RF signal [15].

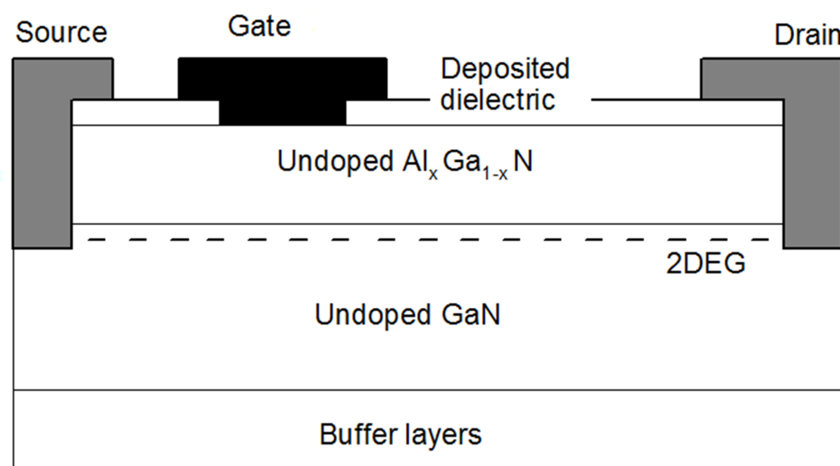

Figure 3. Cross-sectional view of the AlGaN/GaN HEMT structure

1.4. Current status and practical challenges

Electron mobility is the key parameter for the power HEMT performance. Introducing precise methods for measuring this parameter is crucial for analysing HEMT characteristics and developing its performance. Opposite to the gate in the MOSFET, which extends from source to drain [16, 17], the gate of the HEMT divides this device into two main sections: the section underneath the gate and the section outside the gate. The section under the gate is the field-effect section, in which MOSFET-type equations can be employed to model the current–voltage characteristics of this section. However, the section outside the gate is the resistive section and includes the gate-to-drain and gate-to-source resistances. The resistance of the field-effect section is variable by the gate voltage, while the resistive sections have constant resistances; this section can be modelled by fixed resistors. In order to measure the mobility of electrons in the 2DEG section, it is important to separate the 2DEG to these two sections and analyse them separately.

In several studies on electron mobility measurements of the HEMTs, the 2DEG between the source and the drain was treated as a single section [18-20]. Therefore, the measured mobility represents the average mobility between the source and the drain. Also, the common mobility measurement method, Hall measurement, cannot divide the electron

mobility of the 2DEG section outside and under the gate. This method can only be employed to measure the electron mobility of the resistive section.

To solve this issue, Fukui presented a method to divide the source-to-drain region of the GaAs MESFETs into field-effect and resistive sections and measure their resistances separately [21]. Applying that method to the AlGaN/GaN HEMT [22] showed that the measured resistance for the section under the gate was sensitive to the threshold voltage. In order to solve this issue, Menozzi et al. modified Fukui's method [22]. However, Menozzi's method could not differentiate between the voltage between the gate and 2DEG at the source end of the gate and the applied gate-to-source voltage. This means that the voltage over the source-to-gate section of 2DEG was not removed from the gate voltage that controls the 2DEG section under the gate. Therefore, it is important to present a method to measure the 2DEG mobility of the power HEMTs under the gate without the mentioned errors.

In addition to the conditions previously mentioned for a precise electron mobility measurement of the HEMT, it is important to be able to apply the measurement method to the HEMT sample without any requirement to use any extra samples. Different samples may have different characteristics and the characteristics of one sample cannot be used to measure the mobility of the other sample. The other important factor for mobility measurement is the effect of the gate voltage on mobility value. In some studies, it was shown that the HEMT mobility is dependent on the applied gate voltage [20, 23]. Also, it is expected that electron mobility would be influenced by the electric field from the applied gate voltage. However, there are no approved measurements results about the impact of the gate voltage on the behaviour of the HEMT. Therefore, investigating the effect of the gate voltage on mobility is crucial for developing the HEMT.

High breakdown voltage, low ON-resistance, and high power density of the HEMT enable this device to be used at high temperatures. This high temperature may occur because of self-heating or using the HEMT for high-temperature applications [24, 25]. However, mobility dependence on gate voltage at high temperatures was not previously studied. It was well established that the mobility in HEMT at a certified gate voltage reduces when the temperature increases [22, 26-34]. In order to understand the operation of GaN-based HEMT at high temperatures, it is necessary to investigate the physics behind the high-temperature behaviour of the electron mobility in the 2DEG section.

At high temperatures, phonon scattering is the main scattering mechanism limiting electron mobility [35-37]. The relationship between the electron mobility (μ_n) confined by phonon scattering and temperature is explained by [16, 38]:

$$\mu_n = AT^{-\gamma} \tag{1}$$

Here, T shows the temperature, A represents the proportionality constant, and γ is the power coefficient. The value of γ for phonon scattering is 1.5 [16, 38]. Because no other scattering mechanism is identified that can alter the value of mobility at high temperatures [29, 30], the mobility of 2DEG in the case of AlGaN/GaN is expected to have a similar power coefficient. However, it was found that the electron mobility in AlGaN/GaN 2DEG decreases by temperature and follows the power coefficient of between 2.18 and 3.42 [32]. As this issue was not explained in any studies before, investigation of the physical mechanism behind the high value of power coefficient is essential, because it enables the proper modelling of the mobility at high temperatures.

In addition to investigating the mobility measurement methods and the parameters affecting the mobility, such as the gate voltage, temperature, and scattering mechanisms, applying the electron mobility in practice should be taken into consideration. Because the industry continues to promote the GaN-based HEMT technology, the need for its progressive device models becomes increasingly obvious [7]. One of the main abilities of the measured mobility is in the modelling of the HEMT that will be used in power electronic circuits. Designing power electronic circuits is commonly performed by the simulation program with integrated circuit emphasis (SPICE). This software has been adopted by the electronics industry as the standard electronic circuit simulator [39]. It should be noted that SPICE does not include a library model that simulates the HEMT. To simulate the HEMT for circuit design purposes, several studies proposed HEMT models [40-44] that could be incorporated into SPICE by defining external sub-circuits. However, this is a complex process for circuit designers if there are no established parameter-extraction methods, and this can also influence the simulation results. In order to address this issue, proper selection of equations and parameters that match the simulation and experimental DC and AC characteristics of GaN HEMTs is required.

1.5. Original research contributions

The original research contributions developed in this thesis can be summarised as follows:

- A novel method for extraction of the electron mobility in the 2DEG region under the gate of power HEMTs is presented. This method enables the potential impact of the gate metal and the gate voltage on electron mobility in the 2DEG under the gate to be measured without the error caused by the resistive regions outside the gate, which are the gate-to-source and gate-to-drain regions.
- In the presented method, it is determined that the 2DEG mobility between the source and the drain is separated into sections under and outside the gate using the MOSFET-like equations for the section under the gate and the 2DEG constant resistances outside the gate.
- The HEMT mobility is measured in a wide range of temperatures—25ºC to 300ºC—through the other newly presented method that can be used at high temperatures. This method does not consider any assumptions about the mobility dependence on the gate voltage. Comparison of the mobility measurement results by the new method with those measured by existing measurement methods shows a proper matching.
- An experimental demonstration, presented in this thesis, shows that the HEMT mobility is independent of the gate voltage in a wide range of temperatures.
- The mobility at high temperatures is a function of phonon scattering. According to the HEMT mobility dependence on the temperature, the power coefficient, which shows the rate of change for the phonon-limited electron mobility with temperature, for the phonon scattering is 1.5. However, this value is between 2.14 and 3.42 for the GaN-based devices such as AlGaN/GaN HEMT. In this thesis, the increase of the power-law coefficient in the GaN-based devices is investigated physically, which leads to the better understanding of the electron mobility behaviour in GaN structures at high temperatures.
- The application of the measured mobility of the HEMT in the development of the performance of this device is investigated. The measured mobility can be used for modelling the HEMT for circuit designs and simulations. In order to apply the HEMT in electronic circuits, the standard SPICE MOSFET model and the parameters for simulation of power circuits with GaN HEMTs is presented. In order to simulate power GaN HEMTs in circuit designs, carefully selected equations and parameters are

essential. One of these parameters is the mobility, which is extracted by the new presented methods. Applying these parameters to the standard MOSFET *LEVEL 3* model in SPICE leads to matching the DC and AC characteristics of GaN HEMTs.

1.6. Thesis outline

In light of the concerns highlighted in the previous section, this thesis is devoted to investigating the electron mobility of GaN-based power HEMTs. To analyse this parameter, measurement methods for the mobility of the HEMT are studied and novel measurement methods are introduced. These methods are used to identify the dominant parameters affecting the HEMT mobility and to analyse the factors that degrade its value. Also, the application of the measured electron mobility of the HEMT in developing the performance of this device in the electronic circuits is investigated. The key research areas and general outline of this thesis are described in greater detail in the following paragraphs.

Given that the electron mobility is the most important parameter of the HEMT that affects its DC and AC characteristics, a review of various measurement methods of the electron mobility of the HEMT, different definitions of electron mobility, possible sources of errors during its measurements, and parameters degrading its value is presented in **Chapter 2**. Because the HEMT is a promising candidate for high-power and high-temperature applications, the effect of temperature on degrading the mobility and the physical reason behind its reduction is studied and analysed. At the end of the chapter, applying the electron mobility of the HEMT to develop the performance of the HEMT in circuit designs is investigated.

Chapter 3 begins with explaining the importance of separating the electron mobility of the power HEMT in the 2DEG regions underneath and outside the gate. A new method for measuring the electron mobility of the HEMT under the gate, which considers the possible impact of the gate voltage on the electron mobility of the HEMT under the gate and without the error caused by the resistive 2DEG regions, is presented. This method is applied to a fabricated AlGaN/GaN HEMT. The results of the mobility measured under the gate by the new method are compared to the mobility value outside the gate. It is shown that the electron mobility measured underneath and outside the gate is similar.

Although the method presented in Chapter 3 measures the mobility under the gate without the error of the resistive regions, the method not only requires the HEMT but also needs an extra sample, which is the Hall sample. To solve this issue, another method is presented in

Chapter 4, where measurement only requires the HEMT. This method does not consider any assumptions about the dependence of mobility on the gate voltage, and it can be used for mobility measurement at high temperatures. Applying this method to the HEMT for a wide range of temperature, 25ºC to 300ºC, demonstrates that the electron mobility of the HEMT is independent of the gate voltage. Furthermore, it is found that reducing the electron mobility by increasing the temperature has a high value of the power-law coefficient, which is analysed physically in the next chapter.

Reducing the electron mobility of the HEMT by increasing the temperature is investigated in **Chapter 5**. The mobility of the HEMT measured at high temperatures, which is presented in several works, is compared. The main scattering mechanism involved in mobility measurement at high temperatures is the phonon scattering. In the case of phonon scattering, the electron mobility reduction caused by increasing the temperature follows the power-law factor of 1.5. However, the electron mobility of the GaN-based HEMT reduces by an unexpected power-law factor larger than 1.5. It is shown that the effective electron mass, which is a function of temperature, is responsible for this phenomenon.

Application of the measured and analysed mobility in the development of the HEMT for circuit designs purposes is investigated in **Chapter 6**. The measured mobility can be employed for SPICE modelling of the HEMT. It should be noted that there is no available model in SPICE for simulation of circuits including the HEMT. This chapter begins with a critical review of the SPICE modelling of the HEMT and explains why a new model is required. Then, a new model for SPICE simulation of the HEMT is presented, one which is straightforward for circuit designers and that does not require any sub-circuits. The new model is applied to a fabricated HEMT and it is shown that the simulated DC and AC results of the HEMT perfectly match the experimental data.

Finally, the key conclusions and developments made throughout the study, along with recommendations for future work, are summarised in **Chapter 7**.

1.7. Related publications

List of papers constituting this thesis (in the order of the chapters):

- **Amirhossein Aminbeidokhti**, Sima Dimitrijev, Jisheng Han, Xiangang Xu, Chengxin Wang, Shuang Qu, Hamid Amini Moghadam, Philip Tanner, David Massoubre, Glenn Walker, “A method for extraction of electron mobility in power HEMTs,” *Superlattices and Microstructures*, vol. 85, pp. 543–550, 2015.

- **Amirhossein Aminbeidokhti**, Sima Dimitrijev, Anil Kumar Hanumanthappa, Hamid Amini Moghadam, Daniel Haasmann, Jisheng Han, Yan Shen, and Xiangang Xu, “Gate voltage independence of electron mobility in power AlGaN/GaN HEMTs,” *IEEE Transactions on Electron Devices*, vol. 63, no. 3, pp. 1013-1019, 2016.

- **Amirhossein Aminbeidokhti**, Sima Dimitrijev, Jisheng Han, Xiufang Chen, and Xiangang Xu, “The power law of phonon-limited electron mobility in the two-dimensional electron gas of AlGaN/GaN heterostructure,” *IEEE Transactions on Electron Devices*, vol. 63, no. 5, pp. 2214-2218, 2016.

- **Amirhossein Aminbeidokhti**, Sima Dimitrijev, Jisheng Han, and Hamid Amini Moghadam, “SPICE MOSFET equations and parameters as power HEMT model,” to be submitted to *Microelectronics Reliability* journal.

List of papers not included in this thesis (outside the scope of this thesis)

- Hamid Amini Moghadam, Sima Dimitrijev, Jisheng Han, **Amirhossein Aminbeidokhti**, and Daniel Haasmann, “Quantified density of active near interface oxide traps in 4H-SiC MOS capacitors,” *Materials Science Forum*, vol. 858, pp. 603-606, 2016.

- Daniel Haasmann, Hamid Amini Moghadam, Jisheng Han, **Amirhossein Aminbeidokhti**, Alan Iacopi, and Sima Dimitrijev, “Dipole type behaviour of NO grown oxides on 4H-SiC,” *Materials Science Forum*, vol. 858, pp. 453-456, 2016.

- Sima Dimitrijev, Jisheng Han, Hamid Amini Moghadam, and **Amirhossein Aminbeidokhti**, “Power-switching applications beyond silicon: Status and future prospects of SiC and GaN devices,” *MRS Bulletin*, vol. 40, pp. 399-405, 2015.

- Hamid Amini Moghadam, Sima Dimitrijev, Jisheng Han, Daniel Haasmann, and **Amirhossein Aminbeidokhti**, “Transient current method for measurement of active near-interface oxide traps in 4H-SiC MOS capacitors and MOSFETs,” *IEEE Transactions on Electron Devices*, vol. 62, no. 8, pp. 2670-2674, 2015.

- Philip Tanner, Sima Dimitrijev, Hamid Amini Moghadam, **Amirhossein Aminbeidokhti**, and Jisheng Han, “Selection of SPICE parameters and equations for effective simulation of circuits with 4H-SiC power MOSFETs,” *Materials Science Forum*, vol. 778-780, Ch. 5, pp. 997-1000, 2014.

1.8. References

[1] U. K. Mishra, P. Parikh, and Y.-F. Wu, "AlGaN/GaN HEMTs-an overview of device operation and applications," *IEEE Proceedings,* vol. 90, pp. 1022-1031, 2002.

[2] T. Mimura, S. Hiyamizu, T. Fujii, and K. Nanbu, "A new field-effect transistor with selectively doped GaAs/n-$Al_xGa_{1-x}As$ heterojunctions," *Japanese Journal of Applied Physics,* vol. 19, pp. L225-L227, 1980.

[3] M. S. Shur, "Low ballistic mobility in submicron HEMTs," *IEEE Electron Device Letters,* vol. 23, pp. 511-513, 2002.

[4] T. Mimura, "The early history of the high electron mobility transistor (HEMT)," *IEEE Transactions on Microwave Theory and Techniques,* vol. 50, pp. 780-782, 2002.

[5] M. A. Khan, J. Kuznia, D. Olson, W. Schaff, J. Burm, and M. Shur, "Microwave performance of a 0.25 µm gate AlGaN/GaN heterostructure field effect transistor," *Applied Physics Letters,* vol. 65, pp. 1121-1123, 1994.

[6] S. Keller, Y.-F. Wu, G. Parish, N. Ziang, J. J. Xu, B. P. Keller, *et al.*, "Gallium nitride based high power heterojunction field effect transistors: process development and present status at UCSB," *IEEE Transactions on Electron Devices,* vol. 48, pp. 552-559, 2001.

[7] Q. Chen, "Latest advances in gallium nitride HEMT modeling," in *12th IEEE International Conference on Solid-State and Integrated Circuit Technology (ICSICT)*, 2014, pp. 1-4.

[8] M. S. Shur, "GaN-based electronic devices," *World Scientifie Publishing Co., Singapore,* pp. 61-86, 2004.

[9] Y. Développement, "Market and technology analysis," November 2010.

[10] M. A. Briere, "GaN based power devices: Cost-effective revolutionary performance," *Power Electronics Europe,* vol. 7, pp. 29-31, 2008.

[11] M. Golio, *Microwave and RF product applications*: CRC Press, 2003.

[12] M. Mukherjee, *Advanced microwave and millimeter wave technologies semiconductor devices circuits and systems*: Sciyo. com, 2010.

[13] O. Ambacher, B. Foutz, J. Smart, J. Shealy, N. Weimann, K. Chu*, et al.*, "Two dimensional electron gases induced by spontaneous and piezoelectric polarization in undoped and doped AlGaN/GaN heterostructures," *Journal of Applied Physics,* vol. 87, pp. 334-344, 2000.

[14] D. Visalli, "Optimization of GaN-on-Si HEMTs for high voltage applications," Katholieke Universiteit Leuven, 2011.

[15] K. E. Moore, "RF power transistors from wide bandgap materials," in *RF and microwave semiconductor device handbook*, 2003, pp. 9.1-9.16.

[16] S. Dimitrijev, *Principles of semiconductor devices*: Oxford university press, 2012.

[17] B. G. Streetman and S. Banerjee, *Solid state electronic devices* vol. 5: Prentice Hall New Jersey, 2000.

[18] S. Baskaran, A. Mohanbabu, N. Anbuselvan, N. Mohankumar, D. Godwinraj, and C. Sarkar, "Modeling of 2DEG sheet carrier density and DC characteristics in spacer based AlGaN/AlN/GaN HEMT devices," *Superlattices and Microstructures,* vol. 64, pp. 470-482, 2013.

[19] P. Gangwani, R. Kaur, S. Pandey, S. Haldar, M. Gupta, and R. Gupta, "Modeling and analysis of fully strained and partially relaxed lattice mismatched AlGaN/GaN HEMT for high temperature applications," *Superlattices and Microstructures,* vol. 44, pp. 781-793, 2008.

[20] G. R. Valdivia, T. F. Ibáñez, J. Rodriguez-Tellez, A. T. Puente, and A. M. Sánchez, "Measurement of mobility in HEMT devices using high-order derivatives," *IEEE Transactions on Electron Devices,* vol. 51, pp. 1-7, 2004.

[21] H. Fukui, "Determination of the basic device parameters of a GaAs MESFET," *Bell System Technical Journal,* vol. 58, pp. 771-797, 1979.

[22] R. Menozzi, G. A. Umana-Membreno, B. D. Nener, G. Parish, G. Sozzi, L. Faraone*, et al.*, "Temperature-dependent characterization of AlGaN/GaN HEMTs: thermal and source/drain resistances," *IEEE Transactions on Device and Materials Reliability,* vol. 8, pp. 255-264, 2008.

[23] J.-P. Ao, T. Wang, D. Kikuta, Y.-H. Liu, S. Sakai, and Y. Ohno, "AlGaN/GaN high electron mobility transistor with thin buffer layers," *Japanese Journal of Applied Physics,* vol. 42, pp. 1588-1589, 2003.

[24] D. Donoval, M. Florovič, D. Gregušová, J. Kováč, and P. Kordoš, "High-temperature performance of AlGaN/GaN HFETs and MOSHFETs," *Microelectronics Reliability,* vol. 48, pp. 1669-1672, 2008.

[25] W. Tan, M. Uren, P. Fry, P. Houston, R. Balmer, and T. Martin, "High temperature performance of AlGaN/GaN HEMTs on Si substrates," *Solid-State Electronics,* vol. 50, pp. 511-513, 2006.

[26] D. Zanato, S. Gokden, N. Balkan, B. Ridley, and W. Schaff, "The effect of interface-roughness and dislocation scattering on low temperature mobility of 2D electron gas in GaN/AlGaN," *Semiconductor Science and Technology,* vol. 19, pp. 427-432, 2004.

[27] A. Kalavagunta, S. Mukherjee, R. Reed, and R. Schrimpf, "Comparison between trap and self-heating induced mobility degradation in AlGaN/GaN HEMTs," *Microelectronics Reliability,* vol. 54, pp. 570-574, 2014.

[28] K. Takhar, U. Gomes, K. Ranjan, S. Rathi, and D. Biswas, "Temperature dependent DC characterization of InAlN/(AlN)/GaN HEMT for improved reliability," in *IOP Conference Series: Materials Science and Engineering*, 2015, vol. 73, p. 012001-1-012001-4.

[29] D. Pandey, A. Bhattacharjee, and T. Lenka, "Study on temperature dependence scattering mechanisms and mobility effects in GaN and GaAs HEMTs," in *Physics of Semiconductor Devices*, ed: Springer, 2014, pp. 67-70.

[30] N. Maeda, K. Tsubaki, T. Saitoh, and N. Kobayashi, "High-temperature electron transport properties in AlGaN/GaN heterostructures," *Applied Physics Letters,* vol. 79, pp. 1634-1636, 2001.

[31] I. H. Lee, Y. H. Kim, Y. J. Chang, J. H. Shin, T. Jang, and S. Y. Jang, "Temperature-dependent hall measurement of AlGaN/GaN heterostructures on Si substrates," *Journal of the Korean Physical Society,* vol. 66, pp. 61-64, 2015.

[32] S. Arulkumaran, T. Egawa, H. Ishikawa, and T. Jimbo, "High-temperature effects of AlGaN/GaN high-electron-mobility transistors on sapphire and semi-insulating SiC substrates," *Applied Physics Letters,* vol. 80, pp. 2186-2188, 2002.

[33] M. Wang, B. Shen, F. Xu, Y. Wang, J. Xu, S. Huang, *et al.*, "High temperature dependence of the density of two-dimensional electron gas in $Al_{0.18}Ga_{0.82}N$/GaN heterostructures," *Applied Physics A,* vol. 88, pp. 715-718, 2007.

[34] A. Saxler, P. Debray, R. Perrin, S. Elhamri, W. Mitchel, C. Elsass, *et al.*, "Characterization of an AlGaN/GaN two-dimensional electron gas structure," *Journal of Applied Physics,* vol. 87, pp. 369-374, 2000.

[35] O. Katz, A. Horn, G. Bahir, and J. Salzman, "Electron mobility in an AlGaN/GaN two-dimensional electron gas. I. Carrier concentration dependent mobility," *IEEE Transactions on Electron Devices,* vol. 50, pp. 2002-2008, 2003.

[36] A. Anwar, S. Wu, and R. T. Webster, "Temperature dependent transport properties in GaN, $Al_xGa_{1-x}N$, and $In_xGa_{1-x}N$ semiconductors," *IEEE Transactions on Electron Devices,* vol. 48, pp. 567-572, 2001.

[37] M. Gurusinghe, S. Davidsson, and T. Andersson, "Two-dimensional electron mobility limitation mechanisms in $Al_xGa_{1-x}N$/ GaN heterostructures," *Physical Review B,* vol. 72, pp. 045316-1-045316-11, 2005.

[38] H. Morkoç, *Nitride Semiconductor Devices: Fundamentals and Applications*: John Wiley & Sons, 2013.

[39] D. P. Foty, *MOSFET modeling with SPICE: principles and practice*: Prentice-Hall, Inc., 1997.

[40] J. C. Sarker, "Yield sensitivity of HEMT circuits to process parameter variations," *IEEE Transactions on Microwave Theory and Techniques,* vol. 40, pp. 1572-1576, 1992.

[41] S. Khandelwal, C. Yadav, S. Agnihotri, Y. S. Chauhan, A. Curutchet, T. Zimmer, *et al.*, "Robust surface-potential-based compact model for GaN HEMT IC design," *IEEE Transactions on Electron Devices,* vol. 60, pp. 3216-3222, 2013.

[42] L. Yuan, W. Wang, K. B. Lee, H. Sun, S. L. Selvaraj, X. Zhou, *et al.*, "The temperature dependent TCAD and SPICE modeling of AlGaN/GaN HEMTs," in *IEEE 5th International Nanoelectronics Conference (INEC),* 2013, pp. 115-118.

[43] N. DasGupta and A. DasGupta, "A new SPICE MOSFET Level 3-like model of HEMT's for circuit simulation," *IEEE Transactions on Electron Devices,* vol. 45, pp. 1494-1500, 1998.

[44] H. Khakzar, "The extraction of HEMT transistor DC parameters using the transistor electrical characterization and analysis program (TECAP)," in *Proceedings Eighth University/Government/Industry Microelectronics Symposium,* 1989, pp. 211-214.

CHAPTER 2: LITERATURE REVIEW- ELECTRON MOBILITY OF GAN POWER HEMTS

2.1 Introduction 20

2.2 Electron mobility measurement methods for HEMT 21

2.2.1 Hall mobility 22

2.2.1.1 Definition 22

2.2.1.2. Measurement method 23

2.2.1.2.1. Sample configuration 23

2.2.1.2.2. Measurement set-up 24

2.2.1.2.3 Two-dimensional electron gas carrier density measurement 25

2.2.1.2.4. Sheet resistance measurement 26

2.2.2. Effective mobility 28

2.2.3. Field-effect mobility 32

2.3 Works performed on electron mobility measurements of the HEMT 34

2.4 Possible sources of error of electron mobility measurements 42

2.5 Temperature dependence of electron mobility of the HEMT 42

2.6 Scattering mechanisms effects on mobility of the HEMT 50

2.7 Application of the measured electron mobility of the HEMT 53

2.7.1. SPICE simulation of circuits with HEMT 53

2.7.1.1. Importance of SPICE modelling of the HEMT 53

2.7.1.2. Models presented for SPICE simulation of the HEMT 54

2.8 References 61

2.1. Introduction

A high electron mobility transistor (HEMT) is a well-established semiconductor device that uses the formation of two-dimensional electron gas (2DEG) at the intersection of two semiconductor layers. When the HEMT is implemented with AlGaN/GaN heterostructure, it is a promising candidate for high power switching applications [1].

As the name of this transistor infers, the most significant characteristic of this device is its high electron mobility. Electron mobility represents how fast an electron moves through a semiconductor or a metal when an electric field is applied. Investigating the mobility of the HEMT plays an important role in developing its performance and characteristics. In the case of the HEMT, electrons flow throughout the 2DEG region; therefore, this mobility is called 2DEG mobility.

2DEG mobility impacts the HEMT performance through the time and frequency responses of this device in two ways. Initially, the devices with higher mobility have higher currents, which charge capacitances faster and cause a higher frequency response. Second, at low electric fields, carrier velocity is proportional to the mobility. Therefore, higher mobility materials lead to higher frequency responses because carriers need less time to move throughout the device [2]. In order to study the mobility of the HEMT, first of all, it is important to explain the methods available for the mobility measurement. Then, the parameters that affect its mobility need to be analysed.

Different methods are used for measuring 2DEG mobility, including the Hall-effect, field-effect, and effective mobility measurement methods, which are commonly used for the MOSFET [2]. Each of these methods requires a different configuration for measurement, and include different equations. In contrast to the MOSFET, where the gate extends from the drain-to-source, the gate of the HEMT separates the channel to three different regions: source-to-gate, under the gate, and gate-to-drain. The area under the gate is the field-effect section, which can be modelled by the MOSFET, and the area outside the gate is the resistive section. The resistance of the 2DEG under and outside the gate is different. Therefore, the mobility of these regions need to be measured separately. So, it is important to modify these available measurement methods, so they can be applied to the HEMT [3].

Mobility depends on several factors including the material impurity concentrations (acceptor and donor concentrations), defects of the material, carrier (electron and hole) density, and temperature. Temperature plays an important role in the mobility of the HEMT because in

high power semiconductor devices, as the power density increases, the device starts to become heated. Therefore, the device temperature increases, which affects the other characteristics of the device. Analysing the effect of the temperature on the HEMT mobility and rate of the mobility change by temperature requires considering various scattering mechanisms that affect the device at high temperature [2].

After describing the electron mobility measurement methods for the HEMT and analysing the parameters that affect mobility, it is important to investigate applications of the measured HEMT mobility. One of the main performances of the measured HEMT mobility is in the modeling of this device. Because HEMT technology is quickly growing, this device is popular in electronic systems and circuits. Using the HEMT in electronic circuits requires building compact models of this device. The Simulation Program with Integrated Circuit Emphasis (SPICE) is the most common software among circuit designers. Therefore, introducing the HEMT models, which can be applied to the SPICE, and investigating how to apply them to the SPICE, are crucial for simulating circuits that include the HEMT [4].

In this chapter, different methods for mobility measurement of the HEMT are explained in detail and effects of various parameters on its mobility are investigated. Among these parameters, temperature effect is considered as the major effect on HEMT mobility. Analysing the temperature effects on mobility requires investigating different scattering mechanisms. Therefore, in this chapter, effects of temperature and various scattering mechanisms on the HEMT mobility are analysed in detail. Finally, the application of the measured mobility in SPICE modeling of the HEMT is studied.

2.2. Electron mobility measurement methods for HEMT

Three main methods to measure the HEMT mobility include Hall-effect, field-effect, and effective mobility. Mobility measurement by Hall-effect method requires a special test pattern (Hall sample); however, field-effect and effective mobility methods use the HEMT transfer and output characteristics, respectively, for mobility measurement. In the next section, these methods are explained in detail.

2.2.1. Hall mobility

Hall-effect is the most common method for 2DEG mobility measurement. The mobility measured by this method is called Hall mobility. This method is used to measure the 2DEG density and mobility using Van der Pauw technique.

2.2.1.1. Definition

In 1879, Hall investigated the nature of the force acting on a semiconductor carrying a current in a magnetic field [5]. He found that the electric current is deflected by the magnet: in this case a source of stress appears in the conductor toward one side of the sample [2]. He also found that the magnetic field applied to a conductor, which is placed perpendicular to the current direction, causes an electric field perpendicular to the current flow direction and magnetic field [2]. This investigation led to discovering the Hall-effect. Hall-effect refers to the potential difference between opposite sides of a thin sheet of semi-conducting or conducting materials (Hall voltage) through which an electric current is flowing. This phenomenon happens due to the magnetic field applied perpendicular to the Hall sample [2].

The union of the current flowing through the length of the Hall sample and a magnetic field through the sample causes a current. This current is perpendicular to both the current flowing throughout the semiconductor and the magnetic field. It causes a transverse voltage (Hall voltage), which is also perpendicular to both the current and magnetic field. Hall-effect is detected due to the existence of this current. The essential principle of the Hall-effect is the force on a point charge due to electromagnetic fields, which is called Lorentz force. Direction of this force is determined by the right hand rule, based on direction of both carrier movement and applied magnetic field [6]. The Hall-effect can be explained by considering the influence of forces applied to electrons in a magnetic field. When an electron is located in a magnetic field, it experiences the Lorentz force proportional to the field strength. This force is the strongest when the field is perpendicular to the direction of electron movement. When the current is flowing, a steady number of electrons flow through the semiconductor. Applying an external magnetic field leads to an accumulation of electrons at one corner of the Hall sample, which creates a current and a potential difference across the semiconductor, which is the Hall voltage.

The importance of this method for analysing semiconductor material and devices is due to its wide range of applications in various phases of semiconductor materials and devices

technology, from the basic characterization of materials and development of devices to the manufacturing of devices [2], [6]. It can be employed to characterize both high resistance semiconductor materials, such as semi-insulating gallium nitride (GaN), and materials with low resistance including metals, highly doped semiconductor materials, and transparent oxides [6]. The most important parameter determined by Hall-effect measurement is the Hall voltage (V_H), which leads to driving several other important parameters as follows [6]:

- Carrier mobility
- Carrier concentration (n) for a sample with a given thickness
- Doping type (P-type or N-type) of material
- Sheet resistance, from which the resistivity of a sample with a given thickness is determined
- Sheet carrier density of the majority carriers (the number of majority carriers per unit area)

In the next section, performing the Hall measurement in order to drive these parameters is explained.

2.2.1.2. Measurement method

2.2.1.2.1. Sample configuration

In order to perform the Hall measurement, a sample with four Ohmic contacts with the following conditions is required [2]:

- Contacts should be on or as close as possible to sample corners.
- Dimensions of the contacts should be as small as possible.
- All four contacts are required to be from the same material.
- Average diameter of contacts (D) and the distance between contacts (L) result in error in the measurement, which is proportional to D/L.
- Contacts can be connected to wires to ease the measurement. In this case, in order to minimize thermoelectric effects, the materials used for contacts need to be of the same group of materials used for wires.
- Hall samples are usually fabricated in lamella type with arbitrary shape; however, the symmetrical structure is preferred. Lamella-type samples require small contacts, which are placed as close as possible to the periphery. As mentioned above, the location and

size of the contacts are also important. Although Van der Pauw samples need contacts located symmetrically on the periphery, this is not achievable in reality and it involves some error. In order to eliminate the error, Van der Pauw took into account the circular samples with 90◦ intervals between contacts [7].

2.2.1.2.1. Measurement set-up

In order to perform the Hall measurement, a basic Hall-effect measurement configuration including the following components is required:

- Current source: In order to measure the sheet resistance, carrier density in 2DEG (N_{2DEG}) and mobility, a current source is needed to supply the current to one of the contacts of the Hall sample. For samples fabricated based on the materials with low resistivity, the current source should be able to produce an output from milliamps to amps. For samples based on semi-insulators, the source should be able to provide current as low as 1 nA. In case of Hall samples materials with high resistivity (such as intrinsic semiconductors), a source capable of producing 10 µA to 100 mA current is sufficient.
- Voltmeter with high input impedance: The voltmeter should be able to perform accurate measurements from 1 mV to 100 V. For Hall samples with high resistivity materials, the effect of the high input impedance of the voltmeter plays an important role in achieving accurate measurement results.
- Permanent magnetic field: For Hall measurement, a magnetic field with the typical value of 0.5 to 1 T should be applied to the sample.
- Sample holder: The sample holder can be the Hall measurement tool, which keeps the Hall sample while applying a constant magnetic field.

The Hall mobility (μ_H) is calculated by the following equation. As can be seen, measurement of Hall mobility requires measuring the sheet resistance and N_{2DEG}, which are explained in the following sections.

$$\mu_H = \frac{1}{qR_S N_{2DEG}} \tag{1}$$

2.2.1.2.2. Two-dimensional electron gas carrier density measurement

The measurement configuration for N_{2DEG} is illustrated in Figure 1. The first step to determine the value of N_{2DEG} is to measure the Hall voltage by forcing both current and magnetic field to the sample. The combination of the magnetic field and the current results in a transverse current [6]. The current is forced between two diagonal contacts and V_H is measured between two other contacts [6]. For instance, according to Figure 1, the current is forced to contact 1 and flows to contact 3 (I_{13}); the voltage is measured between contact 4 and contact 2 (V_{42}). From this *I*-*V* measurement, the Hall voltage versus the Hall current is drawn.

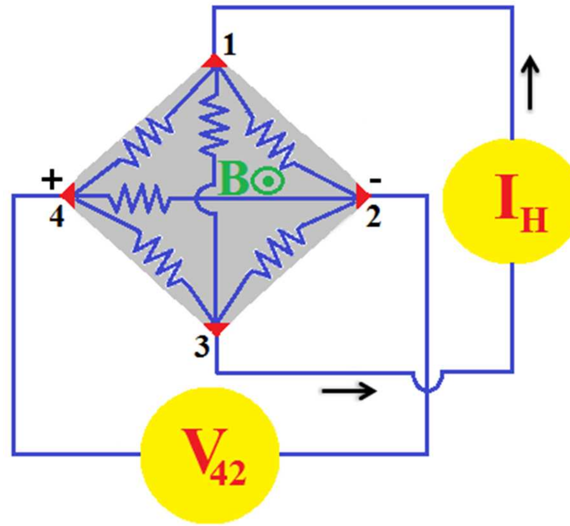

Figure 1. Schematic of N_{2DEG} measurement circuit

It should be noted that the contact resistance does not impact the measured Hall voltage because the voltmeter has very high resistance, so it does not draw any current from the circuit under test and there is no voltage across contact resistances. In order to achieve results with high reliability, the recommended method requires a combination of reversing current source polarity (positive and negative directions of magnetic fields), sourcing on the other three terminals, and reversing the magnetic field direction. Therefore, eight Hall measurements are performed [6]. Equation 2 explains the Hall voltage measured between contacts 2 and 4 at positive and negative magnetic field polarities:

$$V_{H42} = \frac{V_{42P} - V_{42N}}{2} \tag{2}$$

In this equation, V_{42P} is the voltage difference between contacts 2 and 4 (V_4–V_2) with positive magnetic field perpendicular and out of the page, and V_{42N} is the voltage difference between contacts 2 and 4 (V_4–V_2) with negative magnetic field perpendicular and into the page. After performing similar measurement on other contacts, the average Hall voltage can be calculated by:

$$V_H = \frac{V_{H13} + V_{H24} + V_{H31} + V_{H42}}{4} \quad (3)$$

Because the Hall voltage is usually small (mV or less), accurate measurement followed by this averaging technique are critical for obtaining precise mobility results [6]. Considering the achieved Hall voltage, we will have:

$$N_{2DEG} = \frac{BI_H}{qV_H} \quad (4)$$

Here, B is the magnetic field, and in the figure its direction is perpendicular and facing the outside of the sample, I_H shows the Hall current between two diagonal contacts, and q is the charge of an electron $1.6\times10^{-19}\ C$. In order to have an accurate result, the proportion of Hall current over the Hall voltage is extracted from the slope of the measured Hall voltage graph. It is important to mention that the polarity of the Hall voltage shows the type of material; positive polarity indicates the P-type material, while the negative polarity shows the N-type.

2.2.1.2.3. Sheet resistance measurement

After measuring N_{2DEG}, it is essential to measure the sheet resistance (R_S) to calculate the mobility. The sheet resistance is determined using Van der Pauw measurement technique. This technique, which is explained in this section, is used to measure the resistance between contacts with and without a magnetic field. For measuring the sheet resistance through this technique, current is applied between two adjacent contacts and the voltage is measured between the other nodes [6]. As an example, according to Figure 2, which illustrates the measurement configuration of Van der Pauw sheet resistance measurement, current flows through contact 1 to 2 (I_{12}) and the voltage is measured between contact 4 and 3 (V_{43}). Performing this measurement results in the resistance between these contacts ($R_{12,43}$) [2]. The measured resistance can be seen in Equation 5. In this measurement, no magnetic field is applied to the sample.

$$R_{12,43} = \frac{V_{43}}{I_{12}} = \frac{V_4 - V_3}{I_{12}} \tag{5}$$

It is important to mention that similar to the N_{2DEG} measurement, contact resistance does not impact the measured Hall voltage because the voltmeter has very high resistance, so it draws no current from the circuit under test and there is no voltage across contact resistances.

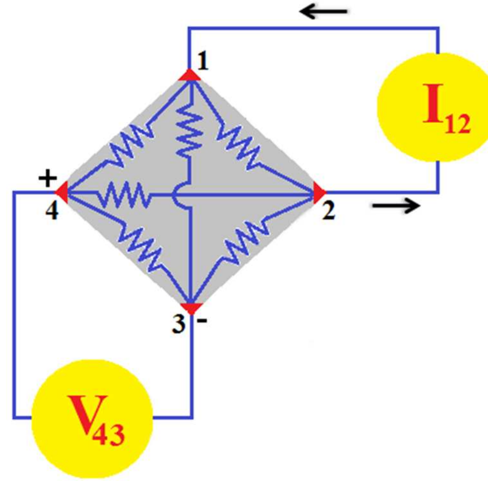

Figure 2. Schematic of resistance and mobility measurement circuit

In order to achieve an accurate result, it is important to perform the same measurement on the other contacts of the Hall sample, which leads to achieving average resistance ($R_{Average}$):

$$R_{Average} = \frac{R_{12,43} + R_{23,14} + R_{34,21} + R_{41,32}}{4} \tag{6}$$

The sheet resistance is calculated by:

$$R_S = 4.5 \times R_{Average} \tag{7}$$

Employing the N_{2DEG} and R_S in Equation 1 results in the Hall mobility.

2.2.2. Effective mobility

Measurement of the HEMT mobility through the Hall method requires fabrication of a special sample with a specific configuration. This sample originates from the same substrate and wafer as the HEMT to extend its measurement result to the HEMT 2DEG mobility. Although the Hall measurement method for mobility is straightforward, the value of the

mobility measured by this method can be different from the real mobility of the HEMT sample. This issue is due to sample-to-sample variation of the results and also because of the different fabrication process for the HEMT and the Hall sample. Therefore, it is important to investigate methods by which the mobility can be measured directly by the HEMT structure and characteristics. In order to achieve this goal, two other definitions for mobility measurement have been presented that use the HEMT transfer and output characteristics for the mobility measurement [3].

These two kinds of definitions for the mobility originate from two popular methods for the MOSFET mobility measurement: field-effect (μ_{FE}) and effective (μ_{eff}) mobility [2]. For the effective mobility, output conductance (g_O) is used for mobility measurements; however, the field-effect method employs the transconductance (g_m). In the HEMT structure, the gate divides the device into three separate sections: gate-to-source region, gate-to-drain region and the region underneath the gate. The region under the gate is the field-effect region that can be modelled by the MOSFET, while the regions outside the gate are resistive regions. Therefore, MOSFET equations and parameters for mobility, including the effective and field-effect definitions, can be developed for mobility measurement of the HEMT. In both methods, it is important to perform the measurements at low drain voltages (V_{DS} < 100 mV) because of the uniformity of the channel charge between the drain and source for these voltages. Both of these methods, which have been originally defined for MOSFET mobility measurement, are capable of being applied in the case of HEMTs [3]. These methods are explained in the following sections.

The effective mobility definition refers to the mobility of MOSFET [2]. Measurement of this mobility is based on the drain current (I_D) of the device. The drain current in an N-channel MOSFET with gate length and width of L and W, respectively, considering its drift and diffusion currents, is given by [2]:

$$I_D = \frac{W\mu_{eff} Q_n V_{DS}}{L} - W\mu_{eff} \frac{KT}{q} \frac{\partial Q_n}{\partial x} \tag{8}$$

Here, Q_n is the density of mobile channel charge (C/cm^2) and V_{DS} is the drain-source voltage. When the value of this voltage is low (<100mV), the channel charge from source-to-drain is uniform and the diffusive second term in the above equation can be neglected. Then, we will have [2]:

$$\mu_{eff} = \frac{g_O L}{W Q_n} \tag{9}$$

In this equation, the output conductance (g_O) is [2]:

$$g_O = \frac{\partial I_D}{\partial V_{DS}} \tag{10}$$

This parameter can be extracted from the output characteristic of the HEMT. The other important parameter in Equation 9 is Q_n, which can be determined through two different approaches. The first approach uses the capacitance of the oxide (C_{OX}), which is the capacitance of AlGaN in case of HEMT. The channel charge density by this method is approximated by [2]:

$$Q_n = C_{OX} (V_{GS} - V_T) \tag{11}$$

Here, V_{GS} is the gate-to-source voltage and V_T is the threshold voltage. Because of the sensitivity of this method to the threshold voltage, determination of the channel charge density by this method is not accurate, which results in an imprecise value for the effective mobility. The second approach determines the Q_n directly from the capacitance measurement by [2]:

$$Q_n = \int_{-\infty}^{V_{GS}} C_{GS} \partial V_{GS} \tag{12}$$

where C_{GS} represents the gate-to-channel capacitance per unit area. Although this method is more accurate than the first-mentioned method for calculation of the charge density, the effective mobility measured even by this method is still influenced by several other sources of error. One error may occur because of the capacitance measurement. C_{GC} (gate-to-channel capacitance) is the summation of C_{GS} and C_{GD}. Neglecting the overlap capacitance in the analysis leads to another error in Q_n measurement, which then results in an error in mobility measurement. C_{GS} measurement should be performed at high frequencies (100 kHz to 1 MHz) because in these frequencies interface traps are not able to follow the AC signal. When the frequency is low, interface traps cause a capacitive component [2]. Also, as mentioned before, effective mobility is calculated from the drain current when $V_{DS} < 100$ mV; however, the g_O determination will be noisy if V_{DS} is too low, and that affects the mobility result. For $V_{DS} > 0$ there will be an error near $V_{GS} = V_T$ due to the reduction in the value of Q_n. A further error occurs if the drain current is assumed to be only the drift current. Although this can be a good approximation for the device performance over the threshold voltage, when V_{GS} is close to V_T

the diffusion current will be significant. It should be remembered that when $V_{GS} < V_T$, the device will operate in the sub-threshold region and the drain current occur principally due to diffusion.

The drain current in the linear region can also be explained without any requirement for charge calculation. It is approximated by:

$$I_D = \mu_n C_{OX} \frac{W}{L}((V_{GS} - V_T)V_{DS} - \frac{V_{DS}^2}{2}) \tag{13}$$

where C_{OX} is the gate insulator capacitance per unit area and W and L represent the width and length of the channel, respectively. When the V_{DS} is small, the second term can be neglected:

$$I_D = \mu_n C_{OX} \frac{W}{L}(V_{GS} - V_T)V_{DS} \tag{14}$$

Using Equation 10 for output conductance calculation leads to:

$$\mu_{eff} = \frac{g_O L}{C_{OX} W (V_{GS} - V_T)} \tag{15}$$

The effective mobility can be also affected by various scattering mechanisms such as the ionized impurity scattering, surface scattering, and lattice scattering, which will be explained in detail in this chapter. Surface and ionized impurity scatterings depend on substrate doping concentration and the gate voltage. The influence of the gate voltage on the effective mobility can be expressed as the impact of the vertical surface electric field (E_{eff}) on the μ_{eff}, according to [2]:

$$\mu_{eff} = \frac{\mu_0}{1 + (\alpha E_{eff})^{\gamma}} \tag{16}$$

Here, α and γ have constant values. The effective mobility reduces if these scattering mechanisms affect the device operation. The reason for decreasing the effective mobility by increasing the gate voltage or electric field is related to the surface roughness scattering increase with increasing the gate voltage, and to its quantisation effects. The effective mobility relation with the gate voltage is explained by [2]:

$$\mu_{eff} = \frac{\mu_0}{1 + \theta (V_{GS} - V_T)} \tag{17}$$

where θ is the mobility degradation factor, which changes by varying the doping density and thickness of AlGaN [8]. Depending on the value of θ, the effective mobility change rate by the gate voltage varies. This parameter is calculated from the slope of the μ_0/μ_{eff} versus $V_{GS} - V_T$, which can be seen in the following figure. In addition, μ_0 represents the low-field electron mobility, which is the intercept of the μ_{eff} versus V_{GS} - V_T, presented in the following figure [2].

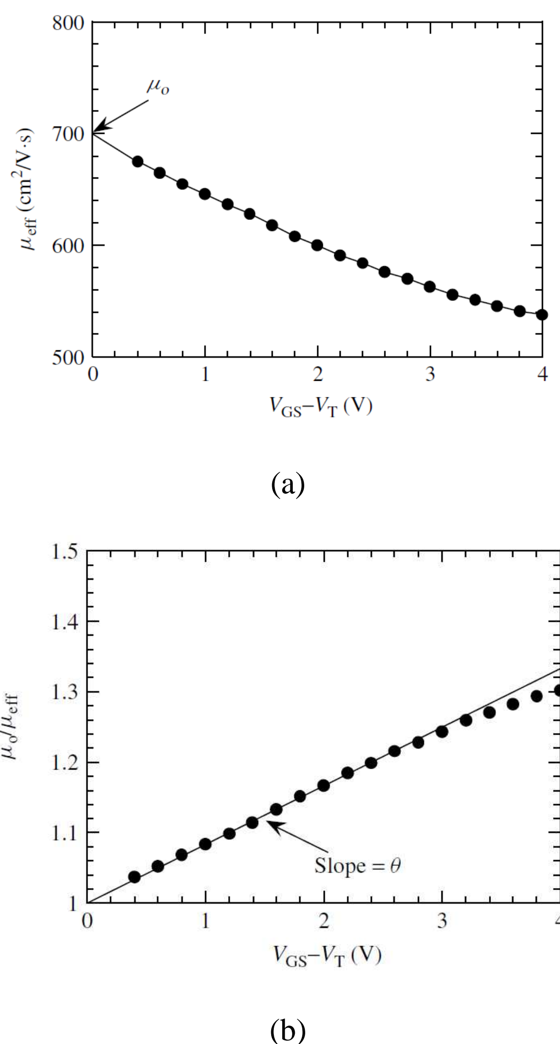

Figure 3. (a) Effective mobility and (b) Normalized effective mobility according to V_{GS}-V_T [2]

2.2.3. Field-effect mobility

Another definition for the mobility measurement is *field-effect mobility*, which is inferred from the field-effect measurement. In contrast to the effective mobility, which uses the conductance for the mobility measurement, this method employs transconductance.

The field-effect mobility measurement method is based on the drain current of the device in the saturation and linear regions [9]. In the saturation region, the drain current is approximated by [9]:

$$I_D = \frac{\mu_n C_{OX}}{2} \frac{W}{L} (V_{GS} - V_T)^2 \tag{18}$$

In this approach, drain-induced barrier lowering (DIBL) has been ignored, which results in an underestimation of the true value of the mobility in practice [9]. By applying the slope of the square root of the saturated current against the gate voltage (m_{sat}), we will have [9]:

$$\mu_{FE} = m_{sat}^2 \frac{2L}{W} \frac{1}{C_{OX}} \tag{19}$$

In order to address the error of the μ_{FE} measurement using I_D in saturation region, the linear region of the I_D (where $V_{DS} < 100$ mV and transistor is in Ohmic mode) is considered for mobility measurement [9]. In the linear region, the drain current is approximated by Equation 14, which leads to having:

$$\mu_{FE} = m_{lin} \frac{L}{W} \frac{1}{V_{DS}} \frac{1}{C_{OX}} \tag{20}$$

where m_{lin} is the slope of the drain current versus the gate voltage in the linear region when V_{DS} is constant. This slope can be determined by the derivative of the drain current versus the gate-source voltage for a constant V_{DS}, as follows:

$$\text{Slope} = g_m = \frac{\partial I_D}{\partial V_{GS}} \quad \text{when } V_{DS} \text{ is constant} \tag{21}$$

Here, g_m shows the transconductance. Considering Equation 14, transconductance will be:

$$g_m = \mu_n C_{OX} \frac{W}{L} V_{DS} \tag{22}$$

Therefore, the field-effect mobility will be:

$$\mu_{FE} = g_m \frac{L}{W} \frac{1}{V_{DS}} \frac{1}{C_{OX}} \tag{23}$$

As field-effect and effective mobility are both measured based on Equation 14 and under identical measurement condition; therefore, the mobility achieved by both methods should have the same value. However, the value of the field-effect mobility measured by the

above equation is usually lower than the effective mobility, which can be seen in Figure 6. This disagreement between μ_{FE} and μ_{eff} happens because of ignoring the dependence of the electric field on mobility during derivation of Equation 22 [10, 11]. By considering the effect of the gate voltage on the μ_{eff}, we will have:

$$g_m = \mu_n C_{OX} \frac{W}{L} V_{DS} (1 + \frac{V_{GS} - V_T}{\mu_{eff}} \frac{\partial \mu_{eff}}{\partial V_{GS}}) \tag{24}$$

that results in:

$$\mu_{FE} = \frac{L g_m}{C_{OX} W V_{DS} (1 + \frac{V_{GS} - V_T}{\mu_{eff}} \frac{\partial \mu_{eff}}{\partial V_{GS}})} \tag{25}$$

Since $\frac{\partial \mu_{eff}}{\partial V_{GS}} < 0$, it is clear that the result of μ_{FE} calculated by Equation 25 is higher than that measured by Equation 23.

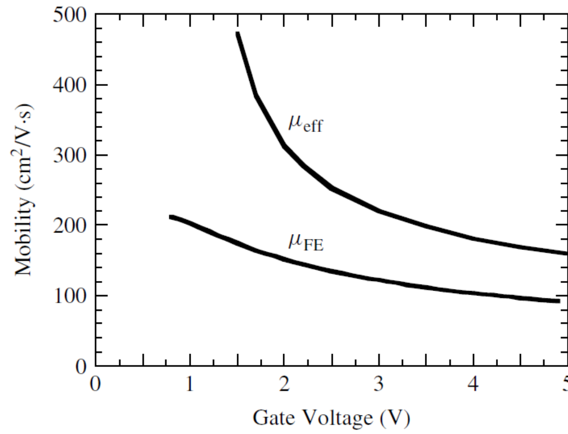

Figure 4. Comparison of the field-effect and effective mobility [2]

In contrast to effective mobility that is sensitive to threshold voltage, field-effect mobility is independent from this parameter. It makes the mobility measured by this method more accurate when the results do not change by threshold voltage.

2.3. Works performed on electron mobility measurements of the HEMT

In recent years, several studies have been performed on investigating the mobility of the HEMT and analysing the parameters that affect its mobility. Some of these works use the basic methods and definitions for measuring the mobility; however, some others modify and develop these basic methods or present new methods to measure the mobility.

As previously mentioned, Hall measurement is one of the main methods for mobility measurement. This measurement is commonly performed at a constant magnetic field with several assumptions. The main assumption is the presence of a single carrier, which has discrete mobility and can only provide the average carrier density and electron mobility for the case of multiple channel transport. In AlGaN/GaN heterostructures, the basic Hall-effect measurement is not able to separate the conductivity of the 2DEG channel from the bulk GaN parasitic conduction [12, 13]. To solve this problem, multi-carrier fitting procedures were employed by Gold and Nelson [14]; however, such an approach includes arbitrary elements, which are not sufficient for modern semiconductor structures. A more beneficial method is employing quantitative mobility spectrum analysis (QMSA) for the Hall-effect measurement and resistivity data in order to separate the conductivity of 2DEG from the rest of the carriers in the sample and measure pure 2DEG mobility [15].

Umana-Membreno et al. measured the 2DEG mobility without any parasitic carrier conduction through the bulk GaN [16]. They studied the 2DEG flow in the AlGaN/AlN/GaN heterostructure by employing Hall-effect and resistivity measurements to extract its mobility [16]. They analysed the 2DEG mobility using a developed analysis technique with a high-resolution mobility spectrum. In addition, they presented the first report on the observation of 2DEG mobility spectra thermal broadening effects [16]. This developed method showed mobility of 1880 $cm^2/V.s$ at room temperature and N_{2DEG} of 9.3×10^{12} cm^{-2}. The results of this work exhibited a Gaussian 2DEG mobility spectra and thermal broadening by increasing the temperature. The reason that they investigated the shape of the mobility spectrum was its importance in analysing the device characteristics. Beck and Anderson reported that the shape of the carriers' distribution line and its thermal broadening helps to understand the carrier spatial fluctuations and their relaxation-time distributions, and helps to analyse the Hall-scattering factor [15]. During the last two decades, several studies investigated on improving the mobility spectrum analysis technique; so it could be used as a powerful practical tool [17-

22]. This tool was employed for characterization and investigation of the 2DEG transport in AlGaN/AlN/GaN heterostructures by Umana-Membreno et al. [23].

In the case of effective mobility, several parameters need to be taken into consideration. Some studies tried to match the experimental results of effective mobility with the results achieved from Equation 17, and these studies led to a number of changes in this equation. Risch [24] considered the effect of the resistive region and applied its effect to the formula. Some other works considered the mobility drop due to the lateral electric fields, which is significant for short-channel semiconductor devices because, in that case, mobility is affected by lateral electric field or drain voltage [25, 26]. In short-channel HEMTs, the value of effective mobility is smaller than the electron mobility in long channel HEMTs [27] because of the ballistic effect, which was first predicted in 1979 [28, 29]. This effect makes the electrons flow from the source to the drain without any collisions with phonons or impurities. Electrons propagate in the channel of the device with a randomly oriented thermal velocity. Therefore, it will have limited time to accelerate in the electric field and acquire drift velocity [27]. As the effective and field-effect mobility originate from the same equation (Equation 14), the effects considered for the effective mobility can also be accounted for by the field-effect mobility.

In addition to the modification of these mobility equations to achieve more accurate results, several studies have shown how to change the device structure to increase the value of this mobility. One of the processes used to increase the mobility of the HEMT is using an insulator under the gate, which was presented by Ye et al. [30]. The new developed device is the metal-oxide-semiconductor high-electron-mobility-transistor (MOS-HEMT). In comparison to the HEMT with the same design, MOS-HEMT presents less gate leakage, higher breakdown voltage, and drain current. Several common insulators are used in MOS-HEMT structure, such as SiO_2, Si_3N4, and Al_2O_3. Among these materials, atomic-layer-deposited (ALD) Al_2O_3 is proven to be a significant gate dielectric for the MOS-HEMT [30]. It has the benefit of a high dielectric constant, large bandgap, high thermal stability, high breakdown electric field, and chemical stability against AlGaN [30]. In addition, ALD equipment for Al_2O_3 leads to a low level of defect density and high uniformity. The measurement results show that the effective mobility of the AlGaN/GaN HEMT is much higher than the Si- and GaN-based MOSFET [30]. Also, Al fraction in $Al_xGa_{1-x}N$ affects the value of N_{2DEG} and mobility, which can be seen in Figure 5.

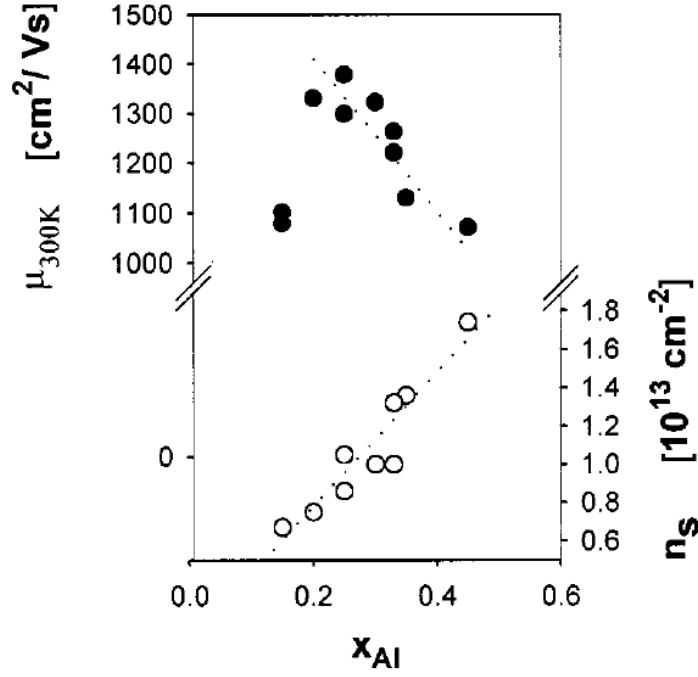

Figure 5. Dependence of electron mobility and sheet carrier density on the Al mole fraction [31, 32]

In addition to these main methods based on Hall, transfer, and output characteristics measurements, several other methods were published for mobility measurement of the HEMT. Sun et al. [33] offered a new method that uses the cut-off frequency to measure the mobility of short channel FETs, which can be applied to the HEMT. This method is based on the effective electron velocity (V_{eff}) equation:

$$V_{eff} = 2\pi L f_T \gamma \tag{26}$$

In this equation, L shows the gate length, f_T is the cut-off frequency measured by current-gain, and γ is:

$$\gamma = \frac{(R_S + R_D + R_{DS})}{R_{DS}} \tag{27}$$

where R_S and R_D are source-to-gate and drain-to-gate resistances, and R_{DS} represents the total resistance between drain and source. It should be mentioned that only a fraction of the applied voltage between drain and source drops across the channel region under the gate. If the applied voltage between the drain and source that is shown by V_{DS} and V_{ds} represents the voltage across the channel under the gate, then V_{ds} can be illustrated by:

$$V_{ds} = \frac{V_{DS}}{\gamma} \tag{28}$$

The average value of the electric field across the channel is given by:

$$E = \frac{V_{ds}}{L} = \frac{V_{DS}}{L\gamma} \tag{29}$$

Considering the average electric field across the channel and the effective velocity of the electrons, the cut-off mobility can be written by:

$$\mu_{FT} = \frac{V_{eff}}{E} = \frac{2\pi f_T (L\gamma)^2}{V_{DS}} \tag{30}$$

The main shortcoming of this method is that it cannot be applied to FETs and HEMTs with long gate lengths.

Moon et al. [34] presented a new method that employed the electron density in the 2DEG channel to measure the average mobility at low electric fields. In this method, which was applied to the MESFET, capacitor-voltage measurement was performed to determine the electron density. In order to restrict the error due to parasitic resistances in mobility measurement, MESFETs with long gate lengths were employed in this work. The gate-to-channel capacitance (C_{gc}) is shown by:

$$qn_S(V_g) = \int_{-\infty}^{Vg} C_{gc}(V)dV \tag{31}$$

In Equation 31, q is the electron charge and n_S shows the electron density per unit area. Assuming that the all of the electrons available for conduction have similar mobility, the average mobility can be calculated by:

$$\mu_{ave} = \frac{\int \mu(x)n(x)dx}{\int n(x)dx} \tag{32}$$

Here, $\mu(x)$ shows the mobility of the channel and $n(x)$ represents the channel electron concentration. The average mobility, considering the electron density at the specific gate voltage, is:

$$\mu_{ave} = \frac{I_{ds}L_{eff}}{qn_S V_{ds} W} \tag{33}$$

where I_{ds} is the drain current, L_{eff} shows the channel effective length, V_{ds} represents the drain voltage, and W is the width of the channel. Parasitic resistances in MESFETs with short gate lengths influence the preciseness of the mobility measurement result, which means that this method cannot be applied to short gate devices.

Another method for the HEMT mobility measurement was presented based on high order derivatives of the current-voltage characteristics [35]. This approach measures the mobility by the following equation:

$$\mu = \frac{\partial^2 I_D L^2}{\partial V_{DS} \partial V_{GS} C_G} \tag{34}$$

Here, I_D shows the drain-to-source current, L represents the length of the gate, and C_G is the gate capacitance. The results of measuring mobility by this method have been compared with the mobility values measured by the cut-off frequency and capacitance-voltage methods. Comparison of the results show that the mobility measured by this new method yields more accurate results than the other methods; however, this method requires complex calculations [35].

The methods mentioned before can measure the average mobility between source and drain of the HEMT because these methods do not separate the mobility under the gate from the mobility outside the gate. In order to solve this issue, it is important to split the characteristics and dc parameters underneath the gate from those outside the gate. These characteristics can be used to measure the HEMT mobility only below the gate. In order to perform the separation, H. Fukui developed a precise method to determine the DC parameters of a MESFET under and outside the gate, separately [36]. In this method, it was assumed that the device can be divided into two regions: 1) an intrinsic resistive region that is influenced by the applied gate voltage (V_G) and follows the gradual channel approximation (GCA), and 2) an extrinsic parasitic resistance region that is not impacted by the gate voltage. The intrinsic resistance is considered as channel resistance (R_{CH}). The extrinsic parasitic resistance includes the drain-to-gate resistance (R_D) and source-to-gate resistance (R_S). Total resistance (R_T) is the summation of intrinsic and extrinsic resistances, which can be explained by:

$$R_T = \frac{V_{DS}}{I_D} = R_S + R_D + R_{CH} \tag{35}$$

Therefore, we have:

$$R_{CH} = (R_S + R_D) - R_T \tag{36}$$

R_{CH} can be represented as a reciprocal of intrinsic conductance, which in turn can be shown as a function of the subtraction of threshold voltage from the gate-source voltage (V_{GS}-V_T). Therefore, Equation 35 can be written by:

$$R_T = R_S + R_D + \frac{1}{f(V_{GS} - V_T)} \tag{37}$$

Plotting R_T as a function of V_{GS}-V_T and employing V_T as the fitting parameter to obtain a linear graph, R_D+R_S value can be determined as the intercept value at the R_T axis. Although this method can be used to determine the value of extrinsic resistances, it results in unstable values for R_D and R_S. In order to solve this problem and also to employ it for mobility measurement, Menozzi et al. modified Fukui's method and developed it; so it could be used for the HEMT. The new method, which is much simpler and more stable than Fukui's method, can be used to determine the source and drain resistances [37]. This work considers the existence of intrinsic resistance in the channel region of the device, which can be declared as a reverse function of intrinsic conductance and shown as a function of V_{GS}-V_T. Menozzi's method also verifies this condition for AlGaN/GaN HEMTs by measuring the electron mobility and that of 2DEG carrier density (n_S). It should be noted that channel conductance is proportional to the product of mobility and 2DEG carrier density. Therefore,

$$f(V_{GS} - V_T) = (\mu_n).(n_S) \tag{38}$$

Self-shielding of 2DEG from Coulomb scattering makes the HEMT mobility a nonlinear function of V_G. In order to satisfy the linear dependence implied by Equation 26, the value of the product of mobility and 2DEG carrier density should be adjusted to make the graph linear, as can be seen in Figure 6.

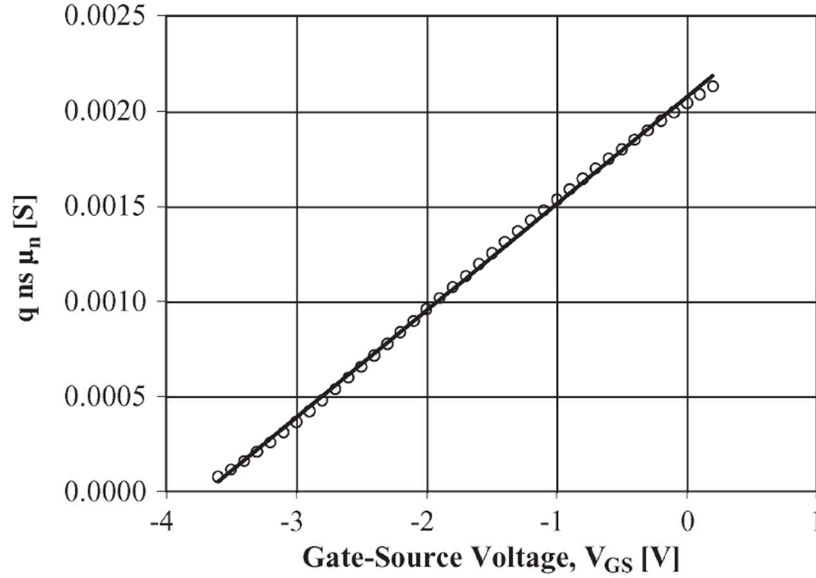

Figure 6. Channel conductance versus gate-source voltage [37]

So, Equation 38 becomes:

$$q.(\mu_n).(n_S) = m(V_{GS} - V_T) \tag{39}$$

In this equation, m is slope of the linear graph, which is equal to 5.611×10^{-4} S/V in Figure 6. In addition, V_T can be determined through the intersection of the $q.(\mu_n).(n_S)$ versus the V_{GS} graph at the V_{GS} axis (V_T = -3.695 V for Figure 6). Considering these parameters, resistance of the intrinsic region can be expressed as:

$$R_{CH} = \frac{L_G}{W_G q n_S \mu_n} = \frac{L_G}{W_G \times 5.611\times10^{-4}(V_{GS} - V_T)} \tag{40}$$

Now, by plotting R_T according to $1/(V_{GS}-V_T)$, the value of R_S+R_D can be found; however, the determined value is not precise enough due to its dependency on the uncertain value of the V_T. In order to solve this problem, Menozzi et al. proposed that instead of plotting R_T versus $1/(V_{GS}-V_T)$, the intrinsic resistance can be drawn for the following equation:

$$\frac{1}{R_{CH}} = \frac{1}{R_T - (R_S + R_D)} \tag{41}$$

Here, instead of using V_T as a fitting parameter, R_S+R_D is used to achieve a linear graph, which has been shown in Figure 7. As can be seen in the figure, the value of R_S+R_D is 18.5 Ω, which is the value that makes the graph linear.

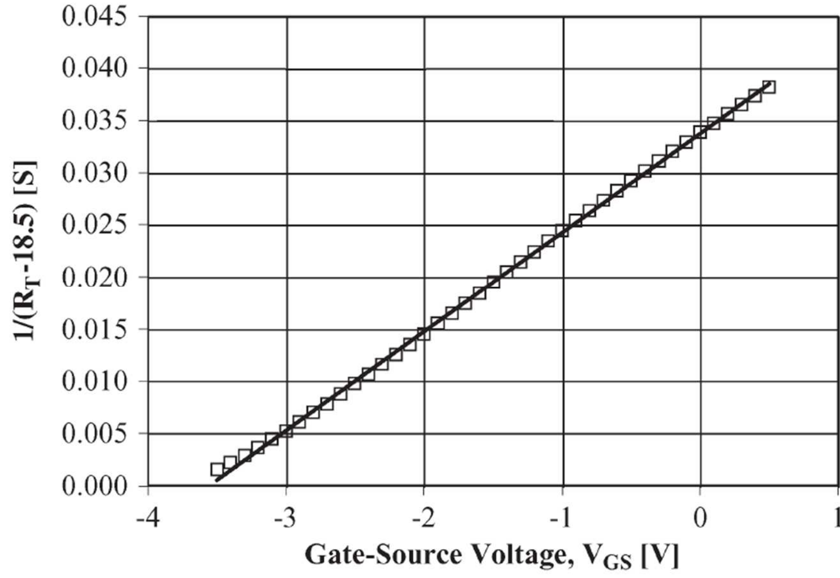

Figure 7. Intrinsic channel conductance versus gate-source voltage [37]

The most fitted graph to the linear graph has the slope of:

$$k = \frac{W_G}{L_G}\mu_n C \tag{42}$$

where W_G shows the gate width, C represents capacitance per unit area, and L_G is the gate length. The accuracy of this modified method can be confirmed by determining the V_T value as the intercept of the graph with the V_{GS} axis. Rearranging Equation 42 leads to:

$$\mu_n = \frac{kL_G}{W_G C} \tag{43}$$

Applying the specific parameters for AlGaN/GaN HEMT, the mobility is shown by:

$$\mu_n = \frac{kL_G t_{AlGaN}}{W_G \varepsilon_{AlGaN}} \tag{44}$$

where t_{AlGaN} and ε_{AlGaN} show the thickness and relative permittivity of the AlGaN layer, respectively. The main shortcoming of the Menozzi's approach is the assumption of independency of the device mobility from the gate voltage. We have developed Menozzi's method to solve this problem, which is presented in Chapter 3.

2.4. Possible sources of error of electron mobility measurements

Analysing the works performed on the mobility measurement shows that there are several sources of error, such as the sample configuration, materials defects, and measurement tools error that affect this measurement.

Gate contact of the HEMT can be leaky, which results in a smaller potential in comparison to the sample with perfect isolation. Although the impact of the gate leakage current can be modified [38], the correction error is large and the accuracy could be questionable. In order to reduce the error due to gate leakage, sample cooling can be used to lower the junction leakage current [39].

In addition to leakage current error in mobility measurement, there are other sources of error that happen due to the measurement process, such as measurement error due to temperature of measurement. The temperature dependence of interface space charge regions and surface should be taken into consideration during carrier density and mobility measurements [40]. The mobility is usually measured at room temperature; however, it should be noted that the mobility measurement is highly dependent on the temperature of the sample. Therefore, it is worthwhile to monitor this temperature, especially if the measurement needs to be repeated several times due to its expected application, and to ensure that the temperature of the sample is adjusted. During the high temperature studies, using a temperature controller and a prober chuck, which is able to cool or heat the sample, is necessary for on-wafer measurements. Also, for low temperature studies, a cryostat can be used to hold the sample inside the liquid nitrogen bath [6].

2.5. Temperature dependence of electron mobility of the HEMT

AlGaN/GaN HEMTs are potential candidates for high-power switching [41], [42] and for high-temperature applications [43-47]. Therefore, studying the reliability of the HEMT at high temperatures and investigating the effects of temperature on the operation of the device is crucial. As mentioned before, the most significant parameter of the HEMT is the 2DEG mobility. This parameter is a function of temperature and it affects the reliability of the device. Because of the large current in the HEMT structure, Joule heating is the main reason of changing the mobility in this device [5]. Temperature dependence of mobility is generally explained by the following equation that relates the mobility to the lattice temperature [48, 49]:

$$\mu(T) = \mu_0 (\frac{T}{T_0})^{-3} \quad (45)$$

where μ_0 is the room temperature mobility and T_0 is 298 K. It can be easily seen that increasing temperature decreases mobility.

Several works study the mobility of the HEMT at high temperatures. Tan et al. investigated the DC characteristic of the AlGaN/GaN HEMT fabricated on a silicon (Si) substrate as a function of temperature [50]. This analysis displayed that mobility and the maximum drain current dropped drastically at high temperatures. Figure 8 below shows the mobility as a function of temperature for a 120 nm gated HEMT [50]. Tan et al. mentioned that HEMTs with short gate length are less temperature dependent than the long gate HEMTs [50].

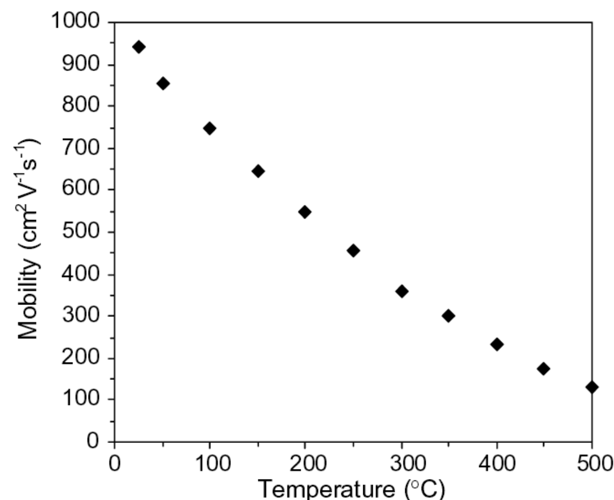

Figure 8. Mobility versus temperature for the HEMT with 120nm gate length [50]

Menozzi et al. studied the effect of temperature on both short gate and long gate HEMTs. The main goal of this work was to analyse the effect of temperature on mobility in the area under and outside the gate (source-to-gate and the drain-to-gate) separately. To achieve this goal, the first step is to divide the channel into these two areas, analyse the characteristics of each area separately, and measure the mobility under and outside the gate individually. Fukui introduced a method to divide the channel and to investigate the characteristics of these areas [36]. They introduced different resistances for the area under and outside of the gate. Two main issues in this work; first, they found that the resistance under the gate was sensitive to the threshold voltage [36]. Second, this work was performed on metal-semiconductor field-effect

transistor (MESFET), not HEMT. In order to address these issues, Menozzi et al. developed Fukui's method to, first, enable it to be applied for the HEMT and, second, solve the sensitivity of resistance to the threshold voltage. In this study, impact of temperature on source-to-gate and the drain-to-gate resistances (R_S + R_D) was investigated, and this was used to exclude the intrinsic channel resistance (R_{CH}) and the mobility in the channel under the gate. It was observed that the parasitic resistance increased by increasing the temperature, while the mobility decreased, which is shown in Figures 9 and 10. They also found that the resistance values become almost double as temperature rises from 75K to 400K.

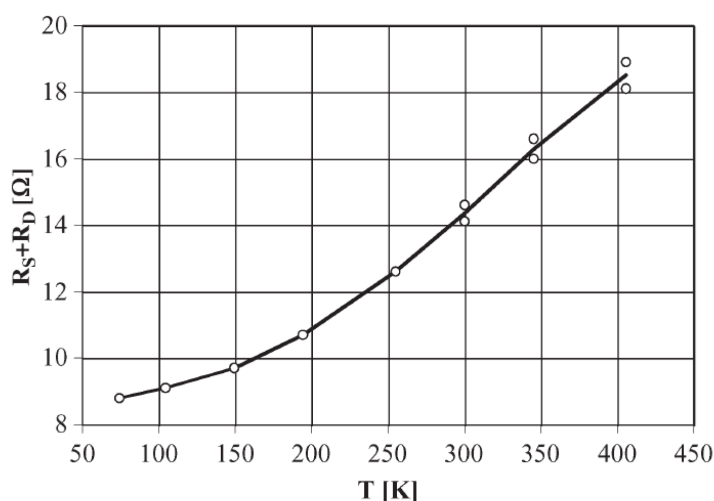

Figure 9. Parasitic resistances according to the temperature [37]

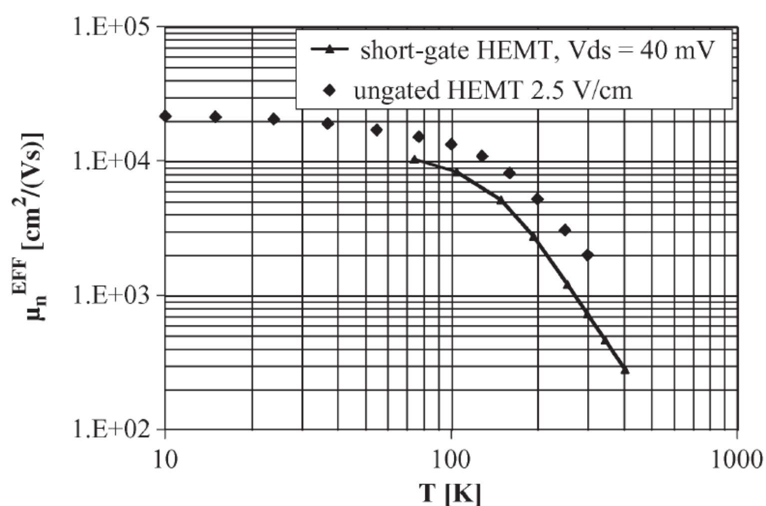

Figure 10. Effective mobility of the short gate and ungated HEMTs by temperature [37]

Investigation of transfer and the output characteristics of un-passivated and passivated AlGaN/GaN HEMTs at high temperatures (up to 425ºC) was presented by Donoval et al. [51]. They found that for both passivated and un-passivated HEMTs, the saturated drain current decreases at high temperatures, and also that transconductance and conductance follow a downward trend. The mobility decreases with increasing temperature following the function of $T^{-1.5}$, which indicates that only phonon scattering is responsible for the mobility drop in these devices. In order to address this issue, an investigation of the effects of different scattering mechanisms on the mobility is very important.

Pandey et al. investigated different scattering mechanisms that affected the mobility of compound semiconductors such as gallium nitride (GaN) and gallium arsenic (GaAs) [52]. They analysed the impact of different carrier scattering mechanisms, such as ionized impurity scattering, piezoelectric scattering, acoustic deformation impurity scattering, and neutral impurity scattering on mobility of GaN and GaAs, which are shown in Figures 11 and 12, respectively. These figures display the mobility of GaN and GaAs for a different scattering mechanism according to the temperature. It can be seen that the mobility increases by temperature for neutral-impurity and ionized-impurity scatterings. However, acoustic deformation impurity and piezoelectric scatterings, which are known as phonon or lattice scatterings, decrease the mobility by increasing the temperature. Even though these scattering mechanisms lead to an increase in the mobility at high temperatures, it can be seen that the total mobility reduces when the temperature is increased. It was also found that the mobility of AlGaAs/GaAs HEMTs behaves similar to the mobility of GaAs bulk material. In addition, it was also noted that increasing the dopant concentration in the semiconductors causes dominant impurity scattering, which further decreases the mobility. In spite of GaN and GaAs mobility dropping by different factors, these materials are still the most preferred for HEMT development [52].

In order improve the mobility of the HEMT, Takhar et al. introduced a new structure for the HEMT [53]. In this structure, a thin layer of indium aluminium nitride (InAlN) and aluminium nitride (AlN) was grown between the gate and the GaN layer, as shown in Figure 13. The dependence of the mobility of the InAlN/AlN/GaN HEMT at high temperature was analysed by developing a simulation model for this device. It was explained that the electron mobility reduction at high temperatures occurs because of lack a proper heat sink at the heterojunction. This leads to an inefficient thermal management and results in increased lattice heating. This lattice heating causes an increase in phonon scattering and gives the mobility a

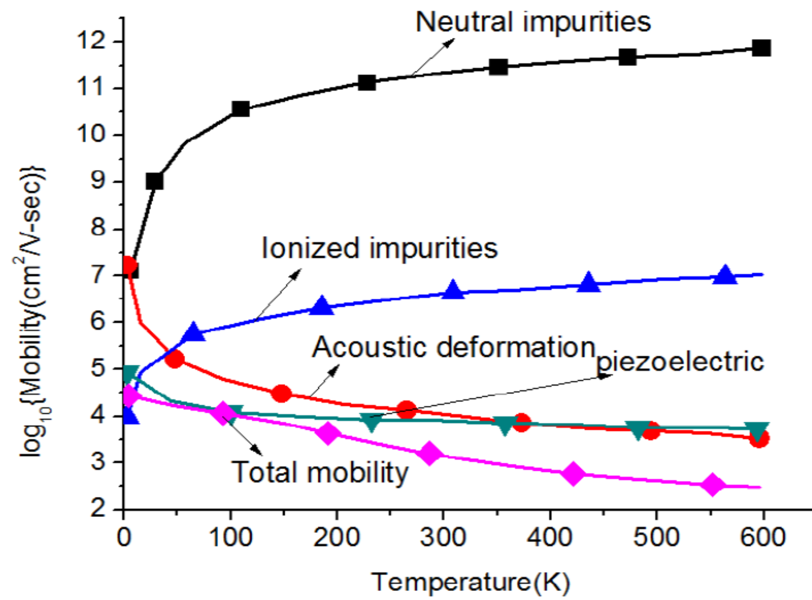

Figure 11. Mobility in bulk GaN for several scattering mechanisms [52]

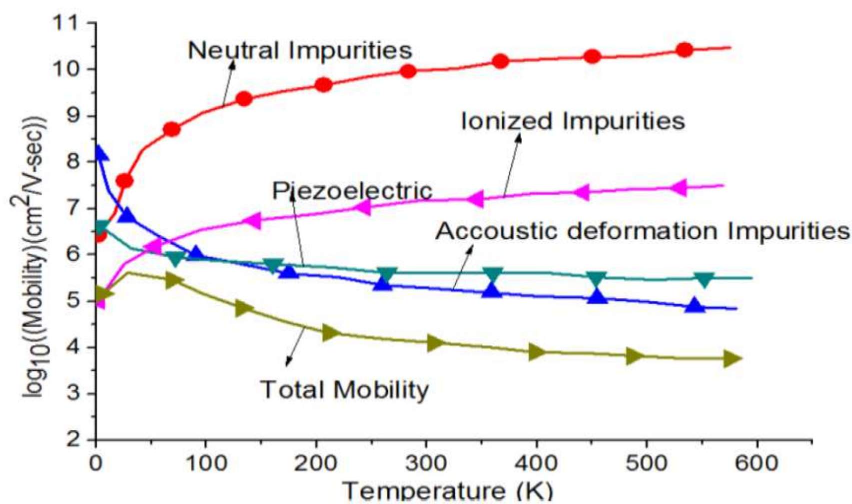

Figure 12. Mobility in bulk GaAs for different scattering mechanisms [52]

downward trend by increasing the temperature. Using a thin layer of AlN between the heterojunction helps to create a better heat sink at the junction, reduce the phonon scattering, and improve the mobility. In another study, it was shown that as the thickness of the spacer layer (which is usually AlN located between AlGaN and GaN) decreases, mobility also decreases [31]. It was also found that the other parameter that degrades the mobility is the defect [54]. Several further works were performed to analyse the effect of charged defect density on degradation of the Mobility [48, 55-58].

Also, it was shown that as the cap layer thickness increases, electron mobility increases as well, while increasing the Al content in AlGaN leads to a reduction in mobility [31, 59, 60].

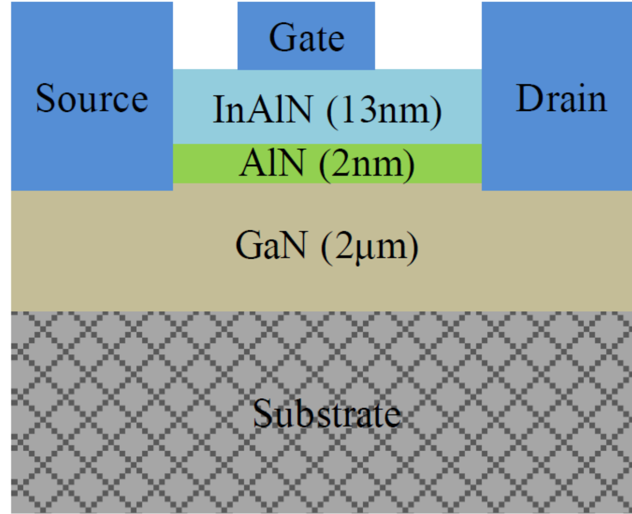

Figure 13. Cross section of the InAlN/AlN/GaN HEMT [53]

It has been frequently reported that increasing the temperature [45, 48, 60-71] or N_{2DEG} [61, 66, 68, 72, 73] decreases the mobility of 2DEG. The degree at which the mobility degrades with temperature is estimated by:

$$\mu = AT^{-\gamma} \tag{46}$$

in which A is the proportionality constant, T is the absolute temperature, and γ is the power coefficient. γ is the exponential factor at which the mobility decreases by temperature. The usual value of γ is 1.5 [45, 74, 75], which follows the mobility trend of phonon scattering at high temperatures. This equation can be written by:

$$\log(\mu) = m\log(T) + \log(A) \tag{47}$$

In this equation, m represents the slope of mobility according to the temperature in log-log scale. This equation matches to the linear equation with the slope of m:

$$y = mx + c \tag{48}$$

By plotting the logarithm of mobility over the logarithm of temperature in Kelvin, the value of m can be determined. This phenomenon occurs because of the increased phonon (or lattice) scattering. Therefore, it can be noted that m is the mobility degradation rate, representing the

degree of the scattering that affects the mobility. This slope (*m*) is always negative, which shows increasing temperature leads to the reduction in mobility [62]. The value of the slope, when only phonon scattering is involved, is 1.5; however, several other scattering mechanisms and factors affect the mobility and cause a change in this value.

When the temperature increases above absolute zero, vibrating atoms of the materials produce pressure (acoustic) waves inside the crystal; these are phonons. Phonons, similar to electrons, are considered particles. Therefore, phonons may collide with electrons and holes and scatter them. By increasing the temperature, phonon concentration increases. Therefore, phonon scattering increases and mobility reduces. Theoretical calculations on mobility of non-polar semiconductors, such as germanium (Ge) and Si, reveal that their mobility is affected mostly by acoustic phonon interaction. The mobility of these semiconductors is expected to be proportional to $T^{-1.5}$; however, the mobility changes caused by the optical phonon scattering is expected to be proportional to $T^{-0.5}$. The experimental values of the mobility temperature dependence for Si, Ge, and GaAs are shown in Table 1 [76].

Table 1. Typical values of m (mobility degradation rate by increasing temperature) [76]

	Si	**Ge**	**GaAs**
Electrons	-2.4	-1.7	-1.0
Holes	-2.2	-2.3	-2.1

In addition to temperature, several other reasons cause the reduction in mobility of the AlGaN/GaN HEMTs. Bulk defects are one of the reasons [48, 77-79]. The drain current degrades because of the cumulative effect of both temperature and charged defects. The region near the drain side of the gate edge has a higher temperature compared to other sides of the device, and this region is called a hot spot. This spot exists because of the high electric fields beside the drain-to-gate region at saturation condition. The mobility of the region with a high electric field is low [80], which increases the resistivity of 2DEG. This increased resistivity causes increased self-heating and even more mobility reduction near the hot spot. When the current density of the HEMT is high, degradation of mobility due to temperature is more significant near the hot spot, while away from the hot spot, charged defect-induced degradation is dominant [48].

To reduce the effect of these temperatures and defects on the reduction of mobility, an AlN interlayer can be employed between the GaN and AlGaN layers. Because of the high crystal quality of this heterostructure, effects of the interface roughness and alloy-disorder scatterings are reduced [69]. In addition to using interface layer, the thickness of the AlGaN cap layer should be optimized to improve the HEMT performance. As the thickness of the AlGaN layer is greater, the scattering time is longer and carrier concentration is larger. However, analysis showed that the DC characteristics of the HEMT with a thin AlGaN layer are better than the thick layer. These DC parameters include higher transconductance (up to 270 mS/mm), lower output conductance, lower threshold voltage, and maximum saturation currents of 1.5 A/mm [63], [81].

Reduction of the mobility of the HEMT results in a drop in the current [71]. In order to investigate whether the reduction of the current during the temperature increase is due to the mobility reduction or to the change in carrier density, the effect of temperature on the 2DEG density has been analysed [82]. It was found that the 2DEG density remains relatively constant from 25 to 500°C [82] and the drain current falls by increasing the temperatures was attributed to the reduction in mobility [46]. It should be noted that in short channel HEMTs operating in the saturation region, the temperature dependence of mobility is weaker than that seen for low-field electron mobility because the carriers flow at the saturation velocity under the gate. This issue has been found previously by Mizutani et al. on AlGaAs/ InGaAs HEMTs [83]. It was also found that another reason for degradation of mobility is quantisation of carriers in the inversion layers [84-86].

2.6. Scattering mechanisms effects on mobility of the HEMT

As mentioned previously, electron mobility is affected by several scattering mechanisms. Each of these scattering mechanisms causes a different mobility that can be measured separately, which was shown previously in Figure 11. The 2DEG measured mobility is a summation of the mobility through each of these scattering mechanisms. According to Mathiessen's rule, the total measured mobility (μ_T) is dependent on various mobilities resulted from each of these scattering mechanisms [87]:

$$\frac{1}{\mu_T} = \frac{1}{\mu_1} + \frac{1}{\mu_2} + \frac{1}{\mu_3} + \ldots \tag{49}$$

According to this equation, it is found that the total mobility is dominated by the lowest mobility. Also these scattering mechanisms reduce the total mobility. The major sources of scattering in the HEMT include ionized impurity, acoustic phonon (also called lattice scattering), piezoelectric, surface roughness, alloy disorder, inelastic, and electron-electron scatterings, as discussed below. In some cases, some other scattering sources, such as optical phonon, neutral impurity, and defect scatterings can be important [88].

Ionized impurity scattering: Deviation of carriers (electrons or holes) because of approaching the ionized impurity in semiconductors is called ionized impurity scattering. This scattering mechanism is related to the doped semiconductors with acceptors or donors, which are ionized and therefore charged. The deviation happens because of the effect of Coulomb forces on carriers approaching the ionized impurity. Two important factors that determine the amount of deviation are proximity of the carriers to the ion and the speed of carriers. By increasing the doping concentration of the semiconductor, the probability of collision of carriers with an ion increases. This reduces the mean time between collisions, and therefore the mobility degrades [89].

While analysing the strength of these interactions, it should be remembered that the total interaction is not only because of Coulomb force; the free carriers and other impurities may also lead to some interactions. Analysis of the scattering mechanism near the interface is complicated because of crystal defects, disorders, and traps near the interface. Free carriers are scattered from traps due to defects linked to dangling bonds. By trapping a charge, the defects will be charged and start colliding with free carriers. For carriers of the inversion layer at the interface, dimensions of the carriers make the case different from the case of bulk impurity, where carriers flow only in two dimensions. In addition, interfacial roughness also limits the mobility of two-dimensional electron gas at the interface of the HEMT [89].

Increasing temperature causes a reduction in ionized impurity scattering because of the increase in the carriers' average thermal speed. Therefore, carriers spend less time near the ionized impurities when passing, and so the effect of ion scattering reduces. A higher effective mass (m^*) of electrons in GaN in comparison to AlGaN makes the impurity scattering role in GaN devices less effective than GaAs devices with the same doping level [89].

Phonon (lattice) scattering: For temperatures above absolute zero, acoustic waves, which are phonons, exist in the crystal due to vibration of atoms. The collision of phonons, which are particles, with the other carriers causes a scatter mechanism. As temperature increases, more

phonons collide with other carriers and reduce the mobility. Phonons are the major source of scattering at high temperature (>150°C) and can even dominate at low temperatures in very pure materials [60], [67].

Piezoelectric scattering: Piezoelectric scattering can be seen in compound semiconductors because of their polar nature. Although this scattering mechanism is not very strong, it may cause local electric fields to scatter and deviate carriers. These electric fields originate from the basic unit cell's distortion when the strain is applied in a certain direction of the lattice. The effect of this scattering can be seen at low temperatures, where the other scatterings are not significant [89]. Also, this scattering has almost no impact on phonon limited mobility [60].

Surface roughness scattering: This is a type of short-range scattering, which is caused by interfacial disorder and limits the mobility of 2DEG at the interface. According to the high-resolution transmission electron micrographs, it is found that the interface is not steep on the atomic level; however, the real position of the interfacial plane changes along the surface of one or two atomic layers. These changes are random and lead to inconstancy in energy levels at the interface, which results in scattering [89]. Interface scattering in bulk materials are usually negligible [89-93]. When the temperature is low ($0<T<150$ K), interface roughness and alloy disorder scattering mechanisms, which are considered as deformation potential scatterings, dominates [60, 67]. For this range of temperature, surface roughness scattering reduces the HEMT mobility below the bulk mobility [94].

Alloy disorder scattering: The random positioning of atoms and the crystal potential perturbation in compound semiconductor materials leads to a scattering that is known as alloy disorder scattering. This scattering happens in ternary or higher alloys because the crystal structure in those materials is formed by randomly replacing atoms in one of crystal structure sub-lattices. The effect of this scattering mechanism is mainly weak; however, it can be the dominant effect in some special circumstances and for certain semiconductors [89].

Electron-electron scattering: When the density of the electrons is less than 10^{17} cm^{-3} or the electric field is lower than 10^{3} V/cm, according to the Pauli's Exclusion Principle, electrons are accounted as non-interacting. However, when the electron density or the electric fields are above those values, electron–electron scattering will be dominant. Nonlinearity and a long range of Coulomb potential, which governs interactions between the electrons, make these interactions complicated to deal with [89-91].

Inelastic scattering: The mentioned scattering mechanism (acoustic phonon, impurity, and piezoelectric scattering) are considered as elastic scatterings. This means that the energy is nearly conserved during the scattering process. For example, because of acoustic phonon scattering, electrons travel from one energy level to the other energy level while they absorb or emit a wave vector phonon. Modelling of this phenomenon is performed by assuming that there is a small shift in energy bands due to the lattice vibrations. Deviations of energy bands, which occur because of these small transitions from the frozen lattice positions, generate a further potential that causes the scattering process [89].

If the energy released from the scattering mechanism is not conserved, this is considered as inelastic scattering. In inelastic scattering processes, significant energy exchange occurs. Similar to the elastic phonon scattering, in the case of inelastic, deformations of energy-bands by atomic vibrations lead to arising the potential. Energy of optical phonons leading to inelastic scattering is between 30 to 50 meV, which is much less than the energy of acoustic phonons (<1 meV). There is a considerable variation in the energy level of carriers while the scattering process is occurring [89].

As mentioned, different scattering mechanisms affect the electron mobility. The average time between two scattering events is named scattering time. The relation between mobility and scattering time (τ) can be simply explained by [95]:

$$\mu = \frac{q}{m^*}\tau \tag{50}$$

In this equation, it is assumed that carriers' motions after each scattering event is randomized; therefore, their average velocity is zero. Then, the carriers are accelerated in the electric field uniformly until they scatter again. Also, in the case that m^* is anisotropic, the effective mass with the same direction of electric field can be used in the equation.

The effective mass is commonly measured using magnetotransport (Shubnikov-de Haas oscillations, SdH) or cyclotron resonance (CR) measurement methods [96]-[99]. These methods require very high values of mobility, therefore they are carried out at low temperatures [97], [99]. Effective mass of electrons in bulk semiconductors and the epitaxial wurtzite GaN is usually temperature independent. However, this effective mass is strongly temperature dependent for 2DEG in AlGaN/GaN structures [97]. Therefore, the value of the 2DEG effective mass measured at low temperatures are not applicable for high temperatures. The variation of the 2DEG effective mass with temperature is caused by variation in its band structure, alloy

disorder, or intrinsic effects of spontaneous and piezoelectric polarization at the interface [98]. These factors are mainly attributed to the growth conditions during the depositing process of AlGaN/GaN heterostructures [97]. Also Fermi level of the 2DEG is high enough in the conduction band for nonparabolicity of electron scattering law to be effective [99]. In addition, strain and polarization charges are dependent on temperature. These reasons cause much larger 2DEG effective mass variation with the temperature than what is typically observed for bulk semiconductors [97].

Comparison of the mobility in the HEMT and MOSFET as two significant power semiconductor devices shows that the mobility of MOSFET is much lower than that of HEMT. This issue is because in MOSFET, conduction electrons occupy a similar space as ionized impurities. Therefore, the channel mobility of the MOSFET is limited at least by the mobility of bulk carriers (μ_B). In practice, the MOSFET mobility is only a fraction of the bulk mobility because of the scattering effects at the interface of the device. This scattering is mainly Coulomb scattering at the interface traps. In the case of GaN-based HEMT with the same transverse electric field as MOSFET, phonon limited mobility is higher than the value of bulk mobility [68].

2.7. Application of the measured electron mobility of the HEMT

Measuring the mobility of the HEMT as its key parameter leads to employing it in the analysis and development of applications for this device. One of the most significant applications of the measured HEMT electron mobility is in the modelling of this device. Measuring the electron mobility precisely and employing it in the modelling of the device makes circuit designers confident about using the HEMT in electronic circuit design. Accurate values of mobility used in device modelling give the simulation results a proper agreement with the experimental data.

2.7.1. SPICE Simulation of circuits with HEMT

2.7.1.1. Importance of SPICE modelling of the HEMT

HEMT technology is growing quickly, and the design of large scale circuits and systems with HEMTs require precise, fast, and physical compact models of this device [100]. Therefore, due to the growing applications of HEMT, development of models for simulating

circuits is essential. SPICE is the most common software among circuit designers for simulation of circuits.

Standardizing and promoting SPICE models of semiconductor devices is organized by the Compact Model Coalition (CMC) Organization [101]. CMC standards are supported by circuit simulators and used by integrated device manufacturers. Previously, the main focus of CMC modelling standardization was on Si-based active and passive devices. However, since 2011, this organization began developing GaN-based HEMTs because of its outstanding applications in power management and green technologies, and they formed a task force to define standard characteristics for modeling GaN HEMTs [42].

2.7.1.2. Models presented for SPICE simulation of the HEMT

In the SPICE simulation software, there is no practical model available for simulation of the HEMT [102, 103]. In order to simulate the circuits including the HEMT, in some studies, MOSFET equations and parameters available in SPICE are modified to be used for simulation of the HEMT [100]. HEMT can be divided into separate regions; under the gate and outside the gate. The region under the gate is the field-effect section and can be modelled by the MOSFET, while the region outside the gate is resistive. Employing MOSFET equations and parameters followed by involving the effect of the resistive section leads to a model for simulation of the HEMT. Many sets of equations for MOSFET in SPICE, called LEVELs, have different parameters that can be used to simulate MOSFETs for various applications, from power to CMOS microprocessors applications [104].

In the early versions of the SPICE, MOSFET LEVEL 1 model, which is the original model of the MOSFET, was introduced. This model contains the analytical model of the FET. In this model, it is assumed that the channel mobility is constant and device dimensions are large. So this model can be applied to only wide and long FETs with large gate oxides, and not short channel FETs. Analysing and developing a MOSFET LEVEL 1 model, whose parameters can be seen in Table 2, provides the fundamental understanding about more complex models. The simplicity of this model makes the extraction of the parameters of this model easy, and this can be seen in Table 2 [4].

Table 2. Parameters for SPICE simulation of MOSFET LEVEL 1 [4]

Parameter	Unit	Explanation
TPG	m	Type of gate material
TOX	m	Gate oxide thickness
NSUB	cm^{-3}	Substrate doping concentration
XJ	m	Drain/source junction depth
UO	$cm^2/V.s$	Zero bias low-field mobility
VTO	V	Threshold voltage
LAMBDA	V^{-1}	Channel length modulation parameter
CGSO	F/m	Zero bias gate-source capacitance
CGDO	F/m	Zero bias gate-drain capacitance
CGBO	F/m	Zero bias gate-bulk capacitance

By decreasing the device geometries and oxide thickness, it is apparent that the LEVEL 1 model is no longer applicable for simulation of the device. In order to address the shortcomings of MOSFET LEVEL 1, this model was developed and the LEVEL 2 model was introduced. This model is developed based on the LEVEL 1 model, and parameters of small geometry effects have been added, which can be seen in Table 3 [4]. Although this model can be applied to small dimension devices, it is mathematically complicated. Therefore, this model is inefficient, and it mostly encounters convergence problems. This model also suffers from the discontinuity of the first derivative at linear to saturation transition point. In addition, this model neglects the possible overlap of depletion regions of the drain and source for very short channel devices, DIBL, and lateral field-effects on the mobility. Furthermore, short channel effects are considered only partially. These reasons limit the extensive use of this model and lead to another more efficient model, the LEVEL 3 model. The LEVEL 3 model was developed to address the shortcomings of the LEVEL 2 model.

Table 3. Parameters for SPICE simulation of MOSFET LEVEL 2 [4]

Parameter	**Unit**	**Explanation**
TPG	m	Type of gate material
TOX	m	Gate-oxide thickness
LD	m	Channel length reduction from drawn value
WD	m	Channel width reduction from drawn value
VTO	V	Threshold voltage
UO	$cm^2/V.s$	Zero bias low-field mobility
UCRIT	V/cm	Critical vertical field for mobility reduction
UEXP		Exponent in the mobility model
RS	Ohm	Source series resistance
RD	Ohm	Drain series resistance
DELTA		Narrow channel effect on the threshold voltage
NSUB	cm^{-3}	Sub-threshold sensitivity parameter
XJ	m	Short channel correction to the substrate sensitivity
VMAX		Maximum carrier velocity
NEFF		Fractional depletion charge reduction due to channel length modulation
NFS	cm^{-2}	Sub-threshold region fitting parameter
CGSO	F/m	Zero bias gate-source capacitance
CGDO	F/m	Zero bias gate-drain capacitance
CGBO	F/m	Zero bias gate-bulk capacitance
XQC		Charge partitioning parameter
UTRA	V^{-1}	Drain bias effect on the vertical field for mobility reduction

Most of the equations and parameters of LEVEL 3 model are similar to LEVEL 2. However, this model involves the effect of channel length modulation, which is different from LEVELs 1 and 2, and which can be seen in the following equations [74]:

$$I_D = \beta[(V_{GS} - V_T)V_{DS} - (1 + F_B)\frac{V_{DS}^2}{2}]$$ Triode region (51)

$$I_D = \frac{\beta}{2(1 + F_B)}(V_{GS} - V_T)^2$$ Saturation region (52)

Here F_B , β, and V_T are [74]:

$$F_B = \frac{\gamma F_S}{2\sqrt{|2\phi_F| + V_{SB}}} + F_n^a$$ for NMOS (53)

$$\beta = KP\frac{W}{L_{eff}}$$ if *KP* is determined (54)

$$\beta = \mu_0 \frac{\varepsilon_{OX}}{t_{OX}} \frac{W}{L_{eff}}$$ if *KP* is not determined (55)

$$V_T = Vto + \gamma(\sqrt{Phi + V_{SB}}) - \sqrt{Phi})$$ (56)

In these equations, V_{DS} and V_{GS} are drain-to-source and gate-to-source voltages, respectively, *Vto* shows the threshold voltage, *KP* represents the transconductance parameter, *Gamma* is the body factor, and *Phi* is the surface potential in strong inversion [74]. As can be seen in Equation 55, mobility is a key parameter for accurate modelling of the device that leads to simulation results that are close to the experimental results. Also, in addition to the DC parameters, AC parameters including the gate voltage should be taken into consideration, which is shown by:

$$C_g = (Cgdo \times W) + (Cgso \times W)$$ (57)

In this equation, Cgso and Cgdo are gate-source and gate-drain overlap capacitance per channel width.

In contrast to LEVEL 2, the LEVEL 3 model employs a semi-empirical approach, in which a parameter reflects the change of the mobility. This model is semi-empirical, simple, straightforward to extract its parameters, possible to be applied to channel lengths even much smaller than 1 μm, able to run faster than the other models, and it rarely encounters convergence issues. Therefore, this model is significantly taken into consideration for SPICE simulation of the MOSFET [4]. The parameters of this model can be seen in the following table. Among these parameters, R_S and R_D are used to include the effect of resistive sections of the HEMT.

Table 4. Parameters for SPICE simulation of MOSFET LEVEL 3 [4]

Parameter	**Unit**	**Explanation**
TPG	m	Type of gate material
TOX	m	Gate-oxide thickness
LD	m	Channel length reduction from drawn value
WD	m	Channel width reduction from drawn value
VTO	V	Threshold voltage
UO	$cm^2/V.s$	Zero bias low-field mobility
THETA	V^{-1}	Reduction parameter of mobility
RS	Ohm	Source series resistance
RD	Ohm	Drain series resistance
DELTA		Narrow channel effect on the threshold voltage
NSUB	cm^{-3}	Sub-threshold sensitivity parameter
XJ	m	Short channel correction to the substrate sensitivity
VMAX		Maximum carrier velocity
ETA		DIBL coefficient
KAPPA	V^{-1}	Channel length modulation effect on the drain current
NFS	cm^{-2}	Sub-threshold region fitting parameter

CGSO	F/m	Zero bias gate-source capacitance
CGDO	F/m	Zero bias gate-drain capacitance
CGBO	F/m	Zero bias gate-bulk capacitance
XQC		Charge partitioning parameter
BEX	V^{-1}	Temperature effect on the low-field mobility

Several works present new models for SPICE simulation of the HEMT by defining new equations [105] or sub-circuits [106], [107, 108]. Some of these sub-circuits include the key physical effects of GaN HEMT, in order to accurately model this device by considering the Schrodinger's and Poisson's equations [100]. Some are defined for RF applications [108], some for large-signal microwave performances [109], and some others are used to better predict the transient performance of the HEMT by providing smooth transitions between different operation regions of the device [110].

The forward and reverse channel current conduction for power electronics applications were presented in [111]. The parameters of this model are easily extracted from C-V and static I-V characteristics. This model considers the effect of reverse channel conduction, which is very important to circuit designers [111].

In addition to MOSFET, implementation of the HEMT model can be performed based on MESFET models [112]. A modified equation for the SPICE simulation of the HEMT drain current using the MESFET drain current equation has been presented [102, 105]. Using the presented equation, a proper matching between the drain current and transconductance of the experimental and simulation results have been achieved [105].

Another model of the HEMT, which is temperature dependent, was proposed and its simulation and measurement results were compared at various temperatures and for several channel lengths [113]. This model includes the temperature effects on the 2DEG mobility, V_{OFF}, saturation velocity, and drain-source resistance [113].

Early models of the HEMT [114, 115] were based on linearized functions of N_{2DEG} for all of its working regions, which is not logical for large forward gate-source potential or for sub-threshold mode. A physically based model of the HEMT should use a three-piece function to be able to describe its different working regions, and these regions are needed to be analysed separately [116]. By that condition, the drain current will be represented by three-piece

conditional functions, which show discontinuity at higher order derivatives and distort analysis results. In addition to the N_{2DEG}, the HEMT model should include the extrinsic drain and source and resistances and intrinsic drain-source current. To solve the problem of discontinuity of the N_{2DEG}, a model was presented in which the 2DEG density was a continuous function of gate voltage. This model combines the sub-threshold, linear, and saturation modes with a single description [117]. This model also features high order continuity for accurate analysis of *I-V* characteristics, gain, and distortion [117].

To solve the problem of linearized assumption for N_{2DEG} by voltage, and also considering the effects of extrinsic drain and source resistive regions for modelling of the HEMT, a model has been presented that takes into account the nonlinear relation of the N_{2DEG} and V_{GS}, which leads to square law type of *I-V* characteristics [103]. Also, it does not extract the parameters values for matching the experimental and simulation results. The simulation results using this model show excellent agreement with experimental data over a wide range of voltage [103].

2.8. References

[1] U. K. Mishra, P. Parikh, and Y.-F. Wu, "AlGaN/GaN HEMTs-an overview of device operation and applications," *Proceedings of IEEE*, vol. 90, no. 6, pp. 1022-1031, 2002.

[2] D. K. Schroder, *Semiconductor material and device characterization*: John Wiley & Sons, 2006.

[3] A. Aminbeidokhti, S. Dimitrijev, J. Han, X. Xu, C. Wang, S. Qu*, et al.*, "A Method for extraction of electron mobility in power HEMTs," *Superlattices and Microstructures,* vol. 85, pp. 543-550, 2015.

[4] D. P. Foty, *MOSFET modeling with SPICE: principles and practice*: Prentice-Hall, Inc., 1997.

[5] E. H. Hall, "On a new action of the magnet on electric currents," *American Journal of Mathematics,* vol. 2, pp. 287-292, 1879.

[6] R. Green, "Hall Effect Measurements in Materials Characterization," *White paper,* pp. 1-12, 2011.

[7] L. van der PAUYV, "A method of measuring specific resistivity and Hall effect of discs of arbitrary shape," *Philips Res. Rep.,* vol. 13, pp. 1-9, 1958.

[8] K. Fu, "Mobility degradation due to the gate field in the inversion layer of MOSFET's," *IEEE Electron Device Letters,* vol. 3, pp. 292-293, 1982.

[9] C. Rost-Bietsch, *Ambipolar and light-emitting organic field-effect transistors*: Cuvillier Verlag, 2005.

[10] F. Fang and A. Fowler, "Transport properties of electrons in inverted silicon surfaces," *Physical Review,* vol. 169, pp. 619-631, 1968.

[11] J. Kang, D. Schroder, and A. Alvarez, "Effective and field-effect mobilities in Si MOSFETs," *Solid-State Electronics,* vol. 32, pp. 679-681, 1989.

[12] Z. Dziuba, J. Antoszewski, J. Dell, L. Faraone, P. Kozodoy, S. Keller*, et al.*, "Magnetic field dependent Hall data analysis of electron transport in modulation-doped AlGaN/GaN heterostructures," *Journal of Applied Physics,* vol. 82, pp. 2996-3002, 1997.

[13] S. Contreras, W. Knap, E. Frayssinet, M. Sadowski, M. Goiran, and M. Shur, "High magnetic field studies of two-dimensional electron gas in a GaN/GaAlN heterostructure: Mechanisms of parallel conduction," *Journal of Applied Physics,* vol. 89, pp. 1251-1255, 2001.

[14] M. Gold and D. Nelson, "Variable magnetic field Hall effect measurements and analyses of high purity, Hg vacancy (p-type) HgCdTe," *Journal of Vacuum Science & Technology A,* vol. 4, pp. 2040-2046, 1986.

[15] W. Beck and J. Anderson, "Determination of electrical transport properties using a novel magnetic field-dependent Hall technique," *Journal of Applied Physics,* vol. 62, pp. 541-554, 1987.

[16] G. Umana-Membreno, T. Stomeo, V. Tasco, A. Passaseo, M. De Vittorio, and L. Faraone, "Thermal broadening of two-dimensional electron gas mobility distribution in AlGaN/AlN/GaN heterostructures," in *Proceedings of the European Solid-State Device Research Conference (ESSDERC),* 2010, pp. 182-185.

[17] Z. Dziuba and M. Gorska, "Analysis of the electrical conduction using an iterative method," *Journal de Physique III,* vol. 2, pp. 99-110, 1992.

[18] J. Antoszewski, D. Seymour, L. Faraone, J. Meyer, and C. Hoffman, "Magneto-transport characterization using quantitative mobility-spectrum analysis," *Journal of Electronic Materials,* vol. 24, pp. 1255-1262, 1995.

[19] I. Vurgaftman, J. Meyer, C. Hoffman, D. Redfern, J. Antoszewski, L. Faraone*, et al.*, "Improved quantitative mobility spectrum analysis for Hall characterization," *Journal of Applied Physics,* vol. 84, pp. 4966-4973, 1998.

[20] S. Kiatgamolchai, M. Myronov, O. Mironov, V. Kantser, E. Parker, and T. Whall, "Mobility spectrum computational analysis using a maximum entropy approach," *Physical Review E,* vol. 66, pp. 036705-1-036705-9, 2002.

[21] J. Antoszewski, L. Faraone, I. Vurgaftman, J. Meyer, and C. Hoffman, "Application of quantitative mobility-spectrum analysis to multilayer HgCdTe structures," *Journal of Electronic Materials,* vol. 33, pp. 673-683, 2004.

[22] J. Rothman, J. Meilhan, G. Perrais, J.-P. Belle, and O. Gravrand, "Maximum entropy mobility spectrum analysis of HgCdTe heterostructures," *Journal of Electronic Materials,* vol. 35, pp. 1174-1184, 2006.

[23] G. Umana-Membreno, J. Antoszewski, L. Faraone, E. Smith, G. Venzor, S. Johnson*, et al.*, "Investigation of Multicarrier Transport in LPE-Grown $Hg_{1-x}Cd_xTe$ Layers," *Journal of Electronic Materials,* vol. 39, pp. 1023-1029, 2010.

[24] L. Risch, "Electron mobility in short-channel MOSFET's with series resistances," *IEEE Transactions on Electron Devices,* vol. 30, pp. 959-961, 1983.

[25] N. Herr and J. J. Barnes, "Statistical circuit simulation modeling of CMOS VLSI," *IEEE Transactions on Computer-Aided Design of Integrated Circuits and Systems,* vol. 5, pp. 15-22, 1986.

[26] M. H. White, F. Van de Wiele, and J.-P. Lambot, "High-accuracy MOS models for computer-aided design," *IEEE Transactions on Electron Devices,* vol. 27, pp. 899-906, 1980.

[27] M. S. Shur, "Low ballistic mobility in submicron HEMTs," *IEEE Electron Device Letters,* vol. 23, pp. 511-513, 2002.

[28] M. Shur and L. Eastman, "Near ballistic transport in GaAs at 77 K," in *Proc. 7th Biennial Cornell Conference Active Microwave Devices and Circuits,* 1979, pp. 389-400.

[29] M. S. Shur and L. F. Eastman, "Ballistic transport in semiconductor at low temperatures for low-power high-speed logic," *IEEE Transactions on Electron Devices,* vol. 26, pp. 1677-1683, 1979.

[30] P. Ye, B. Yang, K. Ng, J. Bude, G. Wilk, S. Halder*, et al.*, "GaN metal-oxide-semiconductor high-electron-mobility-transistor with atomic layer deposited Al2O3 as gate dielectric," *Applied Physics Letters,* vol. 86, pp. 63501-63501, 2005.

[31] S. Keller, G. Parish, P. Fini, S. Heikman, C.-H. Chen, N. Zhang*, et al.*, "Metalorganic chemical vapor deposition of high mobility AlGaN/GaN heterostructures," *Journal of Applied Physics,* vol. 86, pp. 5850-5857, 1999.

[32] S. Keller, Y.-F. Wu, G. Parish, N. Ziang, J. J. Xu, B. P. Keller*, et al.*, "Gallium nitride based high power heterojunction field effect transistors: process development and present status at UCSB," *IEEE Transactions on Electron Devices,* vol. 48, pp. 552-559, 2001.

[33] C. Sun, J. Xu, A. Hagley, R. Surridge, and A. SPRING THORPE, "Electron mobility measurement in short-channel FET's using the cutoff frequency method," *IEEE Electron Device Letters,* vol. 11, pp. 382-384, 1990.

[34] B.-j. Moon, M. J. Helix, and S. Lee, "A new technique to determine the average low-field electron mobility in MESFET using C-V measurement," *IEEE Transactions on Electron Devices,* vol. 39, pp. 1982-1986, 1992.

[35] G. R. Valdivia, T. F. Ibáñez, J. Rodriguez-Tellez, A. T. Puente, and A. M. Sánchez, "Measurement of mobility in HEMT devices using high-order derivatives," *IEEE Transactions on Electron Devices,* vol. 51, pp. 1-7, 2004.

[36] H. Fukui, "Determination of the basic device parameters of a GaAs MESFET," *Bell System Technical Journal,* vol. 58, pp. 771-797, 1979.

[37] R. Menozzi, G. A. Umana-Membreno, B. D. Nener, G. Parish, G. Sozzi, L. Faraone*, et al.*, "Temperature-dependent characterization of AlGaN/GaN HEMTs: thermal and source/drain resistances," *IEEE Transactions on Device and Materials Reliability,* vol. 8, pp. 255-264, 2008.

[38] D. C. Look, "Schottky-barrier profiling techniques in semiconductors: Gate current and parasitic resistance effects," *Journal of Applied Physics,* vol. 57, pp. 377-383, 1985.

[39] N. Johansson, J. W. Mayer, and O. Marsh, "Technique used in Hall effect analysis of ion implanted Si and Ge," *Solid-State Electronics,* vol. 13, pp. 317-335, 1970.

[40] T. Lepkowski, R. DeJule, N. Tien, M. Kim, and G. Stillman, "Depletion corrections in variable temperature Hall measurements," *Journal of Applied Physics,* vol. 61, pp. 4808-4811, 1987.

[41] Y.-F. Wu, D. Kapolnek, J. P. Ibbetson, P. Parikh, B. P. Keller, and U. K. Mishra, "Very-high power density AlGaN/GaN HEMTs," *IEEE Transactions on Electron Devices,* vol. 48, pp. 586-590, 2001.

[42] Q. Chen, "Latest advances in gallium nitride HEMT modeling," in *12th IEEE International Conference on Solid-State and Integrated Circuit Technology (ICSICT),* 2014, pp. 1-4.

[43] M. Akita, S. Kishimoto, and T. Mizutani, "High-frequency measurements of AlGaN/GaN HEMTs at high temperatures," *IEEE Electron Device Letters,* vol. 22, pp. 376-377, 2001.

[44] S. C. Binari, K. Doverspike, G. Kelner, H. Dietrich, and A. Wickenden, "GaN FETs for microwave and high-temperature applications," *Solid-State Electronics,* vol. 41, pp. 177-180, 1997.

[45] R. Hickman, J. Van Hove, P. Chow, J. Klaassen, A. Wowchack, and C. Polley, "Uniformity and high temperature performance of X-band nitride power HEMTs fabricated from 2-inch epitaxy," *Solid-State Electronics,* vol. 42, pp. 2183-2185, 1998.

[46] S. Arulkumaran, T. Egawa, H. Ishikawa, and T. Jimbo, "High-temperature effects of AlGaN/GaN high-electron-mobility transistors on sapphire and semi-insulating SiC substrates," *Applied Physics Letters,* vol. 80, pp. 2186-2188, 2002.

[47] N. Adachi, Y. Tateno, S. Mizuno, A. Kawano, J. Nikaido, and S. Sano, "High temperature operation of AlGaN/GaN HEMT," in *IEEE International Microwave Symposium Digest,* 2005, pp. 507-510.

[48] A. Kalavagunta, S. Mukherjee, R. Reed, and R. Schrimpf, "Comparison between trap and self-heating induced mobility degradation in AlGaN/GaN HEMTs," *Microelectronics Reliability,* vol. 54, pp. 570-574, 2014.

[49] C. Lombardi, S. Manzini, A. Saporito, and M. Vanzi, "A physically based mobility model for numerical simulation of nonplanar devices," *IEEE Transactions on Computer-Aided Design of Integrated Circuits and Systems,* vol. 7, pp. 1164-1171, 1988.

[50] W. Tan, M. Uren, P. Fry, P. Houston, R. Balmer, and T. Martin, "High temperature performance of AlGaN/GaN HEMTs on Si substrates," *Solid-State Electronics,* vol. 50, pp. 511-513, 2006.

[51] D. Donoval, M. Florovič, D. Gregušová, J. Kováč, and P. Kordoš, "High-temperature performance of AlGaN/GaN HFETs and MOSHFETs," *Microelectronics Reliability,* vol. 48, pp. 1669-1672, 2008.

[52] D. Pandey, A. Bhattacharjee, and T. Lenka, "Study on temperature dependence scattering mechanisms and mobility effects in GaN and GaAs HEMTs," in *Physics of Semiconductor Devices*, ed: Springer, 2014, pp. 67-70.

[53] K. Takhar, U. Gomes, K. Ranjan, S. Rathi, and D. Biswas, "Temperature dependent DC characterization of InAlN/(AlN)/GaN HEMT for improved reliability," in *IOP Conference Series: Materials Science and Engineering*, 2015, pp. 012001-1-012001-4.

[54] T. Fink, D. D. Smith, and W. D. Braddock, "Electron-beam-induced damage study in GaAs-AlGaAs heterostructures as determined by magnetotransport characterization," *IEEE Transactions on Electron Devices,* vol. 37, pp. 1422-1425, 1990.

[55] A. Kalavagunta, A. Touboul, L. Shen, R. Schrimpf, R. Reed, D. Fleetwood, *et al.*, "Electrostatic mechanisms responsible for device degradation in AlGaN/AlN/GaN

HEMTs," in *9th European Conference on Radiation and Its Effects on Components and Systems (RADECS)*, 2007, pp. 1-7.

[56] X. Hu, A. P. Karmarkar, B. Jun, D. M. Fleetwood, R. D. Schrimpf, R. D. Geil, *et al.*, "Proton-irradiation effects on AlGaN/AlN/GaN high electron mobility transistors," *IEEE Transactions on Nuclear Science,* vol. 50, pp. 1791-1796, 2003.

[57] A. P. Karmarkar, B. Jun, D. M. Fleetwood, R. D. Schrimpf, R. Weller, B. D. White, *et al.*, "Proton irradiation effects on GaN-based high electron-mobility transistors with Si-doped Al x Ga 1-x N and thick GaN cap Layers," *IEEE Transactions on Nuclear Science,* vol. 51, pp. 3801-3806, 2004.

[58] B. White, M. Bataiev, S. Goss, X. Hu, A. Karmarkar, D. Fleetwood, *et al.*, "Electrical, spectral, and chemical properties of 1.8 MeV proton irradiated AlGaN/GaN HEMT structures as a function of proton fluence," *IEEE Transactions on Nuclear Science,* vol. 50, pp. 1934-1941, 2003.

[59] S.-i. Gozu, K. Watanabe, K. Ishibashi, and Y. Aoyagi, "Very shallow two-dimensional electron gas realized by In/sub x/Al/sub 1-x/As/InAs single quantum well grown on GaAs [111] A substrate," in *International Conference on Molecular Beam Epitaxy,* 2002, pp. 125-126.

[60] M. Gurusinghe, S. Davidsson, and T. Andersson, "Two-dimensional electron mobility limitation mechanisms in $Al_xGa_{1-x}N$/GaN heterostructures," *Physical Review B,* vol. 72, pp. 045316-1-045316-11, 2005.

[61] M. Tischler, B. Parker, J. DeGelormo, T. Jackson, F. Cardone, and M. Goorsky, "Thermal stability of MBE-grown Si-doped InGaAs/InAlAs heterostructures," in *Third International Conference on Indium Phosphide and Related Materials,* 1991, pp. 602-605.

[62] G. Umana-Membreno, T. Fehlberg, S. Kolluri, D. Brown, G. Parish, B. Nener, *et al.*, "Anisotropic two-dimensional electron gas transport in N-polar GaN/AlGaN heterostructures grown on vicinal substrates," in *Conference on Optoelectronic and Microelectronic Materials and Devices (COMMAD)*, 2010, pp. 195-196.

[63] P. B. Shah, D. D. Smith, T. E. Griffin, K. Jones, and S. T. Sheppard, "Carrier transport related analysis of high-power AlGaN/GaN HEMT structures," *IEEE Transactions on Electron Devices,* vol. 47, pp. 308-312, 2000.

[64] M. Miyoshi, A. Imanish, H. Ishikawa, T. Egawa, K. Asai, M. Mouri, *et al.*, "High performance AlGaN/AlN/GaN HEMTs grown on 100-mm-diameter epitaxial

AlN/sapphire templates by MOVPE," in *IEEE Compound Semiconductor Integrated Circuit Symposium,* 2004, pp. 193-196.

[65] L. Hsu and W. Walukiewicz, "Electron mobility in $Al_xGa_{1-x}N$/GaN heterostructures," *Physical Review B,* vol. 56, pp. 1520-1528, 1997.

[66] D. Zanato, S. Gokden, N. Balkan, B. Ridley, and W. Schaff, "The effect of interface-roughness and dislocation scattering on low temperature mobility of 2D electron gas in GaN/AlGaN," *Semiconductor science and technology,* vol. 19, pp. 427-432, 2004.

[67] S. Lisesivdin, S. Acar, M. Kasap, S. Ozcelik, S. Gokden, and E. Ozbay, "Scattering analysis of 2DEG carrier extracted by QMSA in undoped Al0. 25Ga0. 75N/GaN heterostructures," *Semiconductor science and Technology,* vol. 22, pp. 543-548, 2007.

[68] A. Pérez-Tomás and A. Fontserè, "AlGaN/GaN hybrid MOS-HEMT analytical mobility model," *Solid-State Electronics,* vol. 56, pp. 201-206, 2011.

[69] X. Wang, C. Wang, G. Hu, H. Xiao, C. Fang, J. Wang, *et al.*, "MOCVD-grown high-mobility Al 0.3 Ga 0.7 N/AlN/GaN HEMT structure on sapphire substrate," *Journal of Crystal Growth,* vol. 298, pp. 791-793, 2007.

[70] Y. Takahashi, H. Hasegawa, Y. Takahashi, and T. Inabe, "Hall mobility in tin iodide perovskite CH 3 NH 3 SnI 3: evidence for a doped semiconductor," *Journal of Solid State Chemistry,* vol. 205, pp. 39-43, 2013.

[71] S. Vitanov, V. Palankovski, S. Maroldt, and R. Quay, "High-temperature modeling of AlGaN/GaN HEMTs," *Solid-State Electronics,* vol. 54, pp. 1105-1112, 2010.

[72] M. Manfra, N. Weimann, J. Hsu, L. Pfeiffer, K. West, and R. Molnar, "Comparison of high mobility AlGaN/GaN heterostructures grown by MBE on HVPE GaN templates and directly nucleated on sapphire," in *International Conference on Molecular Beam Epitaxy,* 2002, pp. 231-232.

[73] V. Karavolas, M. Smith, T. Fromhold, P. Butcher, B. Mulimani, B. Gallagher, *et al.*, "The effect of interface roughness scattering and background impurity scattering on the thermopower of a 2DEG in a Si MOSFET," *Journal of Physics: Condensed Matter,* vol. 2, pp. 10401-10410, 1990.

[74] S. Dimitrijev, *Principles of semiconductor devices*: Oxford university press, 2012.

[75] H. Morkoç, *Nitride Semiconductor Devices: Fundamentals and Applications*: John Wiley & Sons, 2013.

[76] B. Van Zeghbroeck, "Semiconductor Fundamentals," *Principles of Semiconductor Devices.[Online]. Available: http://ecee. colorado. edu/~ bart/book/book/chapter2/ch2_3. htm,* 2011.

[77] U. V. Bhapkar and M. S. Shur, "Monte Carlo calculation of velocity-field characteristics of wurtzite GaN," *Journal of Applied Physics,* vol. 82, pp. 1649-1655, 1997.

[78] S. J. Pearton, R. Deist, F. Ren, L. Liu, A. Y. Polyakov, and J. Kim, "Review of radiation damage in GaN-based materials and devices," *Journal of Vacuum Science & Technology A,* vol. 31, pp. 050801-1-050801-16, 2013.

[79] A. Y. Polyakov, S. Pearton, P. Frenzer, F. Ren, L. Liu, and J. Kim, "Radiation effects in GaN materials and devices," *Journal of Materials Chemistry C,* vol. 1, pp. 877-887, 2013.

[80] W. Hu, X. Chen, Z. Quan, C. Xia, W. Lu, and P. Ye, "Self-heating simulation of GaN-based metal-oxide-semiconductor high-electron-mobility transistors including hot electron and quantum effects," *Journal of Applied Physics,* vol. 100, pp. 074501-1-074501-9, 2006.

[81] M. S. Shur, R. Gaska, and A. Bykhovski, "GaN-based electronic devices," *Solid-State Electronics,* vol. 43, no. 8, pp. 1451-1458, 1999.

[82] I. Daumiller, C. Kirchner, M. Kamp, K. Ebeling, and E. Kohn, "Evaluation of the temperature stability of AlGaN/GaN heterostructure FETs," *IEEE Electron Device Letters,* vol. 20, pp. 448-450, 1999.

[83] T. Mizutani and K. Maezawa, "Temperature dependence of high-frequency performance of AlGaAs/InGaAs pseudomorphic HEMT's," *IEEE Electron Device Letters,* vol. 13, pp. 8-10, 1992.

[84] M.-S. Lin and M.-S. Lin, "The classical versus the quantum mechanical model of mobility degradation due to the gate field in MOSFET inversion layers," *IEEE Transactions on Electron Devices,* vol. 32, pp. 700-710, 1985.

[85] A. Rothwarf, "A new quantum mechanical channel mobility model for Si MOSFET's," *IEEE Electron Device Letters,* vol. 8, pp. 499-502, 1987.

[86] M.-S. Liang, J. Y. Choi, P.-K. Ko, and C. Hu, "Inversion-layer capacitance and mobility of very thin gate-oxide MOSFET's," *IEEE Transactions on Electron Devices,* vol. 33, pp. 409-413, 1986.

[87] C. Kittel, *Introduction to solid state physics*: Wiley, 2005.

[88] A. K. Singh, *Electronic devices and integrated circuits*: PHI Learning Pvt. Ltd., 2011.

[89] D. Ferry, *Semiconductor transport*: CRC Press, 2000.

[90] H. Ibach and H. Lüth, *Solid-state physics: an introduction to principles of materials science*: springer Berlin, 2003.

[91] A. Bulusu and D. Walker, "Review of electronic transport models for thermoelectric materials," *Superlattices and Microstructures,* vol. 44, pp. 1-36, 2008.

[92] P. Bhattacharya, *Semiconductor optoelectronic devices*: Prentice-Hall, Inc., 1994.

[93] Y. Takeda and T. Pearsall, "Failure of Matthiessen's rule in the calculation of carrier mobility and alloy scattering effects in $Ga_{0.47}In_{0.53}As$," *Electronics Letters,* vol. 17, pp. 573-574, 1981.

[94] J. Schrieffer, "Effective carrier mobility in surface-space charge layers," *Physical Review,* vol. 97, pp. 641-646, 1955.

[95] Y. Peter and M. Cardona, *Fundamentals of semiconductors: physics and materials properties*: Springer Science & Business Media, 2010.

[96] D. R. Hang, C.-T. Liang, C. F. Huang, Y. H. Chang, and Y. F. Chen, "Effective mass of two dimensional electron gas in an $Al_{0.2}Ga_{0.8}N$/GaN heterojunction," *Applied Physics Letters*, vol. 79, no. 1, pp. 66-68, 2001.

[97] T. Hofmann, P. Kühne, S. Schöche, Jr-Tai Chen, U. Forsberg, E. Janzén, N. Ben Sedrine, C. M. Herzinger, J. A. Woollam, M. Schubert, and V. Darakchieva, "Temperature dependent effective mass in AlGaN/GaN high electron mobility transistor structures," *Applied Physics Letters*, vol. 101, pp. 192102-1- 192102-4, 2012.

[98] A. M. Kurakin, S. A. Vitusevich, S. V. Danylyuk, H. Hardtdegen, N. Klein, Z. Bougrioua, A. V. Naumov, and A. E. Belyaev, "Quantum confinement effect on the effective mass in two-dimensional electron gas of AlGaN/GaN heterostructures," *Journal of Applied Physics*, vol. 105, 073703-1-073703-6, 2009.

[99] B. F. Spencer, W. F. Smith, M. T. Hibberd, P. Dawson, M. Beck, A. Bartels, I. Guiney, C. J. Humphreys, and D. M. Graham, "Terahertz cyclotron resonance spectroscopy of an AlGaN/GaN heterostructure using a high-field pulsed magnet and

an asynchronous optical sampling technique," *Applied Physics Letters*, vol. 108, no. 21, pp. 212101-1-212101-4, 2016.

[100] S. Khandelwal, S. Ghosh, Y. Chauhan, B. Iniguez, and T. Fjeldly, "Surface-Potential-Based RF Large Signal Model for Gallium Nitride HEMTs," in *IEEE Compound Semiconductor Integrated Circuit Symposium (CSICS),* 2015, pp. 1-4.

[101] S. D. Mertens, "Status of the GaN HEMT standardization effort at the compact model coalition," in *IEEE Compound Semiconductor Integrated Circuit Symposium (CSICS),* 2014, pp. 1-4.

[102] C. Arnaboldi, A. Cetronio, C. Guazzoni, A. Longoni, and G. Pessina, "Feasibility of a fully integrated HEMT based charge amplifier: design and experiment," in *IEEE Nuclear Science Symposium Conference Record,* 2000, pp. 9/54-9/58 vol. 2.

[103] N. DasGupta and A. DasGupta, "A new SPICE MOSFET Level 3-like model of HEMT's for circuit simulation," *IEEE Transactions on Electron Devices,* vol. 45, pp. 1494-1500, 1998.

[104] P. Tanner, S. Dimitrijev, H. Amini Moghadam, A. Aminbeidokhti, and J. S. Han, "Selection of SPICE Parameters and Equations for Effective Simulation of Circuits with 4H-SiC Power MOSFETs," *Materials Science Forum*, vol. 778-780, pp. 997-1000, 2014.

[105] F. S. Correra and E. Camargo, "18 GHz reverse channel HEMT oscillator," in *IEEE International Microwave Symposium Digest,* 1990, pp. 423-426.

[106] M. Okamoto, G. Toyoda, E. Hiraki, T. Tanaka, T. Hashizume, and T. Kachi, "Loss evaluation of an AC-AC direct converter with a new GaN HEMT SPICE model," in *IEEE Energy Conversion Congress and Exposition (ECCE),* 2011, pp. 1795-1800.

[107] C. G. Diskus, C. Bergamaschi, M. Schefer, W. Patrick, B.-U. Klepser, and W. Baechtold, "Approach for developing a large signal model of a 150 GHz HEMT," in *Third International Workshop on Integrated Nonlinear Microwave and Millimeterwave Circuits,* 1994, pp. 133-137.

[108] M. Basak, A. Biswas, and P. Basu, "Analysis of a radio frequency transimpendance amplifier based on a δ-doped AlInAs-GaInAs HEMT and its performance optimization," in *International Conference on Information and Communication Technology in Electrical Sciences (ICTES),* 2007, pp. 879-883.

[109] J. Zamanillo, H. Ingelmo, C. Perez-Vega, and A. Mediavilla, "A realistic large-signal microwave PHEMT transistors model for SPICE," in *European Gallium Arsenide and Other Semiconductor Application Symposium (EGAAS)*, 2005, pp. 453-456.

[110] H. R. Yeager and R. W. Dutton, "Circuit simulation models for the high electron mobility transistor," *IEEE Transactions on Electron Devices,* vol. 33, pp. 682-692, 1986.

[111] K. Peng and E. Santi, "Characterization and modeling of a gallium nitride power HEMT," in *IEEE Energy Conversion Congress and Exposition (ECCE),* 2014, pp. 113-120.

[112] J. Staudinger, M. Miller, M. Golio, B. Beckwith, and D. Halchin, "An accurate HEMT large signal model usable in SPICE simulators," in *IEEE MTT-S International Microwave Symposium Digest,* 1991, pp. 99-102.

[113] S. Ghosh, K. Sharma, S. Agnihotri, Y. Chauhan, S. Khandelwal, T. Fjeldly*, et al.*, "Modeling of temperature effects in a surface-potential based ASM-HEMT model," in *IEEE 2nd International Conference on Emerging Electronics (ICEE),* 2014, pp. 1-4.

[114] D. Delagebeaudeuf and N. T. Linh, "Metal-(n) AlGaAs-GaAs two-dimensional electron gas FET," *IEEE Transactions on Electron Devices,* vol. 29, pp. 955-960, 1982.

[115] K. Lee, M. S. Shur, T. J. Drummond, and H. Morkoç, "Parasitic MESFET in (Al, Ga) As/GaAs modulation doped FET's and MODFET characterization," *IEEE Transactions on Electron Devices,* vol. 31, pp. 29-35, 1984.

[116] S. J. Mahon, D. J. Skellern, and F. Green, "A technique for modelling S-parameters for HEMT structures as a function of gate bias," *IEEE Transactions on Microwave Theory and Techniques,* vol. 40, pp. 1430-1440, 1992.

[117] G. Qu and A. Parker, "Continuous HEMT model for SPICE," *Electronics Letters,* vol. 32, pp. 1321-1323, 1996.

CHAPTER 3: A Method for Extraction of Electron Mobility in Power HEMTs

This chapter is the following paper:

- **Amirhossein Aminbeidokhti**, Sima Dimitrijev, Jisheng Han, Xiangang Xu, Chengxin Wang, Shuang Qu, Hamid Amini Moghadam, Philip Tanner, David Massoubre, Glenn Walker, "A method for extraction of electron mobility in power HEMTs," *Superlattices and Microstructures*, vol. 85, pp. 543–550, 2015.

Abstract 74

Introduction 75

Extraction method 77

  The new approach 77

  Resistance equations 78

  Extraction of 2DEG mobility under the gate 81

Experimental demonstrations 85

  Device fabrication 85

  Resistances measurements 86

  Extraction of effective and field-effect 2DEG mobilities 87

Conclusion 90

Acknowledgement 90

References 91

A Method for Extraction of Electron Mobility in Power HEMTs

Amirhossein Aminbeidokhti [a,b,*], Sima Dimitrijev [a,b], Jisheng Han [a], Xiangang Xu [c], Chengxin Wang [d], Shuang Qu [d], Hamid Amini Moghadam [a,b], Philip Tanner [a], David Massoubre [a], and Glenn Walker [a]

[a] Queensland Micro- and Nanotechnology Centre (QMNC), Griffith University, Nathan, Queensland 4111, Australia

[b] Griffith School of Engineering, Griffith University, Nathan, Queensland 4111, Australia

[c] Institute of Crystal Materials, Shandong University, 27 Shanda Nanlu, Jinan 250100, P.R. China

[d] Shandong Inspur Huaguang Optoelectronics Co., Ltd., Jinan 250101, P.R. China

Manuscript submitted to:
Superlattice and Microstructures
Date: 25 May 2015

[*] Corresponding author: Email: amirhossein.aminbeidokhti@griffithuni.edu.au

Tel: +61 48 1135 810

Abstract- **In this paper, a novel method for extraction of electron mobility in the two-dimensional electron gas (2DEG) under the gate of power HEMTs is presented. Using this method enables the potential impact of the gate metal and the gate voltage on electron mobility in the 2DEG under the gate to be measured without the error due to the resistive regions outside the gate, which are the gate-to-source and gate-to-drain regions. The application of the new method was demonstrated by measurements on fabricated circular HEMTs.**

Index Terms- Power high-electron-mobility transistor (HEMT), two-dimensional electron gas (2DEG) mobility, mobility extraction method.

1. INTRODUCTION

High-electron-mobility transistors (HEMTs) are well-established semiconductor devices, which utilize the formation of two-dimensional electron gas (2DEG) at the heterojunction between two semiconductor layers. When implemented with $Al_xGa_{1-x}N$–GaN heterojunctions, HEMTs are considered as very promising devices for power applications [1]. HEMT is the most suitable device structure to utilize the unique material properties of GaN: high breakdown field, high electron mobility in the 2DEG, and high-temperature operating capabilities [2].

Electron mobility in the 2DEG is the key parameter for the final HEMT performance in the case of power applications. Unlike the gate in metal–oxide–semiconductor field-effect transistors (MOSFETs), which extends from the source to the drain contacts [3, 4], the gate in HEMTs splits the device in three sections: source to gate, drain to gate, and the section underneath the gate. As illustrated in Fig. 1, the resistances of the 2DEG in these three sections are different. The resistances of the 2DEG sections outside the gate are constant and can be modeled by fixed resistors. However, the 2DEG resistance under the gate depends on the gate voltage, which is modeled by the channel resistance of a field-effect transistor (FET). Given that these resistances depend on both the mobility of electrons and the density of electrons in the 2DEG, it is important to separate the mobility of electrons in the field-effect and resistive sections.

In several reports on mobility measurements in HEMTs [5-7], the 2DEG between the source and the drain was considered as a single section, analogously to the channel between the source and drain in a MOSFET. Therefore, the 2DEG mobilities outside and under the gate were not separated, which means that these results correspond to an average mobility between the source and the drain. A method to separate the source-to-drain channel into field-effect (under the gate) and resistive (outside the gate) sections was proposed by Fukui for GaAs

MESFETs [8]. This method was applied to GaN HEMTs, but it was found that the extracted resistance under the gate was highly sensitive to the threshold-voltage values [9]. To solve this problem, a modified version of Fukui's method was presented [9]. However, this technique could not distinguish between the value of the applied gate-to-source voltage and the voltage between the gate and the 2DEG at the source end of the gate. In other words, the voltage across the gate-to-source section of the 2DEG was not removed from the gate voltage that controls the 2DEG section under the gate.

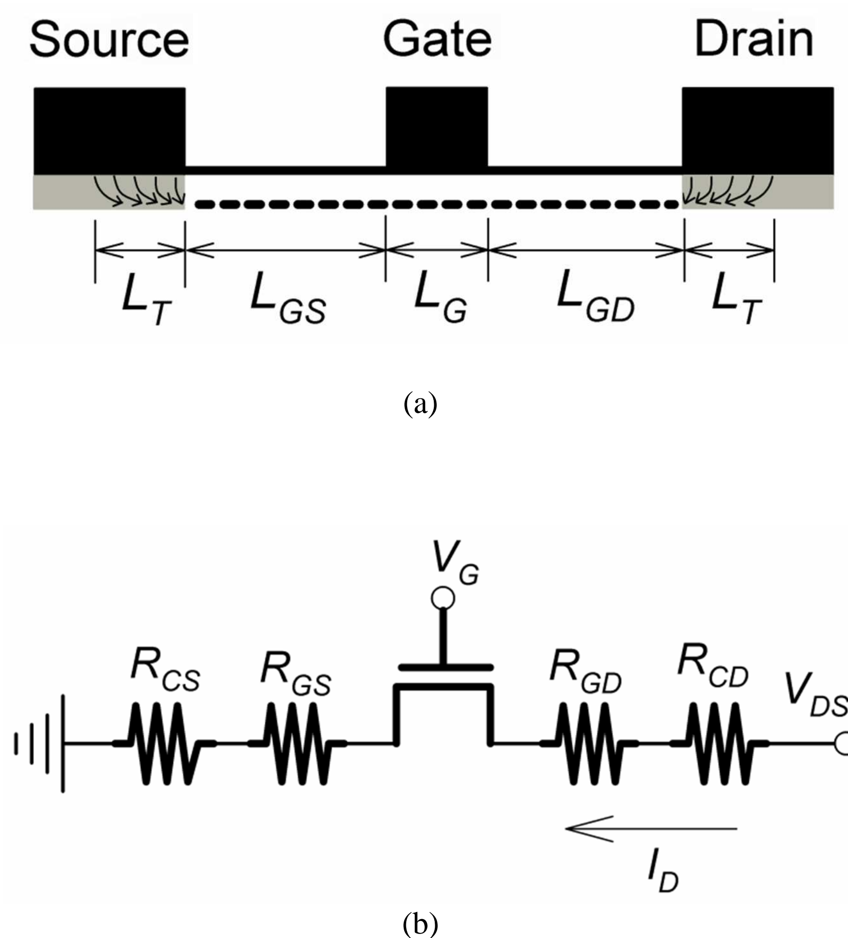

Fig. 1. a) Schematic cross sectional view of a HEMT; b) equivalent circuit showing the resistive sections and the field-effect section under the gate.

In this paper, we present a different method to extract the 2DEG mobility under the gate for power HEMTs. The new method also relies on a separation of the 2DEG between the source

and the drain into sections under and outside the gate to utilize the gradual-channel approximation (MOSFET-like equation) for the section under the gate. However, the new method combines the MOSFET-like equation for the 2DEG section under the gate with 2DEG resistances outside the gate in a way that enables complete separation of the outside-gate resistances from the extracted 2DEG mobility under the gate.

2. EXTRACTION METHOD

2.1 The New Approach

The approach that leads to the new extraction method can be explained by a reference to the HEMT cross-section and equivalent circuit, shown in Figs. 1 (a) and (b), respectively. As can be seen, the 2DEG under the gate is modeled by a field-effect transistor, which is consistent with the fact that the gate voltage impacts the 2DEG and may impact the electron mobility. This section of the 2DEG is analogous to the channel of electrons in a MOSFET, which means that MOSFET-type equations can be used to define the 2DEG mobility.

The 2DEG sections outside the gate are modeled by gate-source (R_{GS}) and gate-drain resistances (R_{GD}) to represent the fact that the resistances of these sections are constant and independent from the gate voltage.

The final set of components in the equivalent circuit are the source and drain contact resistances, R_{CS} and R_{CD}. The contact resistances in HEMTs are proportional to the transfer length (L_T). The transfer length is smaller than the length of the corresponding metal–semiconductor contact because of current crowding at the edge of the contact [10]. Basically, the transfer length is the length within which the current transfers from the metal to the semiconductor.

The equations for the described components of the equivalent circuit are presented in the following sections.

2.2 Resistance Equations

The resistance of a resistor can be expressed as

$$R = R_S n \tag{1}$$

where R_S is the sheet resistance (resistance per unit square), which incorporates all technological parameters (including mobility), and *n* is the effective number of squares, which accounts for the impact of geometric-design parameters. In the case of a basic resistor with length *L* and width *W*, the effective number of squares is:

$$n = \frac{L}{W} \tag{2}$$

HEMTs are frequently designed in closed geometry, utilizing circular or square shapes, as illustrated in in Figs. 2 (a) and (b), respectively. This design approach enables a better control of leakage currents due to the existence of 2DEG in the areas that are not controlled by a gate. Therefore, it is useful to present the resistance equations for these types of HEMTs. The parameter that changes with the design geometry is the effective number of squares. The equations for the effective number of squares for the basic, circular, and square HEMTs, as applied to the source (n_S), drain (n_D), gate (n_G), and contact (n_C) regions, are listed in Table. I.

The sheet resistance of the 2DEG sections outside the gate is constant and does not depend on gate voltage. Labeling this constant sheet resistance by R_{S-O}, the resistances of the gate-to-source (R_{GS}) and gate-to-drain (R_{GD}) sections are given by:

$$\begin{aligned} R_{GS} &= R_{S-O} n_S \\ R_{GD} &= R_{S-O} n_D \end{aligned} \tag{3}$$

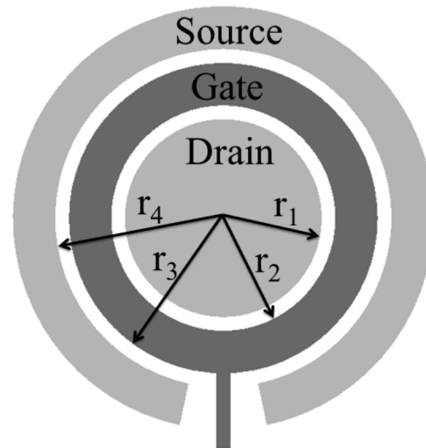

(a)

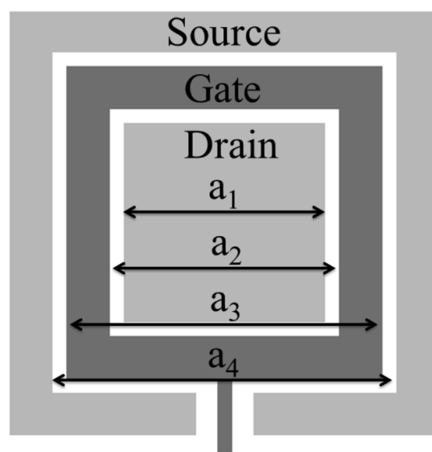

(b)

Fig. 2. Top view of a) circular HEMT and b) square HEMT.

Similarly, the contact resistance for source and drain contacts (R_C) is:

$$R_C = R_{CS} + R_{CD} = R_{S-C} n_C \tag{4}$$

where R_{S-C} is the sheet resistance of the contacts.

The sheet resistance of the 2DEG section under the gate depends on the gate voltage. This variable sheet resistance is labeled by r_{S-U}, which is then multiplied by the effective number of squares for the gate to obtain the variable resistance of the 2DEG under the gate (r_G):

TABLE I
EFFECTIVE NUMBER OF SQUARES FOR THE BASIC, CIRCULAR, AND SQUARE HEMTS

Symbol	Quantity	Basic HEMT	Circular HEMT: r_1- the drain contact radius r_2- the inner radius of the gate ring r_3- the outer radius of the gate ring r_4- the inner radius of the source ring	Square HEMT : a_1 - the drain length a_2- the inner length of the gate a_3- the outer length of the gate a_4- the inner length of the source
n_S	Effective number of squares between the gate and source	$\frac{L_{GS}}{W}$	$\frac{1}{2\pi}\left(Ln\left(\frac{r_4}{r_3}\right)\right)$	$\frac{L_{SG}}{2(a_3+a_4)}$
n_D	Effective umber of squares between the gate and drain	$\frac{L_{GD}}{W}$	$\frac{1}{2\pi}\left(Ln\left(\frac{r_2}{r_1}\right)\right)$	$\frac{L_{DG}}{2(a_1+a_2)}$
n_G	Effective number of squares for the gate	$\frac{L_G}{W}$	$\frac{1}{2\pi}\left(Ln\left(\frac{r_3}{r_2}\right)\right)$	$\frac{L_G}{2(a_2+a_3)}$
n_C	Effective number of squares for source and drain ohmic contacts	$2\frac{L_T}{W}$	$\frac{L_T}{2\pi}\left(\frac{1}{r_1}+\frac{1}{r_4}\right)$	$\frac{L_T}{4a_1}+\frac{L_T}{4a_4}$

$$r_G = r_{S-U} n_G \tag{5}$$

These resistances are used in the mobility equations that are presented in the following section.

2.3 Extraction of 2DEG Mobility Under the Gate

Based on the new approach, which considers several sections between the source and drain contacts, the applied drain-to-source voltage (V_{DS}) is the sum of the voltages across these sections:

$$V_{DS}=V_{2DEG-U}+V_{R-GS}+V_{R-GD}+V_{R-C}=(r_G+R_{GS}+R_{GD}+R_C)I_D \quad (6)$$

In Eq. 6, V_{2DEG-U} is the voltage across the 2DEG under the gate, V_{R-GS} and V_{R-GD} are the voltages across the resistive gate-to-source and gate-to-drain sections of the 2DEG, respectively, which have been shown in Fig. 3.

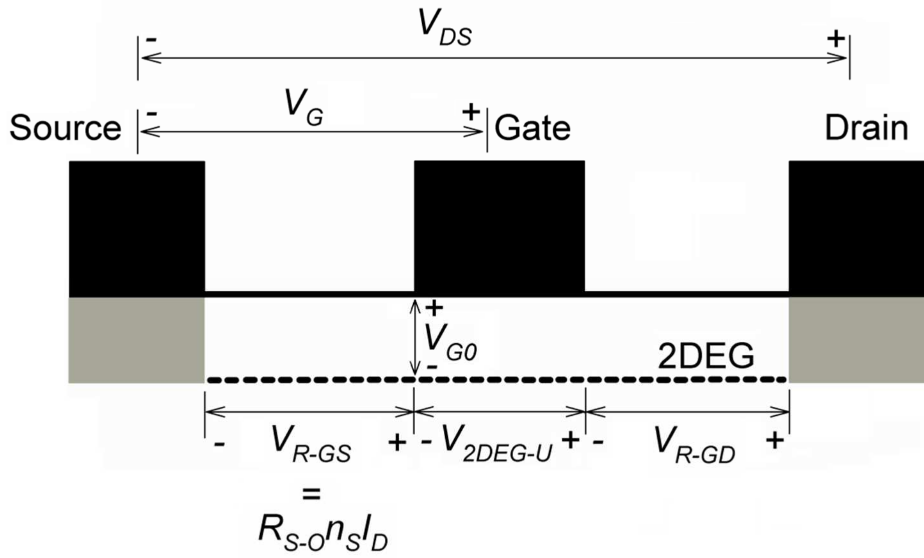

Fig. 3. Potential difference demonstration on cross section of the HEMT.

Moreover, V_{R-C} is the voltage across the contact resistances of the source and the drain, and I_D is the drain current, which flows through the series connection of resistances.

The variable resistance of the 2DEG under the gate (r_G) depends on both the electron density and the electron mobility, which is the mobility parameter that we wish to extract. In this field-effect section, MOSFET-like equations can be applied to relate the variable resistance to the 2DEG mobility under the gate (μ_n). The standard MOSFET equations do provide a model for the dependence of the drain current on the variable gate-to-channel voltage from the source-end toward the drain-end of the channel. More accurate modeling of this impact, such as in the paper by S. Khandelwal et al. [11], is possible but it leads to much more complex equations than the standard MOSFET equations. These equations are not necessary for mobility

extraction, which is based on measurements with very small drain-to-source voltages. According to the drain current equation for a MOSFET, we have:

$$I_D = \mu_n C_d \frac{W}{L}(V_{G0} - V_T)V_{2DEG-U} \quad (7)$$

where $C_d = \frac{\varepsilon_d}{t_d}$ is the dielectric capacitance per unit area, which is determined by the permittivity (ε_d) and the thickness (t_d) of the material between the 2DEG and the gate metal ($Al_xGa_{1-x}N$ in the case of GaN-based HEMTs), V_T is the threshold voltage, and V_{G0} is the voltage between the gate electrode and the 2DEG. In Eq. (7), $\frac{L}{W}$ is equivalent to the number of squares, which can be replaced by the effective number of squares (n_G) to make Eq. (7) applicable to closed-geometry designs:

$$I_D = \mu_n C_d \frac{1}{n_G}(V_{G0} - V_T)V_{2DEG-U} \quad (8)$$

The voltage between the gate electrode and the 2DEG at the source end of the gate (V_{G0}) is equal to the difference between the applied gate-to-source voltage (V_G) and the voltage drop across the gate-to-source resistive segment of the 2DEG:

$$V_{G0} = V_G - R_{S-O} n_S I_D \quad (9)$$

Fig. 3 clarifies the meaning of these parameters. It should be noted that there is no distinction between the V_{G0} and the variable gate-to-2DEG voltage toward the drain end of the gate (V_{2DEG-U}). V_{G0} in the standard MOSFET-type equations used in this paper for gate section is equivalent to the constant gate-to-source voltage in MOSFET theory, which is different from the variable gate-to-channel voltage toward the drain.

Therefore, the variable 2DEG resistance under the gate, which is dependent on the gate voltage, can be expressed as:

$$r_G = \frac{V_{2DEG-U}}{I_D} = \frac{n_G}{\mu_n C_d (V_G - R_{S-O} n_S I_D - V_T)} \tag{10}$$

With this, the equation for applied drain-to-source voltage becomes:

$$V_{DS} = (R_{S-O} n_S + R_{S-O} n_D + R_{S-C} n_C) I_D + n_G \frac{I_D}{\mu_n C_d (V_G - R_{S-O} n_S I_D - V_T)} \tag{11}$$

which leads to the following equation for the drain current:

$$I_D = \frac{V_{DS}}{(R_{S-O} n_S + R_{S-O} n_D + R_{S-C} n_C) + \frac{n_G}{\mu_n C_d (V_G - R_{S-O} n_S I_D - V_T)}} \tag{12}$$

Applying the established mobility extraction techniques for MOSFETs [12] to Eq. (12)—the derived equation for HEMT current—the 2DEG mobility under the gate can be extracted. There are two different mobility definitions, which result from two common techniques for the MOSFET mobility extraction: effective (μ_{eff}) and field-effect (μ_{FE}) mobility. The first technique utilizes measurements of output conductance (g_O), whereas the second technique utilizes measurements of the transconductance (g_m). In either case, the measurements are performed at low drain voltages (V_{DS} < 100 mV), where the channel charge between the source and drain is fairly uniform. Both approaches, leading to extraction of both the effective and the field-effect mobility values, can be applied in the case of HEMTs.

The output conductance,

$$g_O = \frac{\partial I_D}{\partial V_{DS}} \tag{13}$$

can be obtained as the first derivative of I_D with respect to V_{DS} in Eq. (12):

$$g_O = \frac{1}{\left(R_{S-O}n_S + R_{S-O}n_D + R_{S-C}n_C\right) + \dfrac{n_G}{\mu_{eff}C_d\left(V_G - R_{S-O}n_S I_D - V_T\right)}} \tag{14}$$

It should be noted that the generic mobility symbol μ_n, which appears in Eq. (12), has been changed to μ_{eff} in Eq. (14) to indicate that this is the effective mobility, which is determined from measured output conductance of a HEMT. Expressing μ_{eff} in terms of g_O, leads to the final equation for the effective mobility:

$$\mu_{eff} = \frac{n_G}{C_d\left(\dfrac{1}{g_O} - \left(R_{S-O}n_S + R_{S-O}n_D + R_{S-C}n_C\right)\right)\left(V_G - R_{S-O}n_S I_D - V_T\right)} \tag{15}$$

The extraction of the effective mobility by this equation does not require any assumptions for the dependence of the mobility on the gate voltage. Therefore, any experimentally observed dependence of the effective mobility on the gate voltage will be free from errors due to any inconsistent assumptions. However, just as in the case of MOSFETs, the equation for the effective mobility includes the threshold voltage as unknown parameter, whose somewhat arbitrary definition and independent extraction can impact the value of effective mobility. In order to eliminate the impact of the threshold-voltage value on the mobility, the field-effect mobility (μ_{FE}) is obtained from measured transconductance:

$$g_m = \frac{\partial I_D}{\partial V_G} \tag{16}$$

The HEMT equation for the transconductance can be obtained as the first derivative of I_D with respect to V_G in Eq. (12):

$$g_m = \frac{1}{\dfrac{n_G V_{DS}}{\mu_{FE} C_d \left(V_{DS} - \left(R_{S-O} n_S + R_{S-O} n_D + R_{S-C} n_C\right) I_D\right)^2} + R_{S-O} n_S} \tag{17}$$

In this case, the generic mobility symbol μ_n in Eq. (12) has been changed to μ_{FE} in Eq. (17) to indicate that this is the field-effect mobility. Expressing μ_{FE} in terms of measured g_m leads to the final equation for the field-effect mobility:

$$\mu_{FE} = \frac{n_G V_{DS}}{C_d \left(\dfrac{1}{g_m} - R_{S-O} n_S\right)\left(V_{DS} - \left(R_{S-O} n_S + R_{S-O} n_D + R_{S-C} n_C\right) I_D\right)^2} \tag{18}$$

3. EXPERIMENTAL DEMONSTRATION

3.1 Device Fabrication

Typical circular HEMTs were fabricated to provide measurements for the demonstration of the new method. Undoped AlGaN/GaN layers grown on a SiC substrate were employed for the fabrication of the HEMTs. Source and drain ohmic contacts were obtained by sputtering Ti/Al/Ni over a 25-nm-thick $Al_{0.22}Ga_{0.78}N$ and by annealing at 800°C for 30 seconds in N_2 ambient. The HEMT gates were formed by Ni sputtering. The gate-to-drain and gate-to-source distances of the measured devices were 5 µm, whereas the gate length was 15 µm.

In addition to HEMTs, test structures for determination of the contact resistances by the transmission-line method (TLM) [13, 14] were fabricated on the same chip. In this structure, there are several electrodes with various distances.

Figure 4 illustrates the typical transfer and output characteristics of the HEMT, measured by Agilent power device analyzer B1505A. As can be seen in the figure, the threshold voltage, V_T, is -2.2 V.

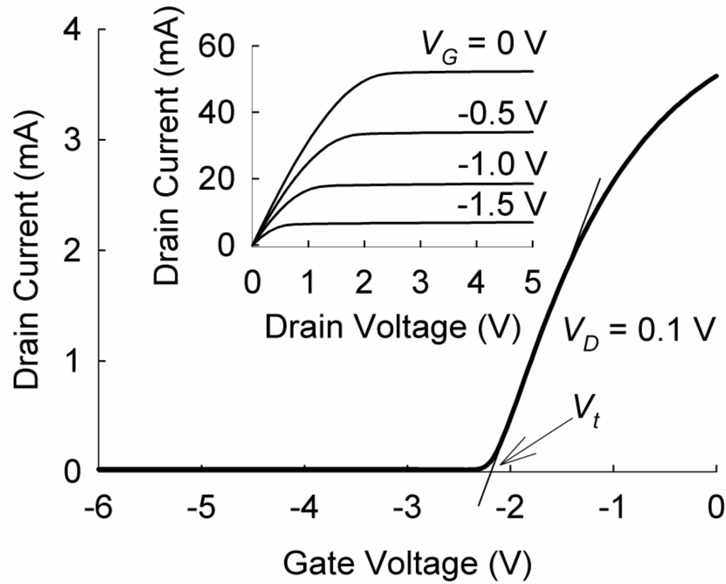

Fig. 4. Transfer and output characteristics of the circular HEMT.

3.2 Resistances Measurements

Figure 5 shows the measured resistances between differently spaced electrodes of the TLM structure. The effective number of squares in the TLM structures is $n_C = \frac{2L_T}{W}$, as shown in Table I. According to Eq. (4), the contact resistance of the source and the drain contacts is $R_C = 2R_{S-C}\frac{L_T}{W}$. This resistance is equal to 36 Ω, as illustrated in Fig. 5. Based on this value and the TLM width, which was 200 μm, the width independent value $R_{S-C}L_T$ is determined as $R_{S-C}L_T = R_C W = 18\times200 = 3600$ Ω.μm. This $R_{S-C}L_T$ value is used in Eqs. (15) and (18) with n_C

for the circular HEMT design (as shown in Table I).

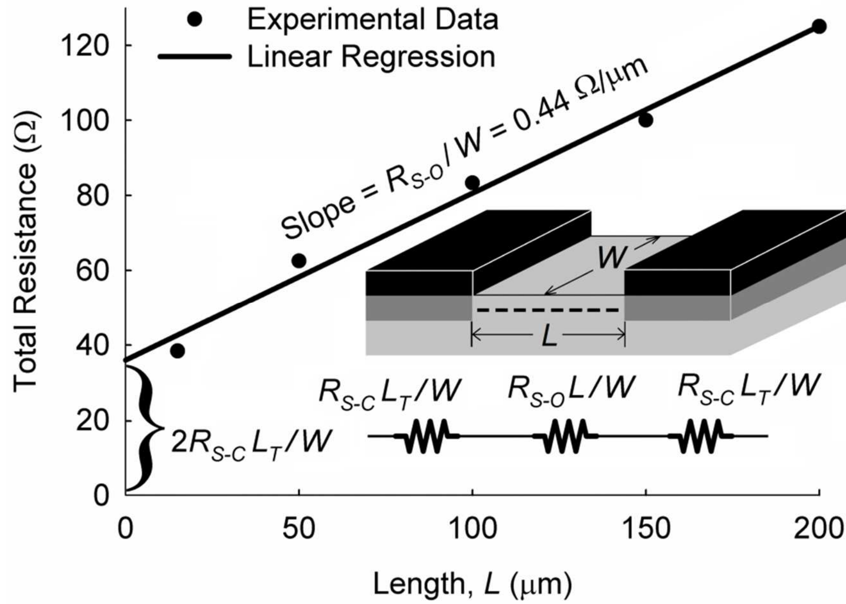

Fig. 5. Extraction of the contact resistance and the sheet resistance of 2DEG outside the gate from the resistance measurements of the transmission-line test structures.

In addition to the value of $R_{S-C}L_T$, the results shown in Fig. 5 are used to determine the sheet resistance of the 2DEG outside the gate, R_{S-O}. As indicated in the figure, this sheet resistance is obtained from the slope of the measured TLM resistances: R_{S-O}= 0.44×200=88 Ω/□.

3.3 Extraction of Effective and the Field-Effect 2DEG Mobilities

The fabricated circular HEMTs were measured to obtain the experimental values for the output conductance (g_O) and the transconductance (g_m). These values were used in conjunction with the values for $R_{S-C}L_T$ and R_{S-O}, obtained from the TLM structures, to determine the effective and the field-effect mobilities, according to Eqs. (15) and (18), respectively. The obtained results are shown in Fig. 6, along with the Hall mobility value that

was determined by Hall-effect measurement on separately fabricated Hall sample. It should be noted that electron mobility can be measured by the Hall-effect method, using samples that only require four ohmic contacts [12], [15]. This method can be used to determine the sheet resistance, the carrier density, and the mobility of the 2DEG [12]. However, it cannot separate the mobilities in the 2DEG sections outside and under the gate. Therefore, the Hall-effect method can only be used to measure the 2DEG mobility in the resistive regions. The sheet resistance measured on the Hall sample agrees with the sheet resistance R_{s-o} that was obtained from the TLM structures. The measured Hall mobility corresponds to the mobility of 2DEG electrons outside the gate, whereas the effective and the field-effect mobilities are for the 2DEG electron under the gate. As can be seen from the results shown in Fig. 6, the Hall mobility of electrons outside the gate is very similar to the effective and the field-effect mobilities that are obtained for the electrons under the gate. This result suggests that there is no significant impact of the gate on the 2DEG mobility.

In the case of MOSFETs, there is a very significant mobility reduction with applied gate voltage. There is no such strong dependence of either the effective or the field-effect mobilities shown in Fig. 6 for the measured HEMTs. It should be noted that the channel of electrons in MOSFETs is created by the electric field of the applied gate voltage, which is increased with an increase in the gate voltage. The increase in the transverse field from the applied gate voltage results in the commonly observed reduction of electron mobility in MOSFET channels. In the case of HEMTs, the applied gate voltage reduces the transverse field, which can explain this difference in mobility behavior in the case of HEMTs. The results for the field-effect mobility, shown in Fig. 6, even indicate a small mobility increase with the applied gate voltage. Based on the observation that the transverse electric field is reduced by the applied gate voltage, this result is not impossible.

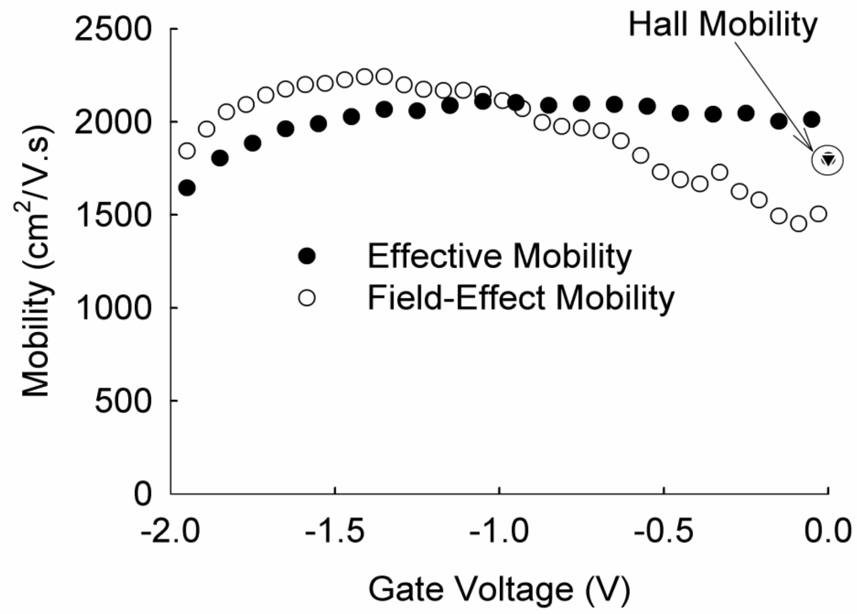

Fig. 6. The extracted effective, field-effect, and Hall mobilities.

CONCLUSION

In this work, a new method for extraction of electron mobility in the 2DEG section under the gate of power HEMTs has been presented. This method enables the possible impact of the gate voltage on the 2DEG mobility under the gate to be measured without the error caused by the resistive 2DEG sections. Applying this technique to fabricated HEMTs showed that the 2DEG mobilities underneath and outside the gate are similar. However, this mobility independence of the gate material and voltage may not be a general feature for all HEMTs. The use of the proposed method with differently fabricated HEMTs will provide a better understanding of the impact of gate material and gate voltage on the 2DEG mobility under the gate.

ACKNOWLEDGEMENT

This work was performed in part at the Queensland node of the Australian National Fabrication Facility, a company established under the National Collaborative Research Infrastructure Strategy to provide nano- and microfabrication facilities for Australia's researchers. The work was partly funded by the Australian Research Council (DP130103145).

REFERENCES

[1] S. Dimitrijev, J. Han, H. Amini Moghadam, A. Aminbeidokhti, Power-switching applications beyond silicon: Status and future prospects of SiC and GaN devices, MRS Bulletin 40 (2015) 399-405.

[2] R. S. Pengelly, S. M. Wood, J. W. Milligan, S. T. Sheppard, W. L. Pribble, A review of GaN on SiC high electron-mobility power transistors and MMICs, IEEE Trans. Microwave Theory Tech. 60 (2012) 1764-1783.

[3] S. Dimitrijev, Principles of Semiconductor Devices: Oxford University Press, 2012.

[4] B. G. Streetman, S. K. Banerjee, Solid State Electronic Devices, Prentice Hall, 2014.

[5] S. Baskaran, A. Mohanbabu, N. Anbuselvan, N. Mohankumar, D. Godwinraj, C.K. Sarkar, Modeling of 2DEG sheet carrier density and DC characteristics in spacer based AlGaN/AlN/GaN HEMT devices, Superlattices and Microstructures 64 (2013) 470-482.

[6] P. Gangwani, R. Kaur, S. Pandey, S. Haldar, M. Gupta, R. S. Gupta, Modeling and analysis of fully strained and partially relaxed lattice mismatched AlGaN/GaN HEMT for high temperatureapplications, Superlattices and Microstructures 44 (2008) 781-793.

[7] G. R. Valdivia, T. F. Ibáñez, J. Rodríguez-Tellez, A. T. Puente, A. M. Sánchez, Measurement of mobility in HEMT devices using high-order derivatives, IEEE Trans. Electron Devices 51 (2004) 1-7.

[8] H. Fukui, Determination of the basic device parameters of a GaAs MESFET, Bell syst. Tech. J. 58 (3) (1979) 771-797.

[9] R. Menozzi, G. A. Umana-Membreno, B. D. Nener, G. Parish, G. Sozzi, L. Faraone, U. K. Mishra, Temperature-dependent characterization of AlGaN/GaN HEMTs: Thermal and source/drain resistances, IEEE Trans. Device and Materials Reliability 8 (2) (2008) 255-264.

[10] H. G. Henry, Characterization of alloyed AuGe/Ni/Au ohmic contacts to n-doped GaAs by measurement of transfer length and under the contact sheet resistance, IEEE Trans. Electron Devices 36 (1989) 1390-1393.

[11] S. Khandelwal, C. Yadav, S. Agnihotri, Y. S. Chauhan, A. Curutchet, T. Zimmer, J.-C. D. Jaeger, N. Defrance, T. A. Fjeldly, Robust Surface-Potential-Based Compact Model for GaN HEMT IC Design, IEEE Trans. Electron Devices 60 (10) (2013) 3216–3222.

[12] D. K. Schroder, Semiconductor Material and Device Characterization: John Wiley & Sons, 2006.

[13] W. Serdijn, C. J. Verhoeven, A. H. V. Roermund, Analog IC Techniques for Low-Voltage Low-Power Electronics: Delft University Press, Delft, The Netherlands, 1995.

[14] Z. Bao and J. Locklin, Organic Field-Effect Transistors: CRC Press, Boca Raton, USA, 2007.

[15] H. H. Henrichsen, O. Hansen, D. Kjaer, P. F. Nielsen, F. Wang, D. H. Petersen, Precision of single-engage micro Hall effect measurements, in Int. Workshop on Junction Technology (IWJT), 2014, pp. 1-4.

CHAPTER 4: GATE VOLTAGE INDEPENDENCE OF ELECTRON MOBILITY IN POWER ALGAN/GAN HEMTS

This chapter is the following paper:

- **Amirhossein Aminbeidokhti**, Sima Dimitrijev, Anil Kumar Hanumanthappa, Hamid Amini Moghadam, Daniel Haasmann, Jisheng Han, Yan Shen, and Xiangang Xu, "Gate voltage independence of electron mobility in power AlGaN/GaN HEMTs," *IEEE Transactions on Electron Devices*, vol. 63, no. 3, pp. 1013-1019, 2016.

Abstract 94

Introduction 94

HEMT mobility measurement method 94

Fabrication process and device structure 96

Measurement of HEMT mobility at room temperature 96

High temperature measurements 98

Conclusion 99

Acknowledgement 99

References 99

Gate Voltage Independence of Electron Mobility in Power AlGaN/GaN HEMTs

Amirhossein Aminbeidokhti, *Student Member, IEEE*, Sima Dimitrijev, *Senior Member, IEEE,* Anil Kumar Hanumanthappa, Hamid Amini Moghadam, *Student Member, IEEE*, Daniel Haasmann, *Student Member, IEEE*, Jisheng Han, Yan Shen, and Xiangang Xu

***Abstract*—The mobility of current carriers in the channel of field-effect transistors usually depends on the applied gate voltage. This paper presents experimental evidence that the electron mobility in the two-dimensional electron gas under the gate of AlGaN/GaN HEMTs is actually independent of the gate voltage. This demonstration of the gate-voltage independence of the electron mobility relates to power HEMTs and it was achieved by introducing a new method for the mobility measurement. The gate-voltage independence of the electron mobility was observed for a wide range of temperature, from 25°C to 300°C. Furthermore, it is confirmed that the HEMT mobility decreases with increased temperature according to the power law (T^{-k}) and with a quite high value of the power-law coefficient (k = 2.45).**

***Index Terms*—High-electron-mobility transistor (HEMT), electron mobility, AlGaN/GaN heterostructure, two-dimensional electron gas.**

INTRODUCTION

AlGaN/GaN high electron mobility transistors (HEMTs) are the most prominent devices that utilize the unique material properties of the AlGaN/GaN heterostructure: high electron mobility in the two-dimensional electron gas (2DEG), high thermal conductivity, high breakdown field, and high saturation velocity [1]-[4]. AlGaN/GaN HEMTs are promising candidates for high power switching applications due to their high breakdown voltage, low on-state resistance, low production cost, capability of fast switching, and compatibility with existing electronic circuits [5]-[7]. These properties enable HEMTs to be operated at high temperatures, either due to self-heating or by using them in high-temperature applications [1], [5], [8], and [9].

High mobility of electrons comprising the 2DEG is the key factor for the HEMT performance in the case of power and high temperature applications [3], [10]. It is well established that the electron mobility in HEMTs exhibits a strong reduction with increased temperature [2], [4], [6], and [11]. However, the complete characterization of the HEMT mobility at high temperatures should include information on the potential mobility dependence on the value of the applied gate voltage. Some published papers present room-temperature measurements that indicate HEMT mobility dependence on the applied gate voltage [12], [13]. It is also expected that the mobility of the current carriers in the channel of a field-effect transistor would be impacted by the electric field from the applied gate voltage. However, there are no confirmed measurements and there are no established data about specific behavior of the HEMT mobility at different gate voltages.

In this paper, we present experimental results that surprisingly show that the HEMT mobility is gate voltage independent in a wide range of temperature, from 25°C to 300°C. This is achieved by introducing a new method for HEMT mobility measurement.

HEMT MOBILITY MEASUREMENT METHOD

Several different methods have been used to measure the HEMT mobility [3], [13]-[16]. Some of these methods considered the 2DEG between the source and the drain as a single section, which is analogous to the channel between the source and drain in MOSFETs [13], [15], and [16]. So, the 2DEG sections under and outside the gate were not separated. Therefore, the mobility results measured by these methods show an average mobility between the source and drain. Fukui introduced a method to separate the channel between source and drain into resistive (outside the gate) and field-effect (under the gate) sections for GaAs MESFETs [17]. Applying this method to the AlGaN/GaN HEMT showed that the

This work was performed at the Queensland Micro- and Nanotechnology Centre (QMNC), Griffith University, Australia.

A. Aminbeidokhti, S. Dimitrijev, and H. A. Moghadam are with the Queensland Micro- and Nanotechnology Centre (QMNC) and with the Griffith School of Engineering, Griffith University, Nathan, QLD 4111 Australia (e-mail: amirhossein.aminbeidokhti@griffithuni.edu.au; s.dimitrijev@griffith.edu.au).

A. K. Hanumanthappa, D. Haasmann, and J. Han are with the Queensland Micro- and Nanotechnology Centre (QMNC), Griffith University, Nathan, QLD 4111 Australia

X. Xu and Y. Shen are with the School of Material Science and Engineering, Qilu University of Technology, Jinan 250353, P. R. China.

resistance under the gate was very sensitive to the threshold voltage [14]. In order to solve this problem, Fukui's method was modified for AlGaN/GaN HEMTs [14]. However, the modified method is based on the assumption that the HEMT mobility is independent from the gate voltage [14]. Another presented method did not have that assumption; however, it requires Hall-effect measurements on a separate sample to be combined with current–voltage measurements on HEMTs [3]. Apart from inconvenience, any sample variations may introduce unwanted variation in the measured mobility. To avoid these issues, a new method for mobility measurement is presented in this section.

In the HEMT structure, the source-to-drain channel can be divided into two separate sections: (1) field-effect section (the section under the gate) and (2) resistive section, which includes the source-to-gate and the gate-to-drain sections outside the gate. To measure the mobility of electrons under the gate, it is important to obtain the resistances of both sections. In the section under the gate, MOSFET-type equations can be applied to model the current–voltage characteristics and the resistance of this section. The section outside the gate can be considered as a gate-voltage independent resistance consisting of the gate-to-source (R_{GS}), the gate-to-drain (R_{GD}), the source contact (R_{CS}), and the drain contact (R_{CD}) resistances.

The voltage applied between the drain and the source terminals (V_{DS}) is the sum of the voltages across all the resistances between the drain and the source:

$$V_{DS} = (R_{GS} + R_{GD} + R_{CS} + R_{CD} + r_G) I_D \quad (1)$$

In (1), r_G is the 2DEG resistance under the gate, which is a variable resistance that changes with the gate voltage, and I_D is the drain current flowing through the series connection of all the listed resistances. Applying the drain current equation for the MOSFET in the linear region to the HEMT section under the gate, we have:

$$I_D = \mu_n C_d \frac{W}{L}(V_G - V_T) V_{2DEG-U} \quad (2)$$

where V_{2DEG-U} is the voltage drop across the 2DEG under the gate, μ_n is the electron mobility in the 2DEG section under the gate, V_G is the applied gate-to-source voltage, V_T is the threshold voltage, C_d is the gate capacitance per unit area, and L and W are the gate length and width, respectively. The gate capacitance per unit area is defined by the thickness (t_d) and permittivity (ε_d) of the material between the 2DEG and the gate metal, which is AlGaN in the case of GaN-based HEMTs:

$$C_d = \frac{\varepsilon_d}{t_d} \quad (3)$$

From (2), the variable 2DEG resistance under the gate (r_G) can be expressed as follows:

$$r_G = \frac{V_{2DEG-U}}{I_D} = \frac{1}{\mu_n C_d \frac{W}{L}(V_G - V_T)} \quad (4)$$

All other resistances can be grouped in a single gate-voltage independent resistance, R_t:

$$R_t = R_{GS} + R_{GD} + R_{CS} + R_{CD} \quad (5)$$

Therefore, the applied drain-to-source voltage, which is the sum of the voltages across r_G and R_t is:

$$V_{DS} = R_t I_D + \frac{I_D}{\mu_n C_d \frac{W}{L}(V_G - V_T)} \quad (6)$$

In (6), there are three parameters that need to be determined from the measurements of the current–voltage characteristics: μ_n, R_t, and V_T. This can be achieved by utilizing two common definitions of mobility, effective (μ_{eff}) and field-effect (μ_{FE}) mobility, which result in two standard techniques for the MOSFET mobility measurements. The first technique is based on calculation of the output conductance ($g_O = \frac{\partial I_D}{\partial V_{DS}}$), whereas the second technique utilizes calculated transconductance ($g_m = \frac{\partial I_D}{\partial V_G}$) [18]. Given that the μ_{eff} and μ_{FE} relate to the same 2DEG mobility (μ_n) in (6), the following condition should be satisfied:

$$\mu_n = \mu_{eff} = \mu_{FE} \quad (7)$$

This condition can be used to determine μ_n, R_t, and V_T from the output conductance and the transconductance that are calculated from measured current-voltage characteristics.

Based on (6), $\mu_{eff} = \mu_n$ is related to the output conductance as follows:

$$g_O = \frac{1}{R_t + \frac{1}{\mu_{eff} C_d \frac{W}{L}(V_G - V_T)}} \quad (8)$$

Likewise, $\mu_{FE} = \mu_n$ can be related to the transconductance:

$$g_m = \frac{\mu_{FE} C_d \frac{W}{L}(V_{DS} - R_t I_D)^2}{V_{DS}} + \frac{\partial \mu_n}{\partial V_G} \frac{C_d \frac{W}{L}(V_{GS} - V_T)(V_{DS} - R_t I_D)^2}{V_{DS}} \quad (9)$$

A comparison between the two terms in (9) shows that the second term is much smaller and can be neglected. This conclusion is based on the observation that $\frac{\partial \mu_n}{\partial V_G} << \frac{\mu_{FE}}{(V_G - V_T)}$. Expressing μ_{eff} and μ_{FE} in terms of g_O and g_m, respectively, results in the following equations:

$$\mu_{eff} = \frac{1}{C_d \frac{W}{L}(V_G - V_T)(\frac{1}{g_O} - R_t)} \quad (10)$$

$$\mu_{FE} = \frac{g_m V_{DS}}{C_d \frac{W}{L}(V_{DS} - R_t I_D)^2} \quad (11)$$

Both μ_{eff} in (10) and μ_{FE} in (11) are derived from the same current-voltage equation (6), so they should both give the same HEMT mobility value that is labeled by μ_n in (6) and (7). This condition can be used to determine the value of the unknown resistance R_t, in addition to setting the value of V_T. So that the difference between μ_{eff} and μ_{FE} obtained from (10) and (11), respectively, is minimized.

Measurements of the electron mobility in the 2DEG section under the gate are influenced by the resistance of the 2DEG outside the gate (R_t in Eqs. 10 and 11). Some of the published measurements ignore the impact of R_t, which could cause apparent dependence of the electron mobility on the gate voltage. The newly presented method extracts the value of the resistance R_t without any assumptions about the impact of the gate voltage on the mobility of the electrons under the gate. Finally, the most important difference and advantage of the new method is that both the value of R_t and the value of electron mobility under the gate are extracted from measurements on a single device. This eliminates the very high sensitivity to sample-to-sample variations.

FABRICATION PROCESS AND DEVICE STRUCTURE

In order to provide experimental data to investigate the influence of the gate voltage on the HEMT mobility, typical circular HEMTs were fabricated utilizing 25 nm undoped $Al_{0.22}Ga_{0.78}N$/GaN, grown on undoped GaN, which was grown on semi-insulating SiC wafer. First, the wafer was cleaned by Piranha before removing the native oxide by HCl. Then, the Ohmic contacts were formed by sputtering Ti/Al/Ni (100nm/300nm/100nm) over the AlGaN layer, followed by annealing at 800ºC for 30 s in nitrogen-rich ambient. This was followed by a photolithography to pattern the source and drain Ohmic contacts. Next, Schottky gates were formed by Ni sputtering, followed by the second photolithography step to pattern the gate metal. The gate lengths of the measured devices were 15 µm, while the gate-to-source and gate-to-drain distances were 5 µm.

Top view of the fabricated circular HEMT is shown in Fig. 1. The closed geometry design was used to avoid any leakage currents due to existence of 2DEG in the areas that are not controlled by the gate. In this figure, L_G shows the gate length, whereas L_{GS} and L_{GD} are the gate-source and gate-drain distances, respectively. HEMT measurements were performed by Agilent power-device analyzer B1505A.

MEASUREMENT OF HEMT MOBILITY AT ROOM TEMPERATURE

Measured transfer and output characteristics of the fabricated HEMTs are shown in Fig. 2. The threshold voltage (V_T), needed in (10), is determined as the intersection of the transfer characteristic with the V_G-axis. As can be seen in Fig. 2 (a), its value is V_T = -2.1 V. The first derivatives of the transfer characteristic with respect to the gate voltage and the drain voltage lead to the transconductance and the output conductance of the HEMT, respectively, which are shown in Fig. 3. These results are used to calculate the

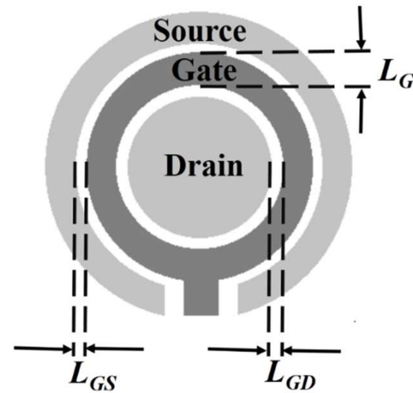

Fig. 1. Top view of the fabricated circular HEMT.

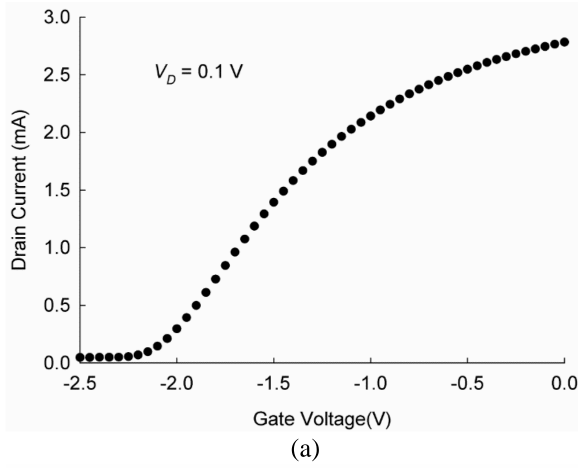

(a)

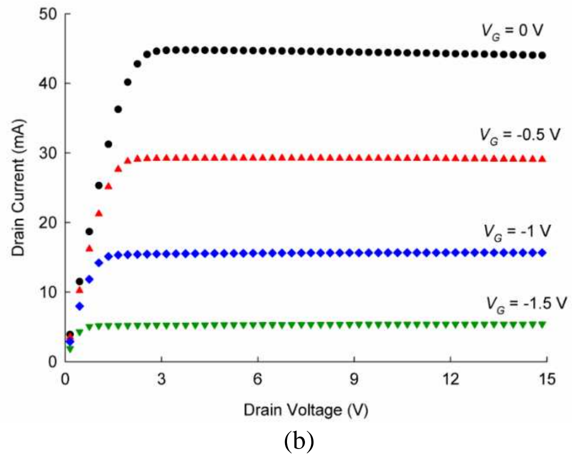

(b)

Fig. 2. The transfer (a) and the output (b) characteristics of the fabricated HEMTs.

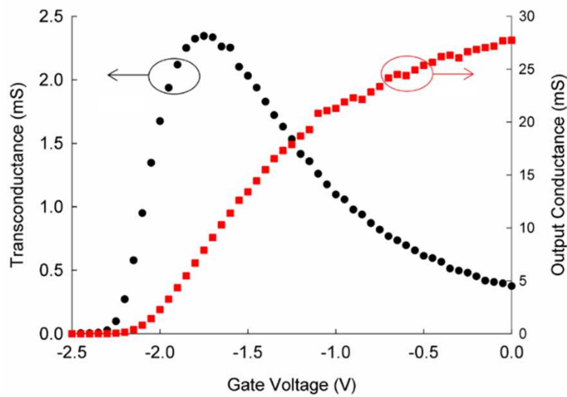

Fig. 3. The transconductance and the output conductance of the fabricated HEMTs.

mobility by the effective and the field-effect mobility equations, (10) and (11), respectively. In these equations, C_d = 3300 μF, W = 770 μm, and L = 15 μm. The value of R_t is determined so that the difference between μ_{eff} and μ_{FE} results is minimized. Figure 4 shows μ_{eff} and μ_{FE} with the best value for R_t. It can be seen that a good agreement is achieved between μ_{eff} and μ_{FE} and that, more importantly, there is no significant dependence of mobility on the gate voltage. This result confirms that the decision to neglect the second term in

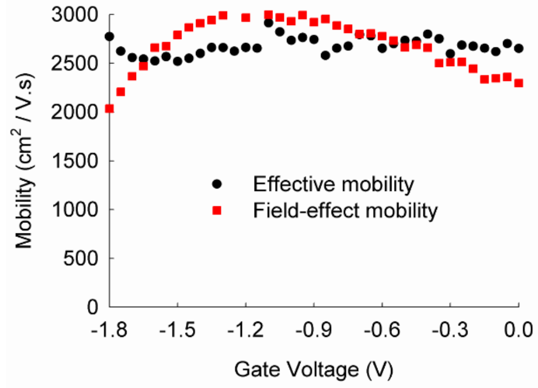

Fig. 4. The best match between the effective and field-effect mobility values of the fabricated HEMTs.

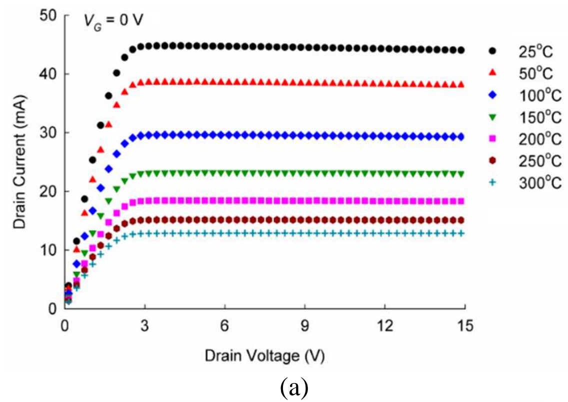

(a)

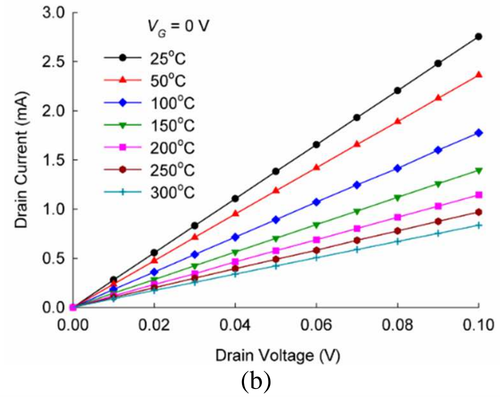

(b)

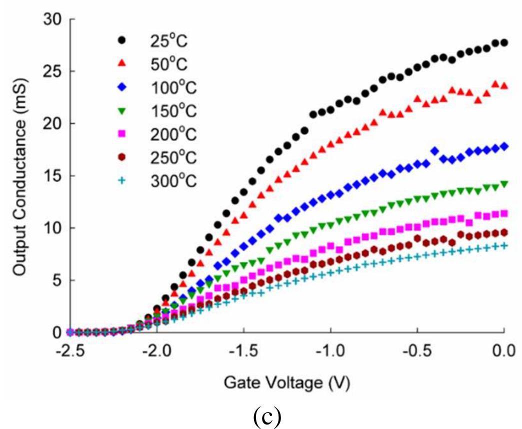

(c)

Fig. 5. The output characteristics (a), the resistive section of the output characteristics where V_{DS} is smaller than 100 mV (b), and the output conductance (c) of the HEMTs at and different temperatures.

(9) is definitely justifiable.

HIGH TEMPERATURE MEASUREMENTS

This section presents the HEMT mobility results, obtained by the new method, for the temperature range from 25ºC to 300ºC.

The measured output characteristics, and the related output conductance, are shown in Fig. 5. The transfer characteristics of the HEMT at drain voltage of 100mV and the related transconductance are shown in Fig. 6. As can be seen in Fig. 6 (a), the threshold voltage of the HEMT does not vary with changing the temperature. The effective and field-effect mobility values, obtained from (10) and (11) using the measured output conductance and transconductance, respectively, are shown in Fig. 7. These results are for the values of R_t that minimize the differences between the μ_{eff} and μ_{FE}. The results clearly show that the HEMT mobility remains independent of the gate voltage up to the temperature of 300ºC.

To understand the reason of HEMT mobility independence from the gate voltage, we can analyze the relationship between different scattering mechanisms and the electric field due to the gate voltage. The relevant scattering mechanisms include phonon, alloy disorder, interface roughness, ionized impurities, dislocation, and dipole scattering. The overall effect of scattering is quantified by the mean time between two scattering events (τ_n), which determines the mobility according to the following fundamental equation:

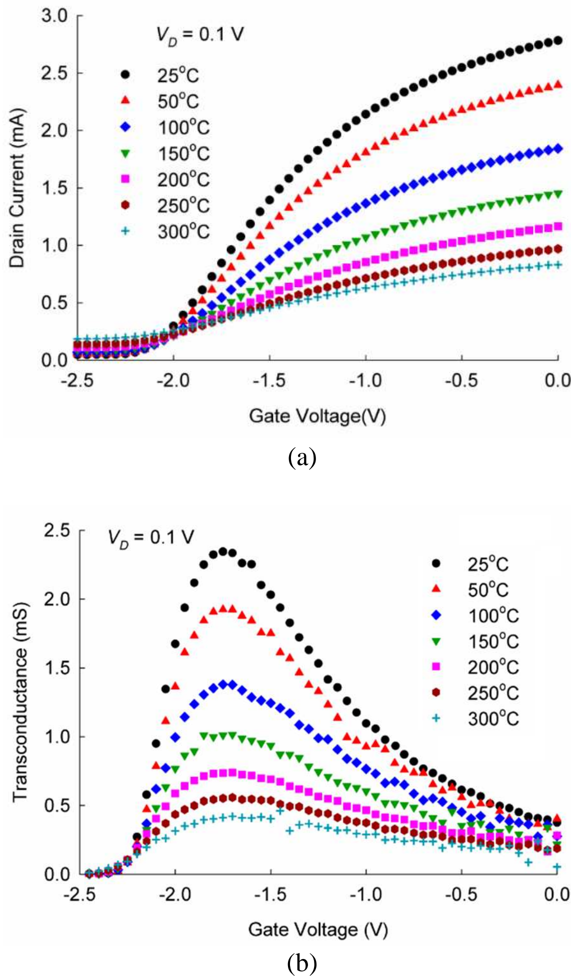

Fig. 6. Transfer characteristics (a) and the transconductance (b) of the HEMTs at different temperatures.

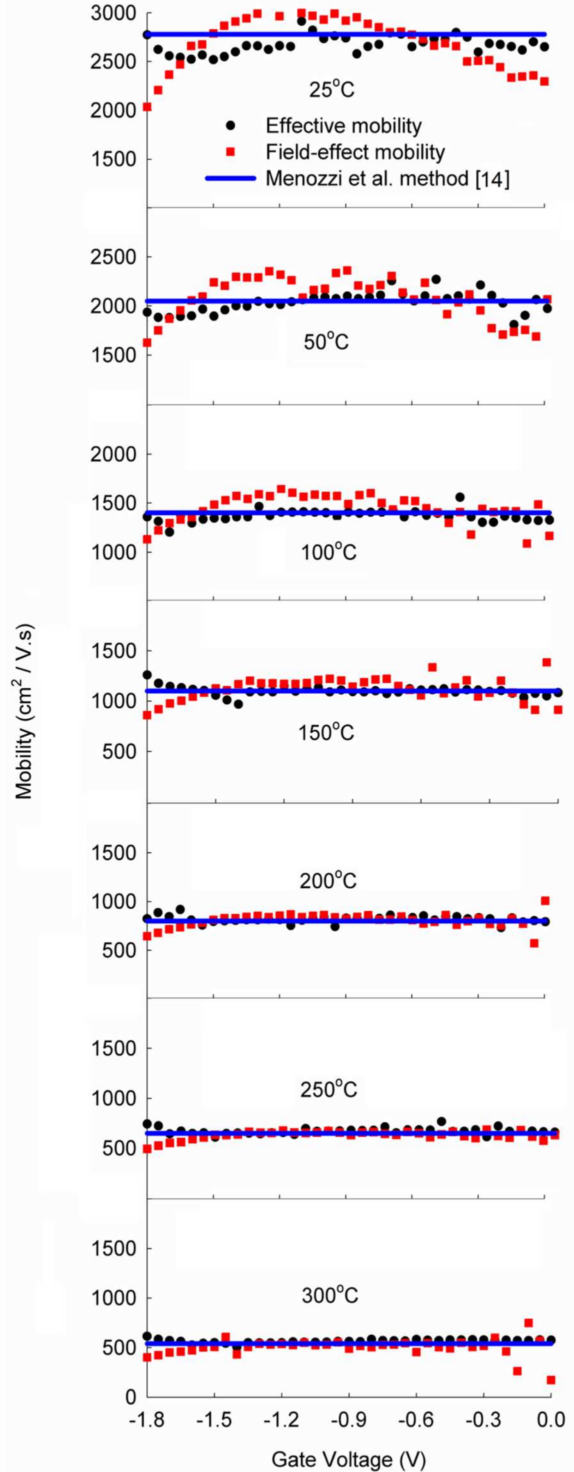

Fig. 7. The measured HEMT mobility is gate-voltage independent in the temperature range from 25ºC to 300ºC.

$$\mu_n = \frac{q\tau_n}{m^*} \quad (12)$$

In Eq. (12), q is the electron charge and m^* is the electron effective mass. The probability per unit time that a carrier will be scattered due to different scattering mechanisms is:

$$\frac{1}{\tau_n} = \frac{1}{\tau_{ph}} + \frac{1}{\tau_{all}} + \frac{1}{\tau_{int}} + \frac{1}{\tau_{ion}} + \frac{1}{\tau_{dis}} + \frac{1}{\tau_{dip}} \quad (13)$$

where τ_{ph} , τ_{all}, τ_{int}, τ_{ion}, τ_{dis}, and τ_{dip} are electron lifetimes due to phonon, alloy disorder, interface roughness, ionized impurities, dislocation, and dipole scattering, respectively. In order to analyze the dependence of these scattering mechanisms on the gate voltage, it is important to observe that the electric field due to the gate voltage is perpendicular to the two-dimensional motion of electrons. Therefore, electrons do not move in the direction of vertical electric field; they appear as standing waves in that direction. Accordingly, interface roughness scattering is the only mechanism that can be influenced by the perpendicular electric field ($E_\perp$) [19]-[23], which is according to the following equation [20], [24]:

$$\frac{1}{\tau_{int}} = \frac{\pi m^*(\Delta\Lambda qE_\perp)^2}{\hbar^3} \quad (14)$$

In Eq. (14), Δ is the root-mean-square deviation of the interface, Λ shows the correlation length, and $\hbar$ is the reduced Planck constant. In the fabricated HEMT, interface roughness scattering is insignificant because the interface is atomically smooth. This is also indicated by the large value of the electron mobility, which shows that most of the scattering mechanisms are not effective. We can conclude that the dominant scattering mechanism that influences the electron mobility in the 2DEG at temperatures above the room temperature is phonon scattering [25], which is independent from the vertical electric field [26].

The result that the HEMT mobility is independent of the gate voltage means that the measurement methods based on the assumption of constant mobility can be used to verify the mobility values obtained by the new method. As can be seen in Fig. 7, there is an excellent agreement between the mobility values obtained by the new method and the method used by Menozzi *et al* [14].

The dependence of the HEMT mobility on temperature is presented in the log–log plot in Fig. 8. The linear dependence on this log–log plot shows that

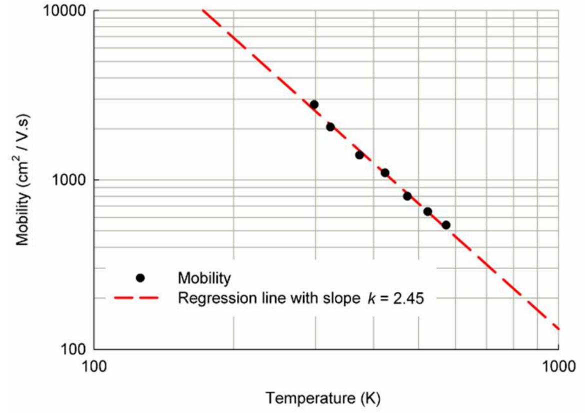

Fig. 8. The measured HEMT mobility follows the power law.

the mobility decrease with temperature follows the following power law [27]:

$$\mu_n = AT^{-k} \quad (15)$$

where A is a temperature-independent proportionality coefficient, T is the absolute temperature, and k is the power coefficient. The value of k, determined from the slope of the mobility versus temperature in the log–log plot, is equal to 2.45. This value corresponds to a much stronger mobility reduction than what is usually observed in the case of phonon scattering (k = 1.5). However, the value of k = 2.45 is in the range of power-coefficient values reported for AlGaN/GaN-based devices (k between 2.18 to 3.42) [28].

Conclusion

In this paper, an experimental investigation of the AlGaN/GaN HEMT mobility dependence on the gate voltage is presented. Using a new method for mobility measurements in HEMTs, it is demonstrated that the HEMT mobility is independent of the applied gate voltage in the temperature range from 25ºC to 300ºC. In addition, it was confirmed that the decrease of mobility with temperature follows the power law and that the power coefficient (k = 2.45) is much higher than the usual phonon-scattering value of k = 1.5.

Acknowledgement

This work was performed in part at the Queensland Node of the Australian National Fabrication Facility, a company established under the National Collaborative Research Infrastructure Strategy to provide nano- and microfabrication facilities for Australia's researchers. We also acknowledge the financial support by the Australian Research Council (DP130103145).

References

[1] D. Donoval, M. Florovič, D. Gregušová, J. Kováč, P. Kordoš, "High-temperature performance of AlGaN/GaN HFETs and

MOSHFETs," *Microelectron. Rel.*, vol. 48, pp. 1669–1672, 2008.

[2] D. Pandey, A. Bhattacharjee, and T. R. Lenka, "Study on temperature dependence scattering mechanisms and mobility effects in GaN and GaAs HEMTs," *Phys. Semicond. Devices, Environmental Sci. Eng.*, pp.67-70, 2014.

[3] A. Aminbeidokhti, S. Dimitrijev, J. Han, X. Xu, C. Wang, S. Qu, H. A. Moghadam, P. Tanner, D. Massoubre, and G. Walker, "A method for extraction of electron mobility in power HEMTs," *Superlattices Microstruct.*, vol. 85, pp. 543–550, 2015.

[4] D. Zanato, S. Gokden, N. Balkan, B. K. Ridley, and W. J. Schaff, "The effect of interface-roughness and dislocation scattering on low temperature mobility of 2D electron gas in GaN/AlGaN," *Semicond. Sci. Technol.*, vol. 19, pp. 427–432, 2004.

[5] C. Fleury, M. Capriotti, M. Rigato, O. Hilt, J. Würfl, J. Derluyn, S. Steinhauer, A. Köck, G. Strasser, and D. Pogany, "High temperature performances of normally-off p-GaN gate AlGaN/GaN HEMTs on SiC and Si substrates for power applications," *Microelectron. Rel.*, to be published.

[6] A. Kalavagunta, S. Mukherjee, R. Reed, R. D. Schrimpf, "Comparison between trap and self-heating induced mobility degradation in AlGaN/GaN HEMTs," *Microelectron. Rel.*, vol. 54, pp. 570–574, 2014.

[7] S. Dimitrijev, J. Han, H. A. Moghadam, A. Aminbeidokhti, "Power-switching applications beyond silicon: The status and future prospects of SiC and GaN devices," *MRS Bull.*, vol. 40, pp. 399-405, 2015.

[8] W. S. Tan, M. J. Uren, P. W. Fry, P. A. Houston, R. S. Balmer, T. Martin, "High temperature performance of AlGaN/GaN HEMTs on Si substrates," *Solid-State Electron.*, vol. 50, pp. 511–513, 2006.

[9] M. Zhao, X. Y. Liu, Y. K. Zheng, Yankui Li, Sihua Ouyang, "Analysis of the device characteristics of AlGaN/GaN HEMTs over a wide temperature range," *Mater. Sci. Eng. B*, vol. 178, pp. 465– 470, 2013.

[10] K. Takhar, U. P. Gomes, K. Ranjan, S. Rathi and D. Biswas, "Temperature dependent DC characterization of InAlN/(AlN)/GaN HEMT for improved reliability," *IOP Conf. Series: Mater. Sci. Eng.*, vol. 73, issue. 1, pp. 1-4, 2015.

[11] S.-I. Gozu, K. Tsuboki, M. Hayashi, C. Hong, S. Yamada, "Very high electron mobilities at low temperatures in $In_xGa_{1-x}As/In_yAl_{1-y}$ As HEMTs grown lattice-mismatched on GaAs substrates," *J. Crys. Growth*, vol. 201/202, pp. 749-752, 1999.

[12] J.-P. Ao, T. Wang, D. Kikuta, Y.-H. Liu, S. Sakai, and Y. Ohno, "AlGaN/GaN high electron mobility transistor with thin buffer layers," *Jpn. J. Appl. Phys.*, vol. 42, pp. 1588–1589, 2003.

[13] G. R. Valdivia, T. F. Ibáñez, J. R.-Tellez, A. T. Puente, and A. M. Sánchez, "Measurement of mobility in HEMT devices using high-order derivatives" *IEEE Trans. Electron Devices*, vol. 51, no. 1, pp. 1-7, 2004.

[14] R. Menozzi, G. A. U.-Membreno, B. D. Nener, G. Parish, G. Sozzi, L. Faraone, and U. K. Mishra, "Temperature dependent characterization of AlGaN/GaN HEMTs: Thermal and source/drain resistances," *IEEE Trans. Device Mater. Rel.*, vol. 8, no. 2, pp. 255-264, 2008.

[15] S. Baskaran, A. Mohanbabu, N. Anbuselvan, N. Mohankumar, D. Godwinraj, and C. K. Sarkar, "Modeling of 2DEG sheet carrier density and DC characteristics in spacer based AlGaN/AlN/GaN HEMT devices," *Superlattices Microstruct.*, vol. 64, pp. 470–482, 2013.

[16] P. Gangwani, R. Kaur, S. Pandey, S. Haldar, M. Gupta, and R. S. Gupta, "Modeling and analysis of fully strained and partially relaxed lattice mismatched AlGaN/GaN HEMT for high temperature applications," *Superlattices Microstruct.*, vol. 44, pp. 781–793, 2008.

[17] H. Fukui, "Determination of the basic device parameters of a GaAs MESFET," *The Bell Sys. Tech. J.*, vol. 58, no. 3, pp. 771–797, 1979.

[18] D. K. Schroder, *Semiconductor Material and Device Characterization*, 3rd ed. New York, NY, USA: Wiley, 2006.

[19] D. Zanato, S. Gokden, N. Balkan, B. K. Ridley, and W. J. Schaff, "The effect of interface-roughness and dislocation scattering on low temperature mobility of 2D electron gas in GaN/AlGaN," *Semicond. Sci. Technol.*, vol. 19, pp. 427–432, 2004.

[20] J. Antoszewski, M. Gracey, J. M. Dell , L. Faraone, T. A. Fisher, G. Parish, Y.-F. Wu, and U. K. Mishra, "Scattering mechanisms limiting two-dimensional electron gas mobility in $Al_{0.25}Ga_{0.75}N$/GaN modulation-doped field-effect transistors," *J. App. Phys.*, vol. 87, pp. 3900-3904, 2000.

[21] Y. Markust, U. Meiravr, H. Shtrikman, and B.Laikhtman, "Anisotropic mobility and roughness scattering in a 2D electron gas," *Semicond. Sci. Technol.*, vol. 9, pp. 1297-1304, 1994.

[22] V. K. Karavolas, M. J. Smith, T. M. Fromhold, P. N. Butcher, B. G. Mulimani, B. L. Gallagher, and J. P. Oxley, "The effect of interface roughness scattering and background impurity scattering on the thermopower of a 2DEG in a Si MOSFET," *J. Phys.: Condens. Matter*, vol. 2, pp. 10401-10410, 1990.

[23] S. Yamakawa, H. Ueno, K. Taniguchi, C. Hamaguchi, K. Miyatsuji, K. Masaki, and U. Ravaioli, "Study of interface roughness dependence of electron mobility in Si inversion layers using the Monte Carlo method," *J. App. Phys.*, vol. 79, pp. 911-916, 1996.

[24] L. Hsu, "Electron mobility in $Al_xGa_{1-x}N$/GaN heterostructures," *Physical Rew. B*, vol. 56, no. 3, pp. 1520-1528, 1997.

[25] M. N. Gurusinghe, S. K. Davidsson, and T. G. Andersson, "Two-dimensional electron mobility limitation mechanisms in AlxGa1−xN / GaN heterostructures," *Physical Rew. B*, vol. 72, pp. 045316-1-045316-11, 2005.

[26] S. B. Lisesivdin,S. Acar, M. Kasap, S. Ozcelik, S. Gokden, and E. Ozbay, "Scattering analysis of 2DEG carrier extracted by QMSA in undoped $Al_{0.25}Ga_{0.75}N$/GaN heterostructures," *Semicond. Sci. Technol.*, vol. 22, pp. 543–548, 2007.

[27] S. Dimitrijev, *Principles of Semiconductor Devices*, 2nd Ed. New York, NY, USA: Oxford Univ. Press, 2011.

[28] Z. H. Liu, S. Arulkumaran, and G. I. Ng, "Temperature dependence of Ohmic contact characteristics in AlGaN/GaN high electron mobility transistors from -50 to 200 ° C," *App. Phys. Lett.*, vol. 94, pp. 142105-1-142105-3, 2009.

CHAPTER 5: THE POWER LAW OF PHONON-LIMITED ELECTRON MOBILITY IN THE TWO-DIMENSIONAL ELECTRON GAS OF ALGAN/GAN HETEROSTRUCTURE

This chapter is the following paper:

- **Amirhossein Aminbeidokhti**, Sima Dimitrijev, Jisheng Han, Xiufang Chen, and Xiangang Xu, "The power law of phonon-limited electron mobility in the two-dimensional electron gas of AlGaN/GaN heterostructure," *IEEE Transactions on Electron Devices*, vol. 63, no. 5, pp. 2214-2218, 2016.

Abstract 102

Introduction 102

Experimental value of the power coefficient 102

    Published results by Hall-effect measurements 102

    New results by Hall-effect and circular-transmission-line (CTL) measurements 103

Analysis of the power coefficient 104

Conclusion 105

Acknowledgement 105

References 105

The Power Law of Phonon-Limited Electron Mobility in the Two-Dimensional Electron Gas of AlGaN/GaN Heterostructure

Amirhossein Aminbeidokhti, *Student Member, IEEE,* Sima Dimitrijev, *Senior Member, IEEE*, Jisheng Han, Xiufang Chen, and Xiangang Xu

***Abstract*—The reduction of electron mobility in AlGaN/GaN heterostructures follows the common power law, but with an unexpectedly high power coefficient. Following experimental verification of the unusual power-coefficient value by a different measurement method, this paper presents an analysis that identifies temperature dependence of the effective electron mass as the responsible physical mechanism for this effect. Based on this result, the measured values of electron mobility are used to calculate the effective mass of electrons in AlGaN/GaN heterostructures over a wide temperature range, from 25ºC to 300ºC.**

***Index Terms*—AlGaN/GaN heterostructure, electron mobility, power coefficient, effective mass.**

INTRODUCTION

Semiconductor devices based on the AlGaN/GaN heterostructure exhibit exceptional characteristics, such as high breakdown voltage, small *on* resistance, high thermal conductivity, and small output capacitance [1]. One of the key material advantages of AlGaN/GaN heterostructures is the high mobility of electrons in the two-dimensional electron gas (2DEG) at the AlGaN/GaN heterojunction. Due to the high electron mobility and the high breakdown field, AlGaN/GaN-based high electron mobility transistors (HEMTs) have been used for high-frequency applications and are now becoming increasingly popular for power-switching applications [2]. The high-power applications result in high power dissipation and increased operation temperatures. For a better understanding of the operation of these devices at high temperatures, it is essential to understand the physics behind the high-temperature behavior of the 2DEG mobility.

At high temperatures, phonon scattering is the only mechanism limiting the carrier mobility in semiconductor devices [3]-[6]. The carrier mobility (μ), limited by phonon scattering at high temperatures, can be expressed by the power-law equation [7]-[9],

$$\mu = AT^{-\gamma} \quad (1)$$

where T is the absolute temperature, A is a proportionality constant, and γ is the power coefficient whose value in the case of phonon scattering is 1.5 [7]-[9]. The electron mobility in AlGaN/GaN 2DEG is expected to follow the same power coefficient, because no additional scattering mechanism that could alter this temperature behavior has been identified [9],[10]. However, numerous results published in the literature show that the power coefficient of the high-temperature dependence of electron mobility in AlGaN/GaN 2DEG is between 2.18 and 3.42 [6],[10]-[18], which is a surprisingly high value in comparison to the expected value of 1.5. There is no published explanation for this unexpected behavior. In this paper, we identify the physical mechanism behind the surprising increase in the power coefficient, which will enable better modeling of the high-temperature mobility behavior and a better understanding of the physics of AlGaN/GaN-based devices.

EXPERIMENTAL VALUE OF THE POWER COEFFICIENT

This section presents the relevant experimental results, both published by other authors and a confirmation of these results by new measurements obtained by a different measurement technique.

Published results by Hall-effect measurements

There are a number of published measurements of the temperature dependence of 2DEG mobility in AlGaN/GaN heterostructures [10]-[17], which are summarized by the grey symbols in Fig. 1. These data

This work was performed at the Queensland Micro- and Nanotechnology Centre (QMNC), Griffith University, Australia.

A. Aminbeidokhti and S. Dimitrijev are with the Queensland Micro- and Nanotechnology Centre (QMNC) and with the Griffith School of Engineering, Griffith University, Nathan, QLD 4111 Australia (e-mail: amirhossein.aminbeidokhti@griffithuni.edu.au; s.dimitrijev@griffith.edu.au).

J. Han is with the Queensland Micro- and Nanotechnology Centre (QMNC), Griffith University, Nathan, QLD 4111 Australia.

X. Chen and X. Xu are with the State Key Laboratory of Crystal Materials, Shandong University, Jinan, Shandong 250100, P.R.China.

include AlGaN/GaN layers grown on sapphire substrates [12]-[17], as well as on Si and SiC substrates [10],[11]. As can be seen in the figure, the substrate type does not impact the mobility values and the power coefficient. In some of the published works, the mobility is measured over a wide range of temperature. In this paper, the focus is on the temperature range from 150 K to 800 K, which is consistent with the expected operational range. In particular, the main focus is on the value of the power coefficient in this

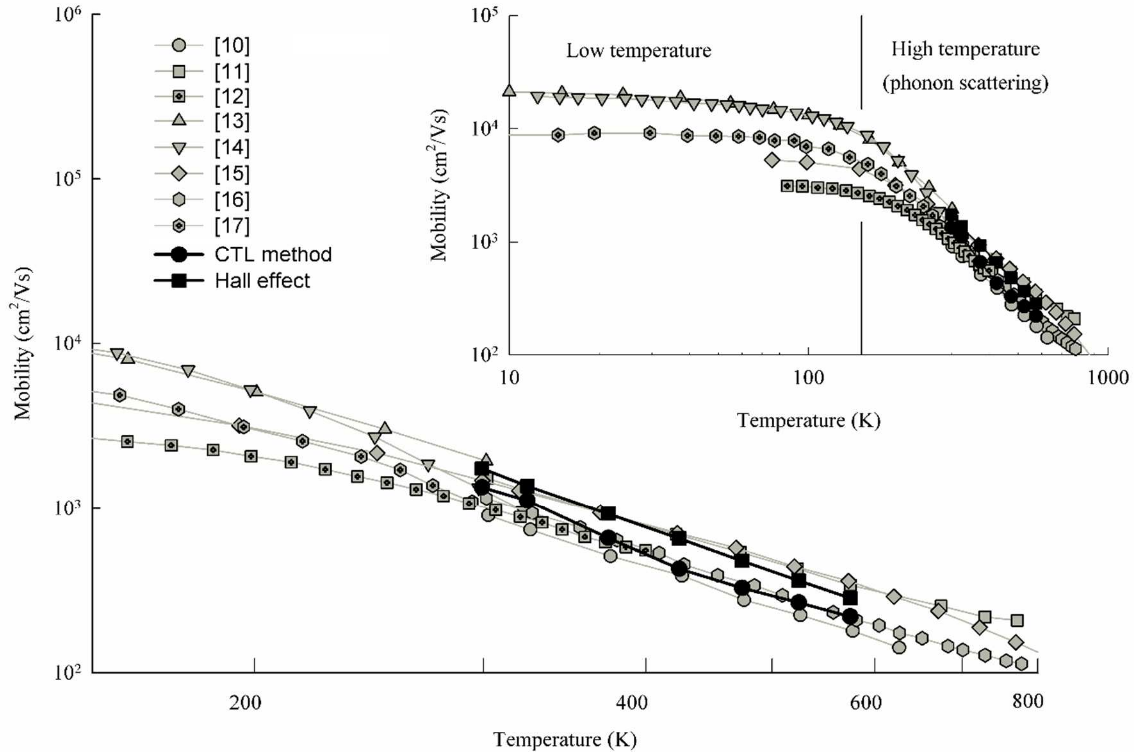

Fig. 1. Published experimental results by Hall-effect measurements (grey symbols), along with new measurements by both Hall-effect and circular-transmission-line (CTL) measurements (black symbols).

specific temperature range. Hence, the main graph in Fig. 1 corresponds to this temperature range, with the experimental data published for lower temperatures shown in the inset.

The results in Fig. 1 are shown as log–log plots, so the linear segment at high temperatures confirms the applicability of the power law given by (1). The absolute value of the slope of this linear segment is equal to the power coefficient γ.

New results by Hall-effect and circular-transmission-line (CTL) measurements

All published results shown in Fig. 1 (the grey symbols) are obtained by Hall-effect measurements. To confirm these results, we performed measurements by both Hall-effect and CTL methods. The CTL method was selected because it enables resistance measurements with well-defined geometry, which avoids errors due to side leakage in the case of the rectangular transmission-line geometry.

The magnetic field for the Hall-effect measurements was 0.52 T. All current–voltage measurements were performed by an HP4145B semiconductor parameter analyzer. The AlGaN/GaN heterostructure used in these measurements was grown on semi insulating SiC wafer. A 25 nm undoped $Al_{0.22}Ga_{0.78}N$ layer was grown on top of undoped GaN layer. For the Hall-effect method, 1×1 cm square shaped samples were cut and four Ohmic contacts were formed on each corner of the sample by sputtering Ti/Al/Ni, followed by annealing at 850ºC for 30 s. For the CTL method, a set of 5 CTLs with different gaps between the CTLs were fabricated on a single sample. The contacts were made by the same process as for the Hall-effect samples.

For both of the Hall-effect and CTL samples, the 2DEG mobility was calculated as [19]

$$\mu = \frac{1}{qR_S N_{2DEG}} \quad (2)$$

where q is the electron charge, R_s is the sheet resistance, and N_{2DEG} is the electron density in the 2DEG, which was obtained by the Hall-effect measurements. It should be noted that N_{2DEG} changes with temperature are negligible [10],[16]. Therefore, the value of N_{2DEG}, obtained from the room-temperature Hall-effect measurements, was used for the mobility calculations

by (2) at both low and high temperatures. The current–voltage measurements, needed to obtain the sheet resistances by both the Hall-effect and CTL methods, were performed over the temperature range from 25ºC to 300ºC.

The obtained mobility values are presented in Fig. 1 by the black symbols (squares for the Hall-effect measurements and circles for the CTL measurements). It can be seen that the measured mobility by the two different methods are in close agreement with each other. The power-coefficient value corresponding to these measurements, which is $\gamma = 2.8$, is approximately equal to the average γ values published in the literature. Therefore, $\gamma = 2.8$ can be considered as the representative power-coefficient value and will be used in the analysis presented in the subsequent section.

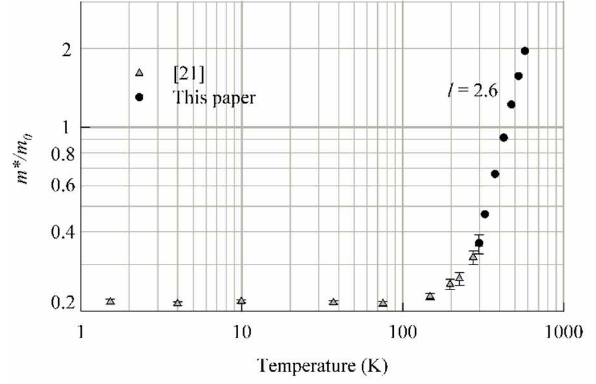

Fig. 2. Experimental values of the effective mass of electrons in AlGaN/GaN heterostructure at different temperatures. The grey symbols are the measured values in [21], whereas the black symbols correspond to the values extracted from the mobility measurements presented in this paper (l is the power coefficient in the power-law dependence of the effective mass on temperature).

ANALYSIS OF THE POWER COEFFICIENT

We begin the analysis by evaluating the various parameters that could affect the electron mobility in AlGaN/GaN heterostructures. Parameters such as background career concentration, quality of the grown AlGaN and GaN, and various scattering mechanisms such as phonon scattering, interface scattering, and background carrier scattering could impact the temperature dependence of the electron mobility in AlGaN/GaN heterostructures. However, published results show that the interface scattering is not a function of temperature and, therefore, has no effect on the temperature dependence of electron mobility [20]. Various publications identify phonon scattering as the dominant mechanism that determines the mobility values at high temperatures [3]-[5],[7],[8]. Regarding the background carrier concentration, published results show that the carrier concentration increases with temperature, thereby increasing the carrier density in the GaN layer. However, this increase in the carrier density is small and is unlikely to significantly impact the measurements of electron mobility [11],[16],[18]. Finally, regarding the quality of the AlGaN and GaN layers, the high electron mobility (1747 cm^2/Vs) recorded at room temperature on these samples demonstrates that the quality of the grown GaN and AlGaN is very high. Therefore, it is safe to conclude that the electron mobility is dominated by phonon scattering at high temperatures.

The relationship between the electron mobility (μ) and the average time between two phonon-scattering events (τ_{ph}) can be expressed as

$$\mu = \frac{q\tau_{ph}}{m^*} \tag{3}$$

where m^* is the effective mass. The phonon-scattering time can be expressed in terms of the phonon-scattering cross-section (σ_{SC}), the concentration of phonons as scattering centers (N_{SC}), and the thermal velocity of electrons (v_{th}) [7]:

$$\tau_{ph} = \frac{1}{v_{th}\sigma_{SC}N_{SC}} \tag{4}$$

The thermal velocity of electrons in two dimensions can be expressed in terms of crystal temperature:

$$\frac{m^* v_{th}^2}{2} = kT \tag{5}$$

where k is the Boltzmann constant. With a linear dependence of phonon scattering cross-section on the absolute temperature [7],

$$\sigma_{SC} = A_1 T \tag{6}$$

where A_1 is a temperature-independent proportionality constant, (4)–(6) lead to the power law of mobility versus temperature and the expected power coefficient value of 1.5:

$$\mu = AT^{-1.5} \tag{7}$$

The coefficient A in (7) is:

$$A = \frac{q}{N_{SC}A_1\sqrt{m^* 2k}} \tag{8}$$

The expected power-coefficient value of 1.5 is experimentally observed in Si devices, which is consistent with the temperature independence of all quantities, including the effective mass, that appear in (8). As distinct from Si, recently published results show that the effective mass of electrons in AlGaN/GaN heterostructures changes with temperature [21]. One possible mechanism for this behavior is due to the quantum confinement effect in

the AlGaN/GaN heterostructure [22]. The measured values of the effective mass at sub-room temperatures, published in [21] are plotted by the grey symbols in Fig. 2. These measurements were performed up to room temperature only, because the measurement methods (cyclotron resonance and Shubnikov-de Haas oscillations) were limited to high mobility values [21].

Rearranging the variables in (7) and (8), the effective electron mass can be expressed as

$$m^* = \frac{q^2}{2kA_1^{\ 2} N_{SC}^{\ 2} \mu^2 T^3} \tag{9}$$

The value of A_1 in (9) can be obtained by substituting the values of the measured mobility (this paper) and the effective electron mass [21] at room temperature, along with the known values of the remaining variables and constants. The obtained value is $A_1 = 6.6\times10^{-25}$ m^2/K. Based on (6), this value corresponds to the scattering cross-section of $\sigma_{SC} = 1.98\times10^{-18}$ cm^2, which is in the range of expected values for the scattering cross-section of phonons in semiconductor devices [7].

Using the determined value for the constant A_1, the concentration of atoms in GaN as the concentration of phonons ($N_{sc} = 8.9\times10^{22}$ cm^{-3}), and the measured electron-mobility values, (9) can be used to calculate the effective electron mass above room temperature. The obtained results are presented by the black circles in Fig. 2. It can be seen that the obtained high-temperature values from the mobility measurements in this work follow the trend of the published results for the temperatures below 300 K.

Inserting the electron mobility from (7), which is the power-law dependence of mobility on temperature, into (9) results in the following equation:

$$m^* = \frac{q^2 A^2}{2kA_1^{\ 2} N_{SC}^{\ 2}} T^{(2\gamma-3)} \tag{10}$$

Equation (10) shows that the effective electron mass also follows a power law at high temperatures, with the power coefficient being equal to $l = 2\gamma\text{-}3 = 2.6$. The slope of the effective-mass increase with temperature on the log–log plot in Fig. 2 (the black circles) is equal to the power coefficient $l = 2.6$.

CONCLUSION

In this paper, we have demonstrated that the effective mass of electrons in AlGaN/GaN 2DEG increases with temperature. Furthermore, we have demonstrated that this increase is according to the power law at temperatures above 300 K, and that the power-law coefficient is $l = 2.6$. This effect accounts for the increased coefficient γ in the power-law dependence of the phonon-limited mobility on temperature. The increase is from the usual phonon-scattering value of $\gamma = 1.5$ to the value of $\gamma = 2.8$, which is experimentally observed in numerous papers and confirmed in this paper by a different measurement method.

Acknowledgements

This work was performed in part at the Queensland Node of the Australian National Fabrication Facility, a company established under the National Collaborative Research Infrastructure Strategy to provide nano- and microfabrication facilities for Australia's researchers. We also acknowledge the financial support by the Australian Research Council (DP130103145).

REFERENCES

[1] R. S. Pengelly, S. M. Wood, J. W. Milligan, S. T. Sheppard, and W. L. Pribble, "A review of GaN on SiC high electron-mobility power transistors and MMICs," *IEEE Trans. Micro. Theory Tech.*, vol. 60, no. 6, pp. 1764-1783, 2012.

[2] S. Dimitrijev, J. Han, H. A. Moghadam, and A. Aminbeidokhti, "Power-switching applications beyond silicon: Status and future prospects of SiC and GaN devices," *MRS Bull.*, vol. 40, no. 5, pp. 399-405, 2015.

[3] O. Katz, A. Horn, G. Bahir, and J. Salzman, "Electron mobility in an AlGaN/GaN two-dimensional electron gas I—carrier concentration dependent mobility," *IEEE Trans. Elec. Devices*, vol. 50, no. 10, pp. 2002-2008, 2003.

[4] A. F. M. Anwar, S. Wu, and R. T. Webster, "Temperature dependent transport properties in GaN, $Al_xGa_{1-x}N$, and $In_xGa_{1-x}N$ semiconductors," *IEEE Trans. Elec. Devices*, vol. 48, no. 3, pp. 567-571, 2001.

[5] M. N. Gurusinghe, S. K. Davidsson, and T. G. Andersson, "Two-dimensional electron mobility limitation mechanisms in AlxGa1−xN / GaN heterostructures," *Physical Rev. B*, vol. 72, pp. 045316-1-045316-11, 2005.

[6] A. Aminbeidokhti, S. Dimitrijev, A. K. Hanumanthappa, H. A. Moghadam, D. Haasmann, J. Han, Y. Shen, and X. Xu, "Gate voltage independence of electron mobility in power AlGaN/GaN HEMTs," *IEEE Trans. Elec. Devices*, vol. 63, no. 3, pp. 1013-1019, 2016.

[7] S. Dimitrijev, *Principles of Semiconductor Devices*, 2nd ed. New York, NY, USA: Oxford Univ. Press, 2011, pp. 124–126.

[8] H. Morkoc, *Nitride Semiconductor Devices: Fundamentals and Applications*, Germany, Wiley-VCH, 2013, pp.140.

[9] D. Pandey, A. Bhattacharjee, and T. R. Lenka, "Study on temperature dependence scattering mechanisms and mobility effects in GaN and GaAs HEMTs," in *Physics of Semiconductor Devices* (Environmental Science and Engineering), Springer, 2014, pp. 67–70.

[10] N. Maeda, K. Tsubaki, T. Saitoh, and N. Kobayashi, "High-temperature electron transport properties in AlGaN/GaN heterostructures," *Appl. Phys. Lett.*, vol. 79, no. 11, pp. 1634-1636, 2001.

[11] I. H. Lee, Y. H. Kim, Y. J. Chang, J. H. Shin, T. Jang, and S. Y. Jang, "Temperature-dependent hall measurement of AlGaN/GaN heterostructures on Si substrates," *J. Korean Phys. Soc.*, vol. 66, no. 1, pp. 61-64, 2015.

[12] S. Arulkumaran, S. L. Selvaraj, T. Egava, and G. I. Ng, "Sheet carrier density enhancement by Si_3N_4 passivation on nonpolar *a*-plane (1120) sapphire grown AlGaN/GaN heterostructures," *Appl. Phys. Lett.*, vol. 92, no. 1, pp. 092116-1-092116-3, 2008.

[13] R. Menozzi, G. A. Umana-Membreno, B. D. Nener, G. Parish, G. Sozzi, L. Faraone, and U. K. Mishra, "Temperature-dependent characterization of AlGaN/GaN HEMTs: Thermal and source/drain resistances," *IEEE Trans. Device Mater. Reliab.*, vol. 8, no. 2, pp. 255-264, 2008.

[14] A. Saxler *et al*., "Characterization of an AlGaN/GaN two-dimensional electron gas structure," *J. Appl. Phys.*, vol. 87, no. 1, pp. 369-374, 2000.
[15] H. Tokuda, J. Yamazaki, and M. Kuzuhara, "High temperature electron transport properties in AlGaN/GaN heterostructures," *J. Appl. Phys.*, vol. 108, no. 10, pp. 104509-1-104509-5, 2010.
[16] M. J. Wang, B. Shen, F. J. Xu, Y. Wang, J. Xu, S. Huang, Z. J. Yang, K. Xu, and G. Y. Zhang, "High temperature dependence of the density of two-dimensional electron gas in Al0.18Ga0.82N/GaN heterostructures," *Appl. Phys. A*, vol. 88, no. 4, pp. 715-718, 2007.
[17] T. Egawa, H. Ishikawa, M. Umeno, and T. Jimbo, "Recessed gate AlGaN/GaN modulation doped field-effect transistors on sapphire," *Appl. Phys. Lett.*, vol. 76, no. 1, pp. 121-123, 2000.
[18] Z. H. Liu, S. Arulkumaran, and G. I. Ng, "Temperature dependence of Ohmic contact characteristics in AlGaN/GaN high electron mobility transistors from 50 to 200 ° C," *Appl. Phys. Lett*., vol. 94, 142105-1-142105-3, 2009.
[19] A. Aminbeidokhti, S. Dimitrijev, J. Han, X. Xu, C. Wang, S. Qu, H. A. Moghadam, P. Tanner, D. Massoubre, and G. Walker, "A method for extraction of electron mobility in power HEMTs," *Superlattices Microstruct.*, vol. 85, pp. 543-550, 2015.
[20] S. B. Lisesivdin, A. Yildiz, N. Balkan, M. Kasap, S. Ozcelik, and E. Ozbay "Scattering analysis of two-dimensional electrons in AlGaN/GaN with bulk related parameters extracted by simple parallel conduction extraction method," *J. Appl. Phys.*, vol. 108, no. 1, pp. 013712-1-013712-7, 2010.
[21] T. Hofmann *et al*., "Temperature dependent effective mass in AlGaN/GaN high electron mobility transistor structures," *Appl. Phys. Lett.*, vol. 101, no. 19, pp. 192102-1-192102-4, 2012.
[22] A. M. Kurakin *et al*., "Quantum confinement effect on the effective mass in two-dimensional electron gas of AlGaN/GaN heterostructures," *J. Appl. Phys.*, vol. 105, no. 5, pp. 073703-1-073703-6, 2009.

CHAPTER 6: SPICE MOSFET EQUATIONS AND PARAMETERS AS POWER HEMT MODEL

This chapter is the following paper:

- **Amirhossein Aminbeidokhti**, Sima Dimitrijev, Jisheng Han, and Hamid Amini Moghadam, "SPICE MOSFET equations and parameters as power HEMT model," to be submitted to *Microelectronics Reliability* journal.

Abstract 108

Introduction 109

Selection of SPIC equations and parameter extraction 109

    Selection of equations and related parameters 109

    Device fabrication 112

    Parameter extraction: Techniques to obtain the values of the selected parameters 112

    Nonlinear fitting 113

Verification by SPICE simulation 117

Conclusion 120

Acknowledgement 120

References 122

In previous chapters, two methods to measure the electron mobility of the HEMT in the 2DEG region were presented and the parameters affecting the value of the mobility were analysed in detail. In this chapter, it is explained that the measured mobility can be used for modelling of the HEMT. HEMT models can be used for SPICE simulation of this device for circuit simulation purposes.

The HEMT includes the field-effect and resistive sections. The field-effect section can be modelled by modifying the MOSFET *LEVEL* 3 model. Therefore, equations and parameters of the MOSFET can be used for modelling of the HEMT. The drain current of the MOSFET is explained by:

$$I_D = [\beta(V_{GS} - \boldsymbol{Vto})(V_{DS} - \boldsymbol{Rs}\, I_D - \boldsymbol{Rd}\, I_D) - (1 + F_B)\frac{(V_{DS} - \boldsymbol{Rs}\, I_D - \boldsymbol{Rd}\, I_D)^2}{2}] \quad \text{Triode region} \quad (1)$$

$$I_D = \frac{\beta}{2(1 + F_B)}(V_{GS} - \boldsymbol{Vto})^2 \quad \text{Saturation region (2)}$$

Here, I_D is the drain current, V_{GS} shows the gate-to-source voltage, *Vto* is the threshold voltage, V_{DS} represents the drain-to-source voltage, and *Rs* and *Rd* are source and drain constant resistances. In both of the equation, β plays an important role and its value changes the value of the drain current in both triode and saturation regions. This parameter is calculated as follows:

$$\beta = \mu_0 \frac{\varepsilon_{OX}}{t_{OX}} \frac{W}{L_{eff}}$$

Here, μ_0 is the low-field mobility, ε_{OX} shows the permittivity of the oxide, which is the permittivity of AlGaN in case of AlGaN/GaN HEMT, t_{OX} represents the thickness of the oxide, W is the gate width and L_{eff} is the effective length of the gate. ε_{OX}, t_{OX}, W, *and* L_{eff} are related to the characteristics and dimensions of the AlGaN layer of the HEMT, however the value of the μ_0 needs to be measured. Therefore, using the value of the HEMT mobility, which can be measured by the presented methods in chapters 3 and 4, leads to calculate the value of β. This issue shows the importance of the mobility measurement in modelling of the HEMT. When the value of the mobility is not known, transconductance parameter (*KP*) needs to be extracted through the transfer characteristic of the HEMT. Extraction of all of the required parameters for SPICE modelling of the HEMT are explained in detail in this chapter.

SPICE MOSFET Equations and Parameters as Power HEMT Model

Amirhossein Aminbeidokhti [a,b,*], Sima Dimitrijev [a,b], Jisheng Han [a], and Hamid Amini Moghadam [a,b]

[a] Queensland Micro- and Nanotechnology Centre (QMNC), Griffith University, Nathan, Queensland 4111, Australia

[b] Griffith School of Engineering, Griffith University, Nathan, Queensland 4111, Australia

[*] Corresponding author:
Email: amirhossein.aminbeidokhti@griffithuni.edu.au
Tel: +61 48 1135 810

We confirm that this manuscript has not been published elsewhere and is also not under consideration by any other journal.

Abstract- Simulation-based analysis and design of circuits with HEMTs is becoming increasingly important, but the device library in the standard circuit simulator (SPICE) does not include a HEMT model. To address this problem, this paper presents a method for overcoming the relevant difference between the HEMT and MOSFET device structures, so that specifically selected MOSFET equations and parameters in SPICE can be used as a model for the current–voltage characteristics of power HEMTs. The proposed method, which includes techniques for determining the values of the selected device parameters, is demonstrated and verified by measured transfer characteristic, output characteristics, and gate capacitance of fabricated HEMTs. Using the selected MOSFET parameters and determining their values by the proposed techniques, circuit designers can simulate circuits with power HEMTs without the uncertainty associated with the unknown parameters and equations in newly developed subcircuit-type HEMT models.

Keywords- **Power high-electron-mobility transistor (HEMT), SPICE simulator, parameter extraction method, SPICE parameters.**

I. Introduction

Design and analysis of power electronic circuits are usually performed by the simulation program with integrated circuit emphasis (SPICE), which is adopted by the electronic industry as the standard analogue electronic circuit simulator [1]. The standard SPICE library of devices was developed at the time when the focus was on bipolar-junction transistors, junction field-effect transistors, and metal–oxide–semiconductor field-effect transistors (MOSFETs), and it does not include a library model for the high-electron-mobility transistor (HEMT). However, there is a growing demand to use HEMTs in power electronic circuits [2-5], especially with the emergence of GaN-based HEMTs that offer blocking voltages well above silicon-based MOSFETs and offer both power efficiency and switching frequencies above SiC-based MOSFETs [6].

To enable simulation of circuits with HEMTs, several papers have proposed HEMT models [4], [7-10] that could be incorporated into SPICE by defining external sub-circuits. This is a complex process for the circuit designers without established parameter-extraction techniques, which can also adversely impact the simulations. To address this problem, we show in this paper that properly selected equations and parameters from the standard MOSFET *LEVEL 3* model in SPICE can be used to match the current–voltage characteristics of GaN HEMTs. The paper also presents parameter-extraction techniques to determine the values of selected parameters from measured HEMT characteristics.

II. Selection of SPICE Equations and Parameter Extraction

A. Selection of Equations and Related Parameters

Figure 1 (a) shows that the two-dimensional electron gas (2DEG), connecting the source and drain contacts of a HEMT, consists of three segments: the source-to-gate segment whose length is L_{GS}, the segment under the gate (L_G) that is subject to the field-effect control by the gate, and

the gate-to-drain segment (L_{GD}) [11]. Figure 1 (b) illustrates that the main difference between a HEMT and a MOSFET is due to the resistive regions outside the gate (gate to drain resistance, ***Rd***, and gate to source resistance, ***Rs***), which do not exist in the case of MOSFETs. However, MOSFET models in SPICE include *parasitic* resistances ***Rs*** and ***Rd*** as parameters. This enables HEMTs to be modeled by the equivalent circuit shown in Fig. 1 (b) and this model to be implemented in SPICE through selected MOSFET equations and parameters, along with properly set values for the parameters ***Rs*** and ***Rd***.

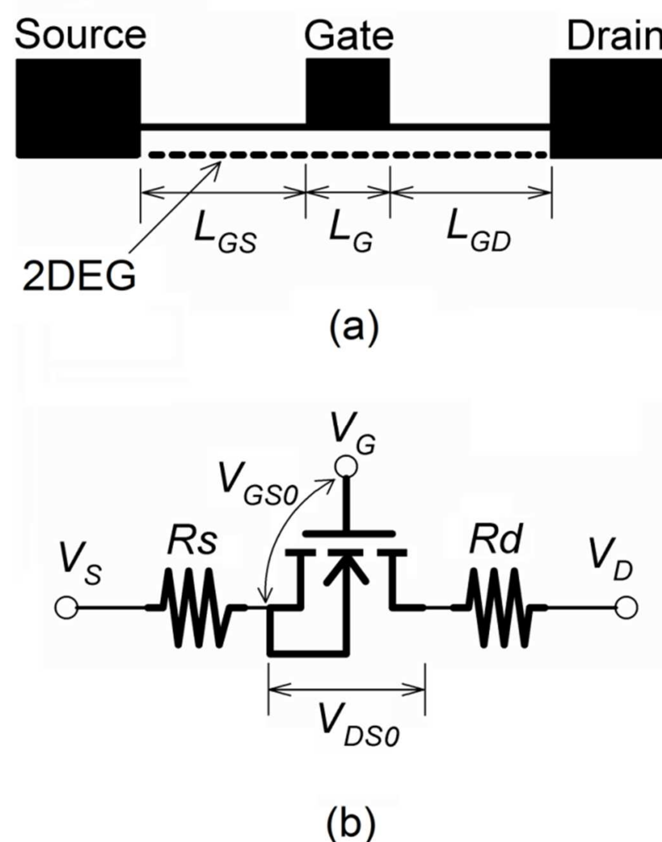

Fig. 1. HEMT cross section showing that the device channel (2DEG) consists of three sections (a), which can be modelled by an equivalent circuit consisting of two resistors and a MOSFET (b).

There are different sets of equations, called model levels in SPICE, with corresponding equation parameters. MOSFET *LEVEL 1* model is based on the rudimentary device equations. It employs a simple MOS capacitor model for the depletion-layer charge, which ignores the effects of the source and drain depletion regions. These effects are included in MOSFET

LEVEL 2 model in a mathematically complicated way [1]. This makes the model inefficient and convergence issues are frequently encountered. Accordingly, *LEVEL 2* model has been superseded by MOSFET *LEVEL 3* model, which is more robust (it rarely encounters convergence problems) and is both simpler and more accurate than *LEVEL 2* model [1]. Therefore, MOSFET *LEVEL 3* model is utilized in this work. In SPICE, a parameter labeled as ***LEVEL*** is assigned to MOSFET devices, which can be set as ***LEVEL***=3 to activate the set of equations that correspond to *LEVEL 3* model.

The equations of MOSFET *LEVEL 3* model that include and define the selected parameters, in addition to the already described ***Rs*** and ***Rd*** parameters, are as follows [12]:

$$I_D = [\beta(V_{GS} - \boldsymbol{Vto})(V_{DS} - \boldsymbol{Rs}\, I_D - \boldsymbol{Rd}\, I_D) - (1 + F_B)\frac{(V_{DS} - \boldsymbol{Rs}\, I_D - \boldsymbol{Rd}\, I_D)^2}{2}] \quad \text{Triode region} \quad (1)$$

$$I_D = \frac{\beta}{2(1 + F_B)}(V_{GS} - \boldsymbol{Vto})^2 \quad \text{Saturation region (2)}$$

$$\beta = \boldsymbol{KP}\frac{\boldsymbol{W}}{\boldsymbol{L}} \quad (3)$$

$$F_B = \frac{\boldsymbol{Gamma}}{2\sqrt{\boldsymbol{Phi}}} \quad (4)$$

In Eqs. (1)-(4), V_{GS} and V_{DS} are the applied gate-to-source and drain-to-source voltages, respectively, I_D is the resulting drain current, and the remaining SPICE parameters are the threshold voltage, ***Vto***, the transconductance parameter, ***KP***, the channel width, ***W***, the channel length, ***L***, the body factor, ***Gamma***, and the surface potential in strong inversion, ***Phi***.

In addition to the described DC parameters, AC parameters are required to enable meaningful simulation of circuits‘ time responses. These parameters, which should be specified to avoid the use of zero-default values by SPICE, are related to the parasitic capacitances. The equation, which is used in SPICE to calculate the gate capacitance (C_g), is as follows:

$$C_g = (Cgdo \times W) + (Cgso \times W) \quad (5)$$

In Eq. (5), ***Cgdo*** and ***Cgso*** are the relevant SPICE parameters, which are called the gate-to-drain and the gate-to-source overlap capacitances per channel width, respectively.

The channel width and length, ***W*** and ***L***, are geometric-design parameters, whereas all the other selected parameters can be considered as technological parameters. The default values of the selected technological parameters in MOSFET *LEVEL 3* model are shown in Table. 1.

TABLE 1
SELECTED PARAMETERS FROM THE MOSFET *LEVEL* 3 EQUATIONS TO BE USED AS HEMT MODEL.

Selected parameters (*LEVEL* = 3)		*Vto* (V)	*KP* (mA/V^2)	*Rd* (Ω)	*Rs* (Ω)	*Phi* (V)	*Gamma* (V$^{1/2}$)	*Cgso* (nF/m)	*Cgdo* (nF/m)
Default values [12, 13]		0	0.02	0	0	0.6	0	0	0
Parameter values to match the measured HEMT	Before nonlinear fitting	-2.2	0.5	5.25	5.25	2	0.28	87.6	87.6
	After nonlinear fitting	-2.2	0.65	7	7	2	0.28	87.6	87.6

B. Device Fabrication

The values of the selected SPICE parameters should be determined from the current–voltage characteristics of a representative HEMT. Measured characteristics of typical circular HEMTs are used to present techniques for determination of the parameter values in this paper. The HEMTs were fabricated from undoped AlGaN/GaN layers, grown on semi-insulating SiC wafers. First, wafer was cleaned by Piranha followed by native oxide removing by HCl. Next, Ti/Al/Ni was sputtered over 25-nm-thick $Al_{0.22}Ga_{0.78}N$, followed by annealing process at 800°C for 30 seconds in N_2 ambient, to form the source and drain Ohmic contacts. Performing photolithography on the sample led to pattern source and drain Ohmic contacts. Following the

formation of the source and drain contacts areas by photolithography, Ni was sputtered and selectively etched to define the gate electrode. The gate-to-source and gate-to-drain distances of the measured devices were 5 µm, whereas the gate length was 15 µm. DC and AC measurements have been performed by Agilent power device analyzer B1505A.

C. Parameter Extraction: Techniques to Obtain the Values of the Selected Parameters

The values of ***Vto***, ***Rs*** and ***Rd*** can be determined from measured transfer characteristic of a corresponding HEMT. The transfer characteristic of the HEMTs fabricated by the process described in the previous section is shown in Fig. 2. This transfer characteristic is measured at V_{DS} = 100 mV. Small V_{DS} value is used during the measured to ensure that Eq. (1) can be simplified to the following linear form:

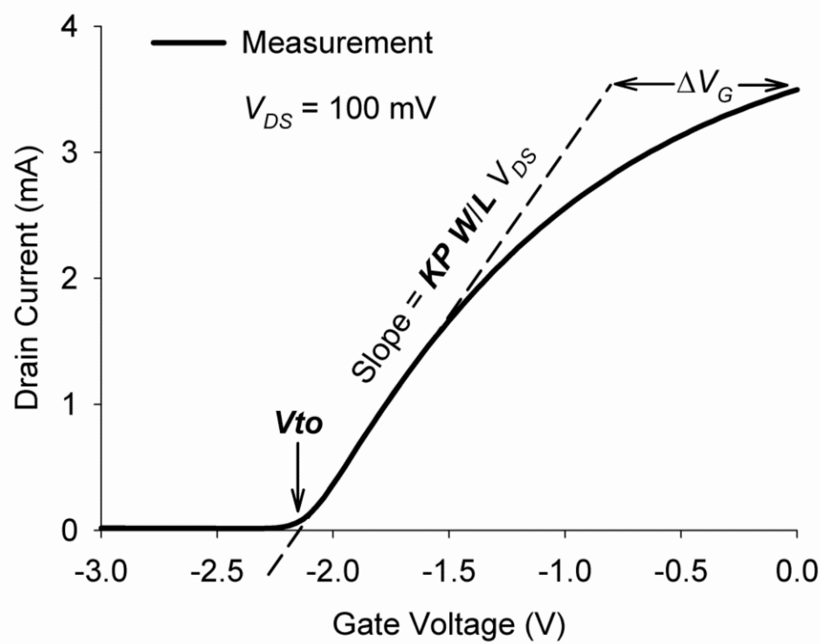

Fig. 2. Extraction of of ***KP***, ***Vto***, ***Rs*** and ***Rd*** from measured transfer characteristic of a fabricated HEMT, in combination with Eqs. (7) and (13).

$$I_D = \boldsymbol{KP}\frac{\boldsymbol{W}}{\boldsymbol{L}}(V_{GS} - \boldsymbol{Vto})(V_{DS} - \boldsymbol{Rs}I_D - \boldsymbol{Rd}I_D) \quad (6)$$

Furthermore, for small currents I_D, the terms $\boldsymbol{Rs}I_D$ and $\boldsymbol{Rd}I_D$ are also negligible, which results

in the linear segment of the transfer characteristic with the slope of $\boldsymbol{KP(W/L)}V_{DS}$:

$$I_D = \boldsymbol{KP}\frac{\boldsymbol{W}}{\boldsymbol{L}}(V_{GS} - \boldsymbol{Vto})V_{DS} \tag{7}$$

Equation (7) corresponds to the dashed line in Fig. 2. It can be seen that the intercept between the dashed line and the V_{GS} axis corresponds to the threshold voltage $\boldsymbol{Vto}$, whereas the slope corresponds to $\boldsymbol{KP(W/L)}V_{DS}$. The parameter $\boldsymbol{KP}$ can be calculated from the determined value of the slope, the known values of the geometric parameters $\boldsymbol{W}$ and $\boldsymbol{L}$, and the value of set V_{DS} voltage. It should be noted that any set of $\boldsymbol{W}$ and $\boldsymbol{L}$ values can be used if the actual values are not known because the current voltage characteristics depend on the combined term $\boldsymbol{KP}(\boldsymbol{W}/\boldsymbol{L})$.

For the case of the measured HEMTs with the transfer characteristic in Fig. 2, the intersection between the extrapolated linear section of the characteristic and the V_{GS} axis is at $\boldsymbol{Vto}$ = -2.2 V. The slope of the linear section is 2.54 mA/V, which corresponds to $\boldsymbol{KP}$=0.5 mA/V^2 for the specific case of V_{DS}=100 mV, $\boldsymbol{W}$=770 µm, and $\boldsymbol{L}$=15 µm.

The solid line in Fig. 2 corresponds to the following equation:

$$I_D = \beta(V_{GS0} - \boldsymbol{Vto})V_{DS0} \tag{8}$$

where $\beta = \boldsymbol{KP}(\boldsymbol{W}/\boldsymbol{L})$, $V_{DS0}=V_{DS}-(\boldsymbol{Rs}+\boldsymbol{Rd})I_D$. From Eq. (8), V_{GS0} can be expressed as

$$V_{GS0} = \frac{I_D}{\beta V_{DS0}} + \boldsymbol{Vto} \tag{9}$$

Obviously, $(\boldsymbol{Rd}+\boldsymbol{Rs})I_D$ is negligible for small I_D currents, and $V_{GS0}=V_{GS}$ in the region where the measured linear segment of the transfer characteristic (the solid line) and the dashed line overlap. For higher I_D currents, however, $(\boldsymbol{Rd}+\boldsymbol{Rs})I_D$ is not negligible and $V_{GS}>V_{GS0}$ is required to achieve the same I_D current. Given that

$$V_{GS} = \frac{I_D}{\beta V_{DS}} + \boldsymbol{Vto} \qquad (10)$$

the following equation for the difference $\Delta V_G = V_{GS} - V_{GS0}$, which is illustrated in Fig. 2, can be obtained from Eqs. (9) and (10):

$$\Delta V_G = \frac{I_D}{\beta}\left(\frac{1}{V_{DS0}} - \frac{1}{V_{DS}}\right) \qquad (11)$$

Replacing $V_{DS0} = V_{DS} - (\boldsymbol{Rs} + \boldsymbol{Rd}) I_D$ we obtain

$$\Delta V_G = \frac{I_D}{\beta}\left[\frac{1}{V_{DS} - (\boldsymbol{Rs} + \boldsymbol{Rd}) I_D} - \frac{1}{V_{DS}}\right] \qquad (12)$$

and

$$\boldsymbol{Rs} + \boldsymbol{Rd} = \frac{V_{DS}}{I_D} - \frac{1}{\dfrac{I_D}{V_{DS}} + \beta \Delta V_G} \qquad (13)$$

Equation (13) shows that $\boldsymbol{Rs}+\boldsymbol{Rd}$ can be determined from ΔV_G, which is the difference between the extrapolated linear segment of the transfer characteristic (the dashed line in Fig. 2) and the actual measured characteristic for a given I_D value. Practically, the highest measured current I_D should be selected for the determination of $\boldsymbol{Rs}+\boldsymbol{Rd}$, because it will result in the largest ΔV_G value and, correspondingly, in the smallest error for $\boldsymbol{Rs}+\boldsymbol{Rd}$.

For the specific data shown in Fig. 2, $I_D = 3.5$ mA, $\Delta V_G = 0.8$ V, and $\boldsymbol{Rs} + \boldsymbol{Rd} = 10.5\ \Omega$. This means $\boldsymbol{Rs} = \boldsymbol{Rd} = 5.25\ \Omega$ for the case of $L_{GS} = L_{GD}$. For HEMTs with different L_{GS} and L_{GD} values, the ratio between these values can be used to partition $\boldsymbol{Rs}+\boldsymbol{Rd}$ into the adequate $\boldsymbol{Rs}$ and $\boldsymbol{Rd}$ values.

The remaining two parameters, ***Gamma*** and ***Phi***, impact the saturation current of the device through the term F_B, as shown by Eq. (4) [12]. The dependence of the saturation current (I_D) on the gate-to-source voltage (V_{GS}), given by Eq. (2), can be linearized if $\sqrt{I_D}$ is plotted versus V_{GS}:

$$\sqrt{I_D} = \sqrt{\frac{\beta}{2(1+F_B)}}(V_{GS} - \boldsymbol{Vto}) \tag{14}$$

As this equation shows, the $\sqrt{I_D}$ -V_{GS} dependence should be linear with the slope equal to $\sqrt{\frac{\beta}{2(1+F_B)}}$. For the case of measured HEMTs in this paper, the $\sqrt{I_D}$ -V_{GS} data are shown in Fig. 3. For these data, the corresponding value of F_B is equal to 0.1. Considering Eq. (4), any set of ***Gamma*** and ***Phi*** values that result in $F_B = 0.1$ is acceptable. If the value of ***Phi*** is set at 2 V, which is the physically expected value of the surface potential in strong inversion, the value for ***Gamma*** that corresponds to $F_B = 0.1$ is ***Gamma*** = 0.28 $V^{1/2}$.

In order to extract the value of selected AC parameters, it should be noted that there are complex dependencies of the gate capacitance on the gate voltage, but their modeling is not absolutely necessary. So the most functional way to model a capacitance is to use constant gate-to-source and gate-to-drain overlap capacitances per unit width (***Cgso*** and ***Cgdo*** in SPICE).

The parameters values obtained by the described procedure are summarized in Table 1 in the raw labeled as “before nonlinear fitting”. The large differences of the extracted values from the default values, which are also shown in Table 1, illustrate the importance of the described extraction procedure.

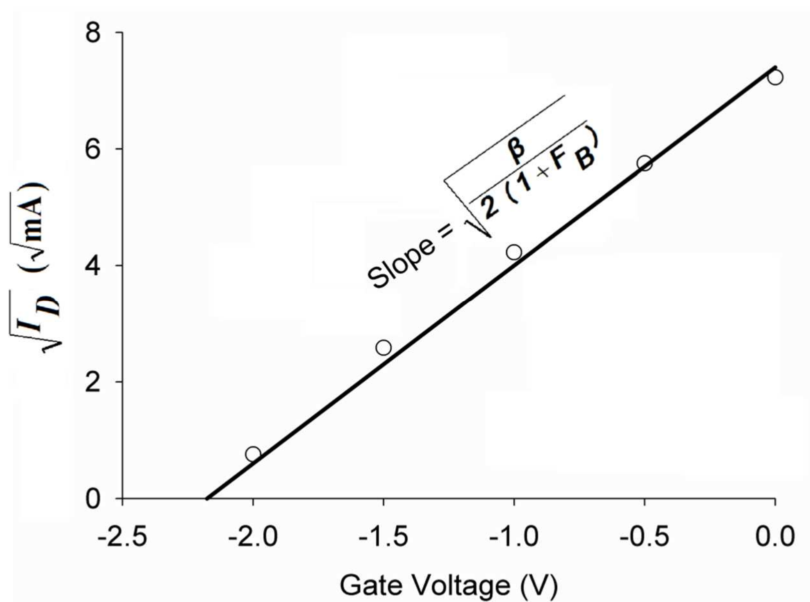

Fig. 3. Determination of F_B from the slope of the linear relationship between the square root of the drain saturation current and the gate voltage.

D. Nonlinear Fitting

The differences between the default values and the extracted values, shown in Table 1, are so large that the default values are not reliable even as the initial values for a possible nonlinear fitting of the selected equations and the measured data. However, the extracted values can be used as the initial values to improve the match between the selected equations and the measured data by nonlinear fitting. The parameter values after nonlinear fitting are also shown in Table 1. As can be seen, the values of extracted parameters after nonlinear fitting are very close to the initial values obtained by the previously described parameter-extraction procedure.

III. VERIFICATION BY SPICE SIMULATION

Setting the values of the selected parameters in MOSFET *LEVEL 3* model, the simulated transfer characteristic, output characteristic, and gate capacitance are compared with the measured results of the fabricated HEMT. Figures 4 (a) and (b) show that an excellent agreement between the SPICE simulation and measurement results is obtained, demonstrating

that the selected MOSFET *LEVEL* 3 equations and parameters can be used as the model for HEMTs in SPICE. In addition, the measured and simulated gate capacitance of the HEMT as a function of gate voltage is shown in Fig. 5, in which ***Cgdo*** and ***Cgso*** have constant values. Due to simplicity of this approach and the familiarity of circuit designers with the standard MOSFET model in SPICE, this approach is ideally suited for analysis and design of circuits with HEMTs.

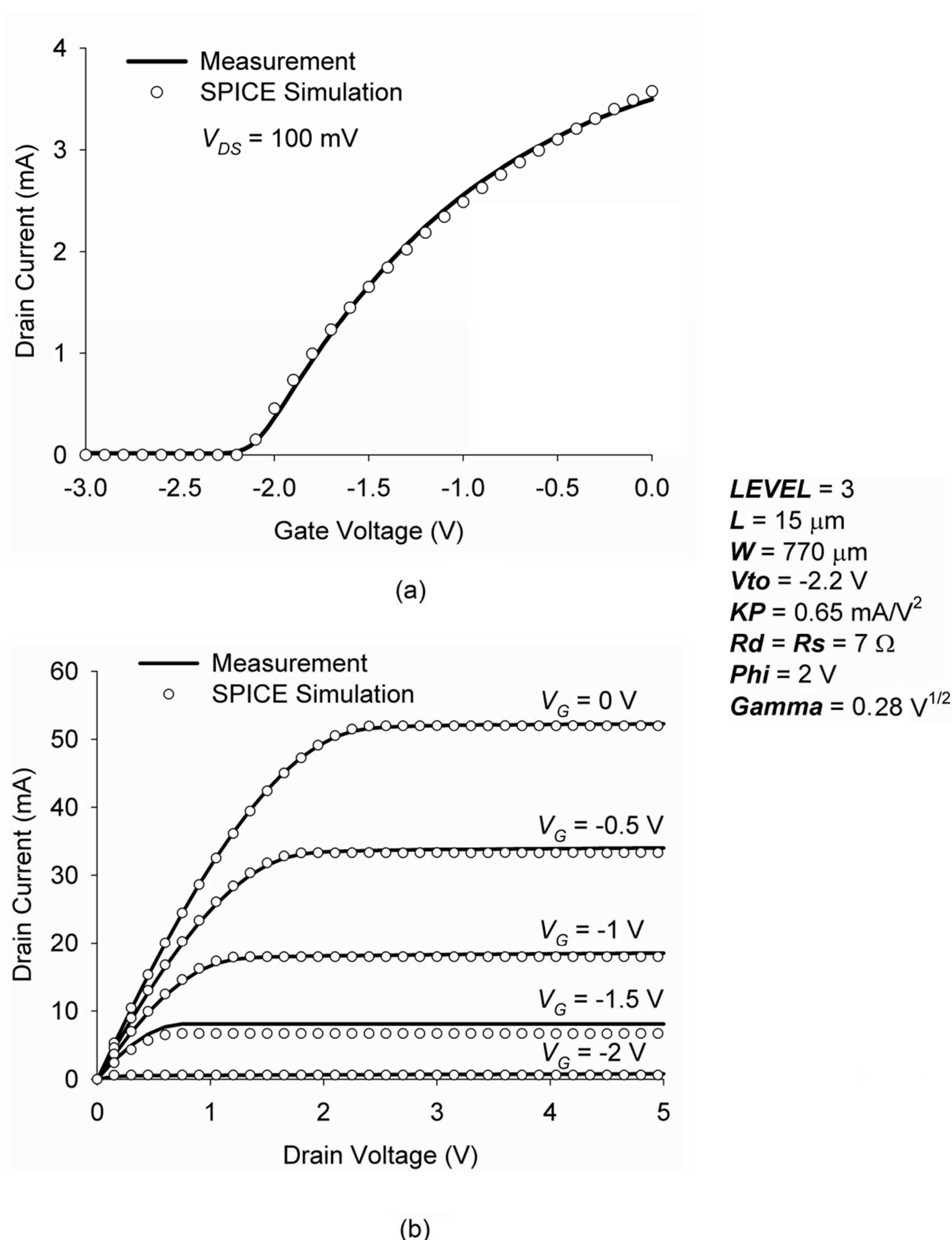

Fig. 4. Verification of the extracted parameters and the selected SPICE equations by measured data: a) transfer HEMT characteristic and b) output HEMT characteristics.

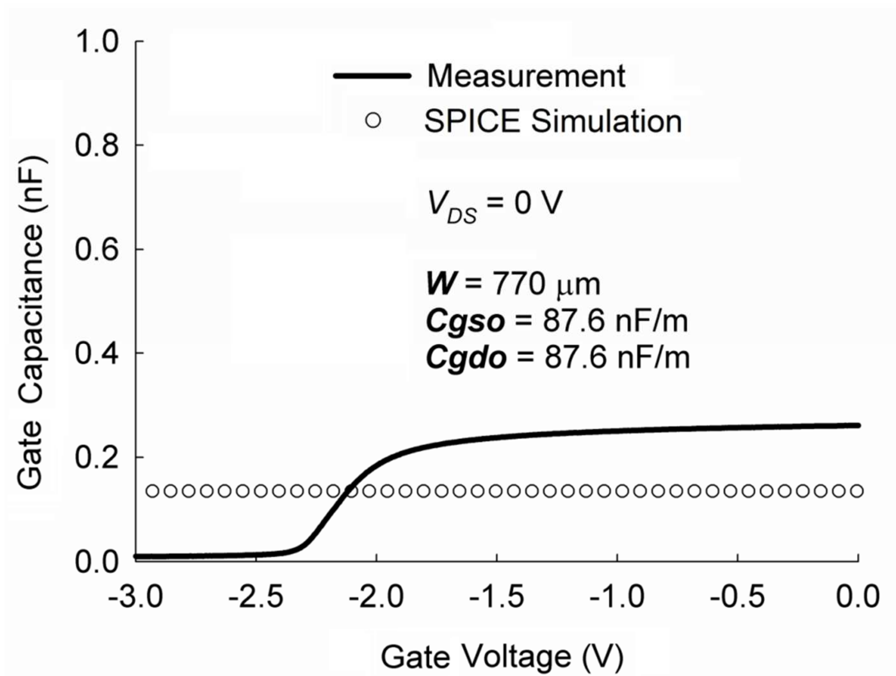

Fig. 5. Comparison of the measured and simulated gate capacitance.

IV. Conclusion

In this work, a method for using standard MOSFET equations and parameters for SPICE simulation of circuits with power HEMTs is presented. A set of MOSFET *LEVEL 3* equations and parameters is selected and techniques for the extraction of the parameter values are presented. The validity of this approach, including the proposed parameter-extraction techniques, is verified by demonstrating an excellent match between simulated and measured transfer characteristic, output characteristics, and gate capacitance of a representative circular HEMT.

Acknowledgement

This work was performed in part at the Queensland node of the Australian National Fabrication Facility, a company established under the National Collaborative Research

Infrastructure Strategy to provide nano- and microfabrication facilities for Australia's researchers. The work was partly funded by the Australian Research Council (DP130103145).

REFERENCES

[1] D. Foty, MOSFET Modeling with SPICE: Principles and Practice, Prentice Hall, New Jersey, 1997.

[2] S. S. Islam and A. F. M. Anwar, SPICE model of AlGaN/GaN HEMTs and simulation of VCO and power amplifier, Int. J. High Speed Electronics Syst. 14 (3) (2004) 853-859.

[3] G. Qu and A. Parker, Continuous HEMT model for SPICE, Electronics Lett. 32 (14) (1996) 1321-1323.

[4] J. C. Sarker and J. E. Purviance, Yield sensitivity of HEMT circuits to process parameter variations, IEEE Trans. Microw. Theory Tech. 40 (7) (1992) 1572-1576.

[5] J. Staudinger, M. Miller, M. Golio, B. Beckwith, and D. Halchin, An accurate HEMT large signal model usable in SPICE simulators, IEEE MTT-S Int. Microw. Symp. Digest 1 (1991) 99-102.

[6] S. Dimitrijev, J. Han, H. A. Moghadam, A. Aminbeidokhti, Power-switching applications beyond silicon: The status and future prospects of SiC and GaN devices, MRS Bull. 40 (2015) 399-405.

[7] S. Khandelwal, C. Yadav, S. Agnihotri, Y. S. Chauhan, A. Curutchet, T. Zimmer, J.-C. D. Jaeger, N. Defrance, and T. A. Fjeldly, Robust surface-potential-based compact model for GaN HEMT IC design, IEEE Trans. Elec. Devices 60 (10) (2013) 3216-3222.

[8] L. Yuan, W. Wang, K. B. Lee, H. Sun, , S. L. Selvaraj, X. Zhou, and G.-Q. Lo, The temperature dependent TCAD and SPICE modelling of AlGaN/GaN HEMTs, IEEE 5th Int. Nanoelectronics Conference (INEC) (2013) 115-118.

[9] N. DasGupta and A. DasGupta, A new SPICE MOSFET Level 3-like model of HEMT's for circuit simulation, IEEE Trans. Electron Devices 45 (7) (1998) 1494-1500.

[10] R. Fiedrich and H. Khakzar, The extraction of HEMT transistor DC parameters using the transistor electrical characterization and analysis program (TECAP), in Proc. of Eighth University/Government/Industry Microelectronics Symposium (1989) 211- 214.

[11] A. Aminbeidokhti, S. Dimitrijev, J. Han, X. Xu, C. Wang, S. Qu, H. Amini Moghadam, P. Tanner, D. Massoubre, G. Walker, A method for extraction of electron mobility in power HEMTs, Superlattices Microstruct. 85 (2015) 543-550.

[12] S. Dimitrijev, Principles of Semiconductor Devices, 2nd Ed., Oxford University Press, New York, 2012.

[13] PSpice Reference Guide, Cadence Design Systems, Inc, 2000.

CHAPTER 7: CONCLUSIONS AND RECOMMENDATIONS

7.1 Conclusions 125

7.2 Suggestions for Future Research 126

7.1. Conclusions

Although GaN-based HEMT was successfully commercialised, the performance of this device required more development. For instance, the AlGaN/GaN HEMT suffered from a lack of an accurate method for measuring its electron mobility in the 2DEG region. Typically, this issue is attributed to the assumption that this mobility is uniform through the whole channel, from the source to the drain. However, the HEMT structure consists of two sections; field-effect and resistive sections. The mobility of these two sections needed to be separately analysed. In addition, there were still several parameters, such as the gate voltage and temperature, whose effects on the mobility of the HMET needed identifying. Finally, the performance of the mobility measurement in the development of the HEMT, especially for the modelling of this device, needed to be known.

In this thesis, a new method for measuring the electron mobility of the 2DEG underneath the gate of the power HEMT is proposed. The mobility measurement by the new method is performed by taking into account the possible effects of the gate voltage on the value of mobility. Also, the new method avoids any errors caused by the resistive sections of the 2DEG. Applying this method to the fabricated HEMTs shows similar values for the mobility underneath and outside the gate.

HEMT is a prominent power device for high-temperature applications. Therefore, a method capable of measuring the mobility at temperatures above the room temperature is presented. This method requires only the HEMT sample, and it does not include any assumptions about the dependence of the mobility on the gate voltage. It is experimentally demonstrated that the electron mobility of 2DEG is independent of the gate voltage at various temperatures. In addition, the mobility reduction caused by increasing the temperature follows a function with the power-law coefficient of 2.45, which is higher than the common phonon-scattering value of this coefficient (1.5).

Increasing the temperature causes a reduction in the value of the mobility. The only scattering mechanism affecting the mobility at high temperatures is the phonon scattering. However, it was found that the rate of the mobility drop by the temperature for the GaN-based devices is different from the case where only normal phonon-scattering is involved. It is demonstrated that this different rate of decrease is because of the effective mass of electrons in the 2-DEG section of the AlGaN/GaN, which is increased by increasing the temperature. This unexpected

value of the power coefficient for the GaN-based devices was found in several other papers and is experimentally confirmed by a mobility measurement method.

The application of the measured mobility for developing the performance of the HEMT is investigated. It is shown that the mobility can be used for the modelling of the HEMT. SPICE, which is the most common circuit simulation software, lacks any models for the HEMT. Therefore, a new model for SPICE simulation of the circuits is introduced. This model uses the standard MOSFET LEVEL 3 equations and parameters for simulation of circuits with the power HEMTs. The technique to extract the value of the parameters is explained in detail. In addition, this model is experimentally verified by applying it to the fabricated HEMT. Comparison of the DC and AC simulated and measured characteristics of the HEMT demonstrates an excellent agreement between these results.

7.2. Suggestions for future research

Power AlGaN/GaN HEMT is the newer technology in comparison to the Si, GaAs and SiC-based power semiconductor devices. Gate leakage current, surface defects, traps, and normally-ON operation of this device are some of the main barriers for commercializing the HEMT. Increasing the temperature makes these undesired effects more prominent. Therefore, taking into account the effects of the following phenomena with temperature helps to more accurately understand the behavior of the HMET:

- Gate leakage currents
- Trapping effects
- Designing and fabricating normally-ON HEMTs without reducing its parameters
- Variation of the source and the drain resistances with the temperature

In chapters 4 and 5, the effect of the temperature on the electron mobility of the 2DEG region of the HEMT was analysed in detail. The future work can include investigation of the methods to decrease the gate leakage and trapping effects at high temperatures. Also the variations of the source and drain resistances with temperatures need to be studied.

In chapter 6, a new model for simulating the HEMT with the SPICE was proposed. The device fabricated for this purpose was normally-ON; however, the circuit designers prefer to use normally-OFF devices. Several structures are proposed for the HEMT to make it normally-OFF. Furthermore, there is evidence suggesting that cascading a MOSFET with the HEMT

makes the device normally-OFF. However, further studies are needed to determine which structure leads to the normally-OFF structure without degrading the other characteristics of the HEMT, such as its breakdown voltage and high power density.